

2 5580155

C-1

MICHIGAN STATE UNIVERSITY LIBRARIES



3 1293 00623 7808



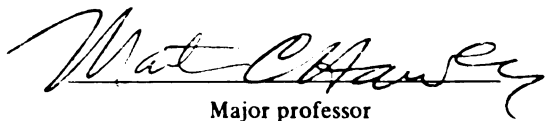
This is to certify that the
thesis entitled
EFFECTS OF FIBERS ON THE CURE CHARACTERISTICS
OF CARBON-REINFORCED EPOXY COMPOSITES

presented by

Cheryl Ann Schwaln

has been accepted towards fulfillment
of the requirements for

M.S. degree in Chemical Engineering


Major professor

Date November 10, 1989.

PLACE IN RETURN BOX to remove this checkout from your record.
TO AVOID FINES return on or before date due.

DATE DUE	DATE DUE	DATE DUE
FEB 0 1985 212	_____	_____
_____	_____	_____
_____	_____	_____
_____	_____	_____
_____	_____	_____
_____	_____	_____
_____	_____	_____

MSU Is An Affirmative Action/Equal Opportunity Institution

**EFFECTS OF FIBERS ON THE CURE CHARACTERISTICS
OF CARBON-REINFORCED EPOXY COMPOSITES**

By

Cheryl Ann Schwalm

A THESIS

**Submitted to
Michigan State University
in partial fulfillment of the requirements
for the degree of**

MASTER OF SCIENCE

Department of Chemical Engineering

1989

ABSTRACT**EFFECTS OF FIBERS ON THE CURE CHARACTERISTICS
OF CARBON-REINFORCED EPOXY COMPOSITES****By****Cheryl Ann Schwalm**

Effects of untreated and surface-oxidized carbon fibers on epoxy-resin cures were experimentally investigated and results were compared with the literature. DSC and FTIR analyses showed no significant difference in extents of cure and glass transition temperatures existed between neat and carbon-reinforced epoxy resins. Reaction rates for neat and carbon-reinforced epoxy resins were fit to a two-equation cure-kinetic model. These two equations represented the autocatalytic polymerization and diffusion-controlled crosslinking reactions. Gelation times increased and crosslinking rate constants decreased by ten percent when the carbon-fiber concentration equalled 0.60. Frequency factors decreased by 99 percent and activation energies decreased by 35 percent with a carbon-fiber concentration equal to 0.60. Carbon-fibers affected the epoxy-resin cure reactions by restricting the molecular mobility of reactants and forming chemical interactions with epoxy molecules.

Dedicated to my father, Harold,
and my mother, Leona.

ACKNOWLEDGEMENTS

I express my deepest gratitude to my family and friends, for their endless love and encouragement. I acknowledge the United States Naval Office and Michigan State University Chemical Engineering department for financial support. I wish to thank Dr. Martin Hawley, my advisor, for his wisdom and guidance during the course of this research. Appreciation is also extended to John DeLong, Jinder Jow, and Mark Finzel for their knowledge and suggestions. I want to thank Mike Rich and Javad Kalantar for assistance with the experimental apparatus. In conclusion, I would like to thank Dave Gagliardi, Carol Kelly, and Allen Magolan for their moral support and helpful ideas.

TABLE OF CONTENTS

LIST OF TABLES	vii
LIST OF FIGURES	ix
LIST OF NOMENCLATURE	xiii
I. INTRODUCTION	1
A. History	1
B. Advantages and Uses of Carbon-Reinforced Epoxy Resins	3
C. Motivation of Thesis	3
D. Thesis Statement	5
II. BACKGROUND AND LITERATURE REVIEW	7
A. Carbon Fibers	7
1. Fabrication	9
2. Topography	12
a. Fiber Structure	12
b. Untreated Surface	15
c. Surface-Oxidized	18
B. Epoxy Resin	24
1. Time-Temperature-Transformation, TTT, Diagrams — A Model of the Isothermal Cure Behavior	26
2. Cure Reactions	29
3. Cure Characteristics	31
a. Reaction Exotherm	33
b. Glass Transition Temperature	34
c. Cure-Kinetic Models	36
C. Reinforced Epoxy Composite	42
1. Types of Adhesion	43
2. Interphase Reactions	50
a. Glass-Epoxy	50
b. Carbon-Epoxy	52
3. Cure Characteristics	54
a. Reaction Exotherm	55
b. Glass Transition Temperature	56
c. Cure-Kinetic Models	58
4. Mechanical Properties	63
D. The Role of Cure Kinetics in Composite Manufacturing	66
1. Composite Cure	66
2. Laminate-Autoclave Curing	69

E. Instrumentation Overview	73
1. Differential Scanning Calorimeter, DSC	73
a. Theory	74
b. Analysis Techniques	76
2. Fourier Transform Infrared, FTIR, Spectrometer	77
a. Theory	77
b. Analysis Techniques	79
III. EXPERIMENTAL STUDY	86
A. Sample Preparation	86
B. Experimental Instrumentation	94
1. DSC	94
2. FTIR Spectrometer	97
C. Experimental Procedure	99
1. DSC-Cured and DSC-Analyzed	99
2. Convectionally-Cured and FTIR-Analyzed	102
D. Experimental Results and Discussion	105
1. Carbon Fiber Experiments	106
a. Carbon Fiber and Hardener Experiments	109
b. Carbon Fiber and Epoxy Experiments	109
2. Neat and Reinforced Epoxy-Resin Experiments	112
a. Ultimate DSC Reaction Exotherm, H_{ult}	112
b. Initial FTIR-Spectroscopy Epoxy-Intensity Ratio	115
c. Full-Cure Time, t_f (Isothermal Cure Temperature, T_c)	117
d. Full-cure Extent of Cure, $\alpha(T_c)$	125
e. Cure Kinetics	131
f. Glass Transition Temperature, $T_g(T_c)$	149
g. Reproducibility and Accuracy	155
(1) Hardener Addition	155
(a) Stoichiometric Variations	156
(b) Extent of Cure	156
(2) Fiber Impregnation	157
(3) Prevention of Environmental Contamination	159
(4) Transmission- and Diffuse-Reflectance, DRIFT, FTIR Spectroscopy	161
IV. CONCLUSIONS	167
V. RECOMMENDATIONS	174
A. Problems and Suggestions	174
B. Further Research	177
APPENDICES	
A. Maximum Exotherm Between Carbon Fibers and Epoxy Matrix	181
B. TTT Diagram Transitions	183
C. DSC and FTIR-Spectroscopy Experimental Data	186
LIST OF REFERENCES	190

LIST OF TABLES

Table II.1. Comparison of high-strength and high-modulus carbon fibers [17].	9
Table II.2. Principal bond defects in carbon fibers [22].	17
Table II.3. Volatiles on surface-oxidized carbon-fibers [22]: (a) composition versus temperature; and (b) total and incremental amounts of desorbed volatiles.	21
Table II.4. Atomic percentages of constituents on the carbon-fiber surface [8,31].	23
Table II.5. Experimentally-determined ultimate reaction exotherm, H_{ult} , for an epoxy resin.	34
Table II.6. Mijovic et al. [44] cure-kinetic model for a neat and 40% glass-reinforced epoxy resin.	63
Table II.7. Composite manufacturing processes [2].	67
Table III.1. Cure characteristics.	106
Table III.2. Specimens for carbon-fiber experiments.	109
Table III.3. Ultimate reaction exotherm, H_{ult} , versus fiber weight fraction, w_f .	115
Table III.4. Total reaction exotherm, H_T , glass transition temperature, T_g , and full-cure time, t_f , versus cure temperature, T_c , for neat epoxy-resin cures between 120°C and 250°C.	119
Table III.5. Analysis of variance, ANOVA, of the total reaction exotherm, H_T , for the following sources of variation: (a) cure temperature, T_c ; and (b) fiber-weight fraction, w_f .	126
Table III.6. Gelation time, t_{gel} , versus cure temperature, T_c , and fiber-weight fraction, w_f , for: (a) untreated carbon-reinforced epoxy resin; and (b) surface-oxidized carbon-reinforced epoxy resin.	135

Table III.7. Reaction-rate constants, k_1 , k_2 , and k_3 , as a function of cure temperature, T_c , and fiber-weight fraction, w_f , for: (a) untreated carbon-reinforced epoxy resin; and (b) surface-oxidized carbon-reinforced epoxy resin.	139
Table III.8. Cure kinetic parameters for the neat and: (a) untreated carbon-reinforced epoxy resin; and (b) surface-oxidized carbon-reinforced epoxy resin.	142
Table III.9. Calculation of the entropy for: (a) untreated carbon-reinforced epoxy resin; and (b) surface-oxidized carbon-reinforced epoxy resin.	144
Table III.10. Comparison of activation energy, E_A , for epoxy resins modeled with the autocatalytic cure-kinetic equation in Equation 13.	146
Table III.11. Extent of cure, α , after hardener addition and fiber impregnation.	159
Table III.12. FTIR-spectroscopy sample-preparation errors.	163
Table C.1. DSC extent of cure, α , versus time, t , for the neat, untreated carbon-reinforced, and surface-oxidized carbon-reinforced epoxy resin isothermally DSC-cured at 170°C, 200°C, and 220°C.	186
Table C.2. FTIR-spectroscopy epoxy-intensity peaks.	188

LIST OF FIGURES

Figure I.1. Conceptualization of the fiber-matrix interphase.	5
Figure II.1. Decomposition of polyacrylonitrile, PAN, at 200°C under reduced pressure [11].	10
Figure II.2. Dehydrogenation and denitrogenation of polyacrylonitrile, PAN, [11].	11
Figure II.3. A schematic model of the crystallite columns in a carbon fiber. The S_1 , S_2 , and S_3 represent voids, basal-plane boundary and intercrystallite boundary, respectively [10].	13
Figure II.4. A schematic model of the axial hexagonal arrays of carbon atoms in a graphitic basal plane [11].	14
Figure II.5. A schematic three-dimensional structural model of a carbon fiber [23].	14
Figure II.6. Common graphitic basal-plane defects on the carbon-fiber surface [22]: (a) hole defects; (b) claw defects; and (c) twinning-line defects. Note: A "twinning-line" is defined as a region in which the defect causes a sequence of alternating four- and eight-atom rings instead of the normal six-atom hexagonal rings.	16
Figure II.7. Volatiles from surface-oxidized carbon fibers [8]: (a) composition versus temperature; and (b) total amount desorbed versus temperature.	22
Figure II.8. Schematic illustration of the potential carbon-fiber surface groups [18].	23
Figure II.9. Reaction of epichlorodiyfrin and bisphenol A, diphenyl propane A produces the epoxy monomer, difunctional diglycidyl ether of bisphenol A, DEGBA [33].	24
Figure II.10. Typical cure schedule for an epoxy resin.	25

Figure II.11. Schematic representation of a: (a) branched polymer; and (b) crosslinked polymer [33].	27
Figure II.12. Time-temperature-transformation, TTT, diagram [36].	32
Figure II.13. Representation of: (a) wetting of a solid with a liquid; and (b) nonwetting of a solid with a liquid. Note: θ = contact angle.	44
Figure II.14. Fiber-matrix adhesion between isolated contact points on a carbon fiber.	46
Figure II.15. Chemical reaction in the fiber-matrix interphase between the carbon-fiber surface and epoxy resin.	48
Figure II.16. Illustration of a: (a) glass-silane coupling-agent; and (b) the R groups covalently bonding with the epoxy resin [2].	51
Figure II.17. Experimental results reproduced from Dutta et al. [43]: (a) k_1 for a carbon-black filled epoxy resin; (b) k_2 for a carbon-black filled epoxy resin; (c) k_1 for a glass-filled epoxy resin, and (d) k_2 for a glass-filled epoxy resin.	60
Figure II.18. A schematic of a laminate-fabrication sequence [62].	71
Figure II.19. Nonuniformity in conventionally-cured epoxy composite.	72
Figure II.20. Illustration of the Michelson Interferometer [28].	78
Figure II.21. FTIR-spectroscopy analysis techniques: a) transmission; b) single internal reflection, IRS; and c) diffuse-reflectance, DRIFT [83].	80
Figure III.1. The molecular structure of: (a) Dow Epoxy Resin, DER 332 [90]; and (b) Diaminophenyl sulfone, DDS [91].	87
Figure III.2. Photograph of a prepregger machine manufactured by the Research Tool Company.	89
Figure III.3. A 500X photograph of a carbon-reinforced epoxy composite with a fiber-weight fraction, w_f , of 0.60.	92
Figure III.4. Cross-section of the DuPont 9900 DSC cell [93].	95

Figure III.5. Photograph of the DuPont thermal analyzer, TA, and 9900 DSC.	96
Figure III.6. Photograph of the Perkin-Elmer 1800 FTIR spectrometer.	97
Figure III.7. Illustration of the Perkin-Elmer diffuse-reflectance, PEDR, accessory [94].	98
Figure III.8. Experimental DSC curves of: (a) the ultimate reaction exotherm, H_{ult} , for an uncured epoxy resin; (b) the total reaction exotherm, H_T , for an uncured epoxy resin; and (c) the glass transition temperature, T_g , for a fully-cured epoxy resin.	101
Figure III.9. FTIR-spectroscopy absorbance spectra of: (a) an uncured epoxy resin; and (b) a cured epoxy resin.	104
Figure III.10. Total reaction exotherm, H_T , versus DSC-heating rate for an epoxy resin.	113
Figure III.11. DSC analyses of the: (a) total reaction exotherm, H_T , versus the cure temperature, T_c ; and (b) the glass transition temperature, T_g , versus T_c .	118
Figure III.12. Illustration of the: (a) total reaction exotherm, H_T , versus the \log_{10} (glass transition temperature, T_g); and (b) \log_{10} (residual extent of cure, $\alpha_{rid} = 1 - \alpha$), versus the T_g .	121
Figure III.13. Illustration of the full-cure line. The cure temperature, T_c , versus log time, t .	122
Figure III.14. Time-temperature-transition, TTT, diagram for a stoichiometric DER 332-DDS epoxy resin.	125
Figure III.15. Full Cure extent of cure, α , versus cure temperature, T_c , for the (a) DSC-cured and DSC-analyzed untreated carbon-reinforced epoxy resin; (b) DSC-cured and DSC-analyzed surface-oxidized carbon-reinforced epoxy resin; and (c) convectionally-cured and FTIR-analyzed surface-oxidized carbon-reinforced epoxy resin.	128
Figure III.16. Extent of cure, α , versus time, t , for a: (a) DSC-cured and DSC-analyzed untreated carbon-reinforced epoxy resin; and (b) DSC-cured and DSC-analyzed surface-oxidized carbon-reinforced epoxy resin.	134

Figure III.17. Reduced: (a) polymerization reaction rate, α_{red1} , versus extent of cure, α , for the neat epoxy resin; and (b) crosslinking reaction rate, α_{red2} , versus α for the neat epoxy resin.	137
Figure III.18. Logarithm of the rate constants, k_1 , k_2 , and k_3 , versus inverse absolute cure temperature, T_c , for: (a) untreated carbon-reinforced epoxy resin; and (b) surface-oxidized carbon-reinforced epoxy resin.	138
Figure III.19. DSC analyses of fully-cured epoxy resin at: (a) 170°C; (b) 190°C; (c) 200°C; (d) 210°C; (e) 220°C; (f) 230°C; and (g) 250°C.	153
Figure III.20. Glass transition temperature, T_g , versus cure temperature, T_c , for: (a) untreated carbon-reinforced epoxy resin; and (b) surface-oxidized carbon-reinforced epoxy resin.	158
Figure III.21. The extent of cure, α , versus time, t , for a neat epoxy resin cured at 80°C.	158
Figure A.1. Chemical reaction of a carbon fiber and an epoxy resin.	179

LIST OF NOMENCLATURE

A - frequency factor

$A(1184)$ - absorbance at 1184 cm^{-1} of fully-cured epoxy resin,

$A(916)$ - absorbance at 916 cm^{-1} of fully-cured epoxy resin,

$A_0(1184)$ - absorbance at 1184 cm^{-1} of unreacted epoxy resin,

$A_0(916)$ - absorbance at 916 cm^{-1} of unreacted epoxy resin,

$A_{916\text{ cm}^{-1}}/A_{1184\text{ cm}^{-1}}$ - FTIR-spectroscopy epoxy intensity
ratio

$(A_{916\text{ cm}^{-1}}/A_{1184\text{ cm}^{-1}})_0$ - initial FTIR-spectroscopy epoxy
intensity ratio

ATR - attenuated total reflection

a_m - molar absorption coefficient

B - ratio of hardener equivalents to epoxy-monomer
equivalents

$B(\nu)$ - source intensity

C - proportionality constant

C_A - hardener concentration

C_{A0} - initial hardener concentration

C_E - epoxy-monomer concentration

C_{E0} - initial epoxy monomer concentration

c - filler content

c_m - molar concentration

DDS - diaminodiphenyl sulfone

DEGBA - diglycidyl ether of bisphenol A
 DER 332 - Dow Epoxy Resin 332
 DRIFT - diffuse reflectance
 DSC - differential scanning calorimeter
 d_p - prepreg density
 d_w - water density
 E_A - activation energy
 E_m - unreacted epoxy-monomer lattice energy
 E_x - full-cure epoxy-polymer lattice energy
 $F(R_\infty)$ - Kubelka-Munk function
 F_m - unreacted epoxy-monomer segmental mobility
 F_x - full-cure epoxy-polymer segmental mobility
 FTIR - Fourier transform infrared spectrometer
 f - frequency
 f_e - epoxy-monomer functionality
 $f_1(c)$ - function of filler content for the catalyzed
 reaction rate
 $f_2(c)$ - function of filler content for the autocatalyzed
 reaction rate
 g_e - hardener functionality
 H - reaction exotherm
 H_T - total reaction exotherm
 H_{ult} - ultimate reaction exotherm
 $I(x)$ - interferogram intensity
 ITCA - International Confederation for Thermal Analysis
 i - reaction mechanism occurring chronologically during the
 cure

K - overall reaction-rate constant
K' - initial reaction-rate constant
k_i - rate constant for the i reaction mechanism
k₁ - catalyzed reaction-rate constant
k₂ - autocatalyzed reaction-rate constant
k₃ - crosslinking reaction-rate constant
M - specimen weight
m - autocatalyzed-polymerization reaction order
m' - moles
m'₀ - initial moles
N - overall reaction order
n - catalyzed-polymerization reaction order
PAN - polyacrylonitrile
PEDR - Perkin-Elmer diffuse-reflectance
R - universal gas constant
R_s - sample diffuse reflectance
r/R - normalized radius
SEM - scanning electron microscopy
S₁ - voids
S₂ - basal-plane boundary
S₃ - intercrystallite boundary
s - scattering coefficient
T - absolute temperature
T_i - internal transmittance
TEM - tunneling electron microscopy
T_c - cure temperature
T_g - glass transition temperature

T_{g_0} - unreacted glass transition temperature
 $T_{g_{gel}}$ - gelled glass transition temperature
 T_{ult} - ultimate reaction exotherm
 TA - thermal analyzer
 TTT - time-temperature-transformation
 t_f - full-cure time
 t_{gel} - gelation time
 VHT - vacuum heat treatment
 W_A - work of adhesion
 w - absorption coefficient
 w_f - fiber-weight fraction
 XPS - x-ray photoelectron spectroscopy
 x - mirror displacement
 y - uniform sample thickness
 α - extent of cure
 α_{gel} - extent of cure at gelation
 α_{rid} - residual extent of cure
 α_{red1} - reduced polymerization reaction rate
 α_{red2} - reduced crosslinking reaction rate
 τ_1 - epoxy resin surface free energy
 τ_2 - carbon fiber surface free energy
 τ_{12} - epoxy-hardener surface free energy
 θ - contact angle
 ϵ - molar absorptivity

Chapter I

INTRODUCTION

In a carbon-reinforced epoxy composite, carbon fibers act as the reinforcement and epoxy resin serves as the matrix which holds the fibers. Carbon fibers have superior mechanical properties, but are in a difficult to use form. An epoxy resin has poor mechanical properties, but can easily function as a structural element. The resultant composite is a material with superior mechanical properties, but in a form which can be easily handled [1,2].

A. History

Fiber composites are neither new materials nor always man-made. Wood is a fiber composite consisting of cellulose chains embedded in a lignin matrix which has existed for more than 350 million years — since the Middle-Devonian period of the Paleozoic era. What is new and man-made are the realms of fiber composites which have developed since the mid-twentieth century.

Laying groundwork for the study of composites, Herrick [3] stated that the bond between a carbon fiber and an epoxy resin is both physical and chemical. Since the discovery that an enhanced carbon-fiber surface aids the composite's mechanical integrity, the focus has shifted to chemical bonding. For example, Drzal et al. [4] reported that surface-oxidized carbon-reinforced composites have improved interfacial-mechanical properties over untreated carbon-reinforced composites. They implied that these improved properties are the result of enhanced chemical bonding between fiber and matrix. Fitzer et al. [5] used scanning electron microscopy, SEM, and wet chemical analyses to probe the chemical nature of the carbon-fiber surface. Their results suggested that both covalent and hydrogen bonding occurred between the carbon fiber and epoxy resin.

While the last decade has witnessed much fruitful research, "a priori" prediction of composite properties based on fiber type, fiber-surface treatment, and resin properties is not currently possible. Nevertheless, manufacturers add surface-oxidized carbon fibers to epoxy resins to form very useful composites.

B. Advantages and Uses of Carbon-Reinforced Epoxy Resins

Synergistic union of carbon fibers with an epoxy resin creates a composite with strength and modulus values in the direction of the oriented fibers which are comparable to those of conventional materials, such as steel and aluminum. Carbon-reinforced epoxy composites also possess better thermal and electrical properties, less tendency toward corrosion, reduced density, and lower thermal expansion than conventional materials. Today, carbon-reinforced epoxy composites are being used: (1) by the aviation industry in wings and fuselages for aircrafts; (2) in defense-related naval equipment such as ship masts, hulls, and decks; (3) for recreational equipment, which includes sailboats, motorboats, skis, bicycles, fishing rods, bowling balls, golf clubs, and tennis rackets; and (4) by the automobile industry for bumpers, distributor caps, integrated front-end panels, leaf springs, and other components.

C. Motivation of Thesis

All manufacturing processes are designed to produce a desired product from starting materials through a succession of physical and chemical treatments. During the manufacture of a carbon-reinforced epoxy composite, carbon fibers and epoxy resin undergo a number of physical

treatments. Fiber-surface treatments or resin purification prepare them for chemical treatment. During the chemical treatment, carbon fibers and epoxy resin are combined and cured to form a carbon-reinforced epoxy composite. This composite may undergo further physical treatment, such as forming and trimming, before the final desired product is obtained. The chemical treatment or curing is the heart of any composite fabrication process, the step that determines a successful process.

This study is to serve as an aid for manufacturing high-performance composite materials. In the past, carbon-reinforced epoxy-composite cures have been modeled with neat, or fiberless, epoxy-resin cure kinetics. Today, researchers [6] postulate that either physical or chemical interactions exist in the region between the carbon fibers and epoxy resin [7,8].

In this study, it will be determined whether more or less epoxy molecules polymerize when carbon fibers are added to the epoxy resin. Also the carbon-fiber effects on thermal cure characteristics, such as the reaction exotherm and glass transition temperature, will be considered. Finally, this work will address carbon-fiber effects on epoxy-resin cure kinetics.

D. Thesis Statement

A literature review is conducted to study the chemical composition of the carbon fiber, epoxy resin, and fiber-matrix interphase. A three-dimensional fiber-matrix interphase concept has been developed by Sharpe [4]. He stated that the interface is only part of the three-dimensional fiber-matrix interphase. The interphase extends between the bulk matrix through the interface to the bulk fiber. This interphase is unlike either the bulk matrix or fibrous material. Figure I.1. illustrates a schematic model of the fiber-matrix interphase in a fiber-reinforced composite.

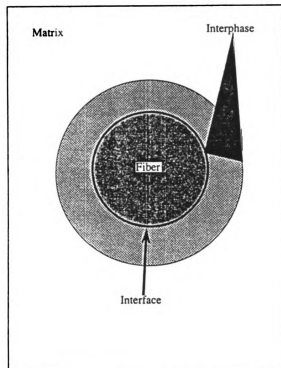


Figure I.1. Conceptualization of the fiber-matrix interphase.

The experimental study involves fabrication and curing of carbon-reinforced epoxy-resins. A differential scanning calorimeter, DSC, and a Fourier transform infrared, FTIR, spectrometer are used to determine the carbon-fiber effects on epoxy-resin cure characteristics. DSC should show an increase in the reaction exotherm if additional epoxy molecules react with carbon-fiber surface groups. FTIR spectroscopy should show a decrease in the epoxy-intensity ratio if additional epoxy molecules react with carbon-fiber surface groups. Then, the cure data is fit to an autocatalytic cure-kinetic and Arrhenius-temperature model. Any thermal or kinetic differences between neat and carbon-reinforced epoxy-resin cures is attributed to interactions in the fiber-matrix interphase.

CHAPTER II

BACKGROUND AND LITERATURE REVIEW

Before the experimental study was performed, a review of related literature was conducted. First, the chemical structure of the carbon fiber and epoxy resin was discussed. Next, the epoxy-resin cure was described and several cure-kinetic models were evaluated. Finally, the chemical nature of the fiber-matrix interphase and experimental results from other composite characterization studies were summarized.

A. Carbon Fibers

Appreciable interest in carbon fibers had originated in 1880, when the incandescent lamp was created by Thomas Edison [12]. He made carbon fibers by carbonizing natural cellulose fibers, such as cotton or linen. In the 1950s, the Wright-Patterson Air Force Base had produced carbon fibers from pyrolyzed viscose rayon [13]. A significant breakthrough in carbon-fiber technology had occurred around 1965, when researchers discovered that they could form high-strength carbon fibers. These high-strength fibers were formed by subjecting mesophase petroleum pitch to a

continuous tensile stress at high temperatures. Today, the most common carbon fibers used in composite technology are those prepared by the carbonization of polyacrylonitrile, PAN [14].

The basic goal in carbon-fiber development was to produce a high density of graphitic basal planes which were oriented parallel to the fiber axis [15,16]. A distinction between carbon and graphite fibers should be made. Carbon fibers were usually fabricated at temperatures of 1000°C to 1500°C and contain only 96% carbon [18,19]. On the other hand, graphite fibers, were fabricated at temperatures up to 2500°C and contain at least 99% carbon [20]. Graphite fibers have a higher degree of orientation than carbon fibers. Manufacturers primarily used carbon fibers in composite fabrication; therefore, only carbon fibers were tested in this study.

Both high-strength and high-modulus carbon fibers exist. Table I.1 lists several properties of commercial high-strength and high-modulus carbon fibers [21]. The difference between these two fibers was, simply, high-strength carbon fibers have a higher tensile strength and high-modulus carbon fibers have a higher Young's modulus. In this study, only high-strength carbon fibers were considered.

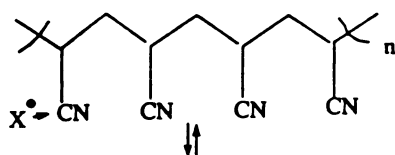
Table II.1. Comparison of high-strength and high-modulus carbon fibers [21].

Fiber Type	High-Strength	High-Modulus
Modulus (psi)	30.0×10^6	55.0×10^6
Tensile Strength (psi)	3.9×10^5	3.2×10^5
Density (g/cm ³)	1.8	1.9
Fiber Diameter (μm)	≈ 8	≈ 8

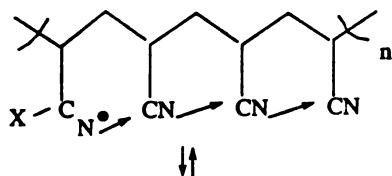
1. Fabrication

High-strength carbon fibers were formed by forcing the polyacrylonitrile, PAN, precursor material through an orifice. The chemistry of formation of the PAN precursor is given in Figure II.1. [14]. The degradation of PAN was initiated by an impurity anion, X, (Figure II.1(b)) which was derived from a cyclization to yield an impurity or degradation product (Figure II.1(a)). This initiation was succeeded by a cyclization to yield an imine structure (Figure II.1(c)), which tautomerized into an enamine structure (Figure II.1(d)). Then, this enamine oxidized to give the final pyridone structure (Figure II.1(e)). The sequence of cyclized groups in the ladder structure provided rigidity along the chain and maintains this structure by extensive interchain bonding between the polymer chains through C=O and N-H groups.

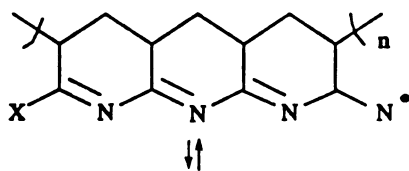
a.



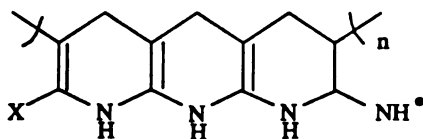
b.



c.



d.



e.

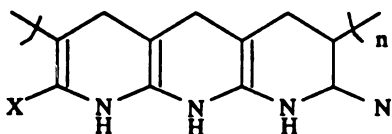


Figure II.1. Decomposition of polyacrylonitrile, PAN, at 200°C under reduced pressure [14].

These fibers were then heated in an oxygenated atmosphere at temperatures up to 400°C, and partially graphitized in the presence of an inert gas at temperatures up to 600°C, shown in Figure II.2. When the temperature reached 600°C, dehydrogenation occurred, and singular hexagonal chains began to form small graphitic basal planes.

Next, the temperature was increased from 600°C to 1500°C denitrogenation occurred [14]. During the denitrogenation step, the small graphitic planes combined to form larger graphitic basal planes and evolved volatiles such as H_2 , HCN , NH_3 , CO , CO_2 , and N_2 [3,7,14,18-21]. A few of these volatiles remained as functional groups on the carbon-fiber surface. These functional groups aided in adhesion and were an important part of the fiber-matrix interphase.

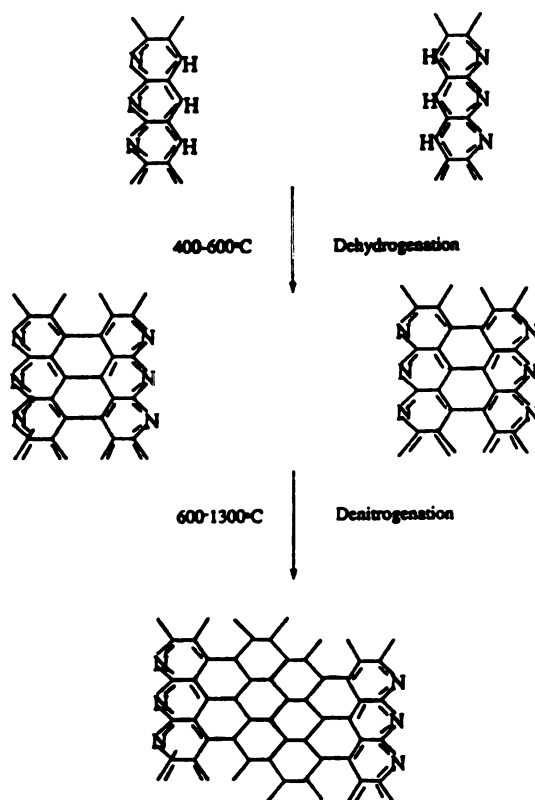


Figure II.2. Dehydrogenation and denitrogenation of polyacrylonitrile, PAN [11].

2. Topography

The carbon-fiber structure was very important when considering the fiber effects on epoxy-resin cures. Chemical constituents on the carbon-fiber surface were responsible for adhering to the epoxy resin in the fiber-matrix interphase.

a. Fiber Structure

The main structural units of the carbon fiber were crystallitic columns. These crystallite columns contained numerous arrays of graphitic basal planes oriented roughly parallel to the carbon-fiber axis, as shown in Figure III.3. The average length of the graphitic column was estimated to be 12 basal arrays and the average graphitic column is between 40 and 120 Å [1,10].

Figure II.4 shows that these basal planes were stacked on top of each other in a regular abab...packing sequence [11]. Such a sequence meant that starting with one layer (a) and using an axis normal to it as a reference, the third layer (c) was similarly placed with respect to this axis; whereas the second layer (b) was slightly shifted off axis. The distance between two adjacent basal planes was approximately 3.35 Å.

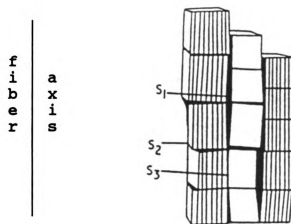


Figure II.3. A schematic model of the crystallite columns in a carbon fiber. The S_1 , S_2 , and S_3 represent voids, basal-plane boundary, and intercrystallite boundary, respectively [10].

In these graphitic basal planes, the carbon atoms were arranged in a near-ideal hexagonal matrix [22]. The hexagonals in a graphitic basal plane have angles of 60° between side faces, have carbon atoms at each of its vertices, and were in parallel arrangement.

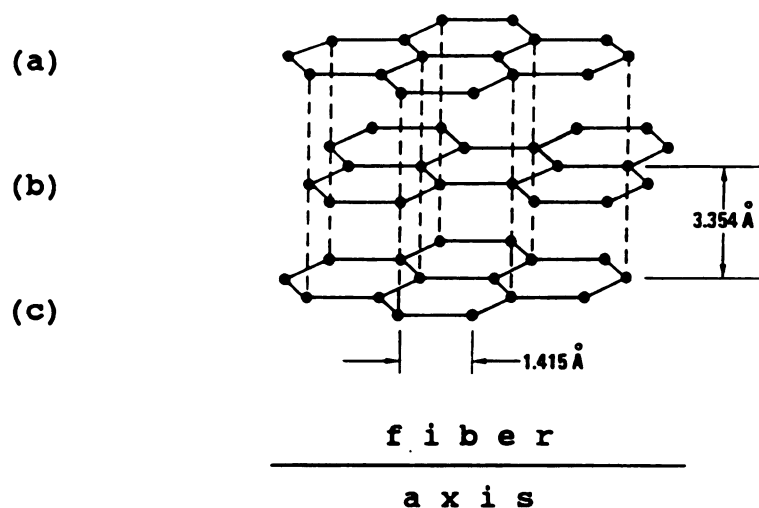


Figure II.4. A schematic model of the axial hexagonal arrays of carbon atoms in a graphitic basal plane [11].

Figure II.5 [23] shows that a carbon fiber contained three distinct regions, inner, middle, and outer. The development and orientation in the inner layer was poor, the crystallite columns were twisted and undulated. The middle layer was better developed and highly ordered.

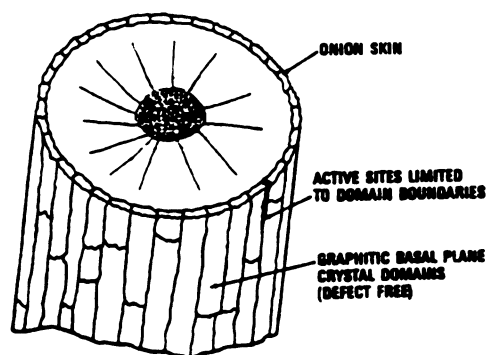


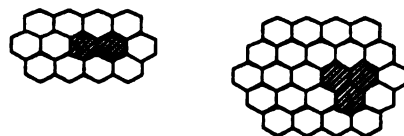
Figure II.5. A schematic three-dimensional structural model of a carbon fiber [23].

Diefendorf et al. [23] have used tunneling electron microscopy, TEM, and described the outer untreated carbon-fiber surface as being similar to an onion-skin structure. Folding of the surface skin was caused by differences in the thermal expansion coefficients of the poorly-ordered fiber interior and the highly-ordered fiber exterior. Upon cooling from the cure temperature, the outer carbon-fiber surface cooled prior to the inner fiber layers. This differential contraction placed the outer fiber surface in compression and caused cracking and buckling of the carbon-fiber surface.

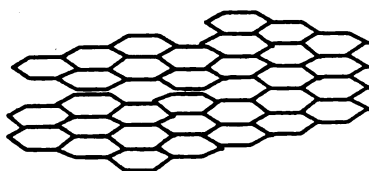
b. Untreated Surface

Many macroscopic defects in carbon fibers were located at the boundaries between single-crystal domains and within non-basal plane regions of the surface. Significance of the defects in the carbon-fiber surface comes from the fact that the ideal graphite basal plane was inert. Thus, chemical reactivity of a carbon-fiber was limited to these basal-plane defect regions [24]. Figure II.6 shows common basal-plane defects. Table II.1 lists the principal types and causes of these defects in the carbon-fiber surface [22].

a.



b.



c.

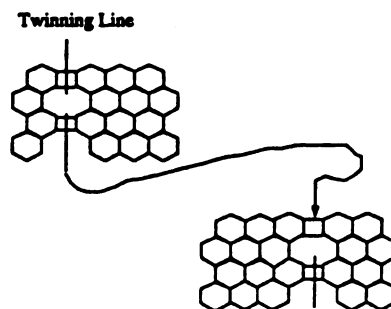


Figure II.6. Common graphitic basal-plane defects on the carbon-fiber surface [22]: (a) hole defects; (b) claw defects; and (c) twinning-line defects. Note: A "twinning-line" is defined as a region in which the defect causes a sequence of alternating four- and eight-atom rings instead of the normal six-atom hexagonal rings.

Table II.2. Principal bond defects in carbon fibers [22].

Types of Defects	Causes of Defects
Edge Effects	Occurs wherever a C-C bond cannot be formed, due to foreign atoms or molecules or misalignment of carbon atoms.
Bond Isomerism Defects	Occurs when atoms become attached at carbon atoms whose hybridization is sp^3 in the carbon hexagonal network, instead of the usual sp^2 .
Chemical Effects	Incorporation of foreign atoms or molecules in the carbon hexagonal network.
Radiation Damage Effects	Caused by bombardment with neutrons or other high-energy radiation causing carbon atoms to displace from their normal lattice position.
Gross Effects	Partly graphitized carbon, where only small regions or crystallites of the carbon polymer approximates the ideal graphite hexagonal network; joined together by various kinds of isomorphous carbon structures.

Since the untreated fiber-surface consisted of mainly basal planes, X-ray photoelectron spectroscopy, XPS, analyses of the bare, as-received, untreated carbon fiber exhibited only a very small adsorption of oxygen after exposure to air [24]. In an XPS study performed by Grant et al. [8], the untreated carbon-fiber surface was found to consist of 92 atomic percent of carbon, 5 atomic percent of oxygen and 2 atomic percent of nitrogen, and negligible amounts of sodium and sulfur.

c. Surface-Oxidized

Manufacturers have added oxidized functional groups to the carbon-fiber surface to enhance the adhesion of the carbon fiber and epoxy resin. These oxidizing treatments were performed by wet-chemical methods with either sodium hypochlorite or nitric acid. Drzal et al. [25] have described the oxidizing treatments through a two part mechanism: First, the weak, outer fiber layer was removed; second, the functional surface groups were added.

Oxidizing treatments changed the surface of the untreated carbon fiber by [7,25]: (1) increasing the surface area, (2) increasing the surface rugosity, (3) reducing the tensile strength, (4) changing the chemical functionality or reactivity, (5) removing the original surface layer, and (6) changing the surface energy. A chemically and structurally new region was created, much different from the onion-skin structure of the untreated carbon fiber.

The constituents on a surface-oxidized carbon-fiber surface have been investigated by using wet-chemical analyses. Donnet et al. [11] have performed chemical reactions with the carbon-fiber surface groups and showed that oxidative treatments add carboxylic acids, lactones, carbonyls, and hydroxyls to the carbon-fiber surface.

Boehm et al. [20] have performed similar wet chemical analyses on surface-oxidized carbon fibers. Their results showed equivalent amounts of free carboxyl groups, lactones with structures similar to that of fluorescein or to a lactol of a formyl-carboxylic acid, phenolic hydroxyl groups, and carbonyl groups.

Several researchers [6-8,18,21] have used XPS to identify the chemical constituents on the carbon-fiber surface. Kozlowski et al. [21] have performed XPS analyses on carbon fibers and detected the presence of keto-enol type groups and carboxyl-ester groups. Denison et al. [18] have used XPS and determined that carboxyl, carbonyl, and hydroxyl groups present on the carbon-fiber surface. Grant et al. [8] have found carboxylic and carbonyl groups to be the most prevalent functionalities present, with small amounts of phenolic and lactone functionalities.

Thomas et al. [6] have used XPS and concluded that the carbon-fiber surface chemisorbed nitrogen. Other surface XPS studies have shown that nitrogen in the form of cyano or amino groups and trace impurities due to the manufacturing process, such as silicon, sodium, and iron were present on the carbon-fiber surface [7].

In spite of these past efforts, Sellitte et al. [27] believed the structure of the oxidized carbon-fiber surface

was not well understood due to the analyses used. They claimed the wet-chemical and XPS analyses were not sufficiently sensitive to detect minor chemical structural differences which were important in understanding fiber-matrix adhesion. They characterized the surface-oxidized carbon fibers with attenuated total reflection, ATR, FTIR, spectroscopy. Their results yield similar carbon-fiber constituents: phenols, hydroxyls, carboxyls, and carbonyls. Unfortunately, the ATR-FTIR spectroscopy analysis of carbon fibers was not fully reliable either, because spectra were distorted by the severe scattering phenomena and high absorbance of the carbon fibers [27-29].

To determine the constituents on the surface-oxidized carbon fibers, Grant et al. [8] have performed desorption studies in which carbon fibers were thermally heated under a vacuum. The zero-order reduction of their mass data is listed in Table II.3 (a) and plotted in Figure II.7 (a). These data showed that the most abundant volatile removed after 60 minutes at 150°C was carbon-monoxide. This implied many C=O groups were present on the carbon-fiber surface or the most prevalent carbon-fiber surface groups were carbonyls and carboxyls. Other carbon-fiber surface components were hydrogen, methane, amine, water, nitrogen, and carbon dioxide. Quantification of the total amounts of volatiles desorbed are listed in Table II.3 (b) and plotted in Figure II.7 (b).

Table II.3. Volatiles on surface-oxidized carbon-fibers [22]: (a) composition versus temperature; and (b) total and incremental amounts of desorbed volatiles.

a.

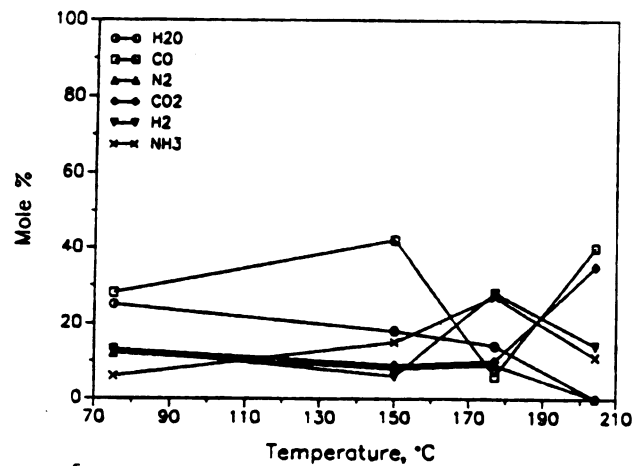
	75°C VHT/ 130 min (mole %)	150°C VHT/ 60 min (mole %)	177°C VHT/ 90 min (mole %)	204°C VHT/ 90 min (mole %)
H ₂	13	6	28	14
CH ₄	3	2	6	-
NH ₃	6	15	27	11
H ₂ O	25	18	14	-
CO	28	42	6	28
N ₂	12	8	9	-
CO ₂	13	9	10	35

b.

Treatment	Incremental Amount (monolayers)	Total Amount (monolayers)	Monolayer Capacity (moles/gm)
75°C VHT 130 min	1.6×10^{-2}	1.6×10^{-2}	2.61×10^{-6}
150°C VHT 60 min	4.6	4.62	2.61×10^{-6}
177°C VHT 90 min	3.8×10^{-2}	4.62	3.43×10^{-6}
204°C VHT 90 min	1.1×10^{-3}	4.63	3.43×10^{-6}

Note: VHT = vacuum heat treatment.

a.



b.

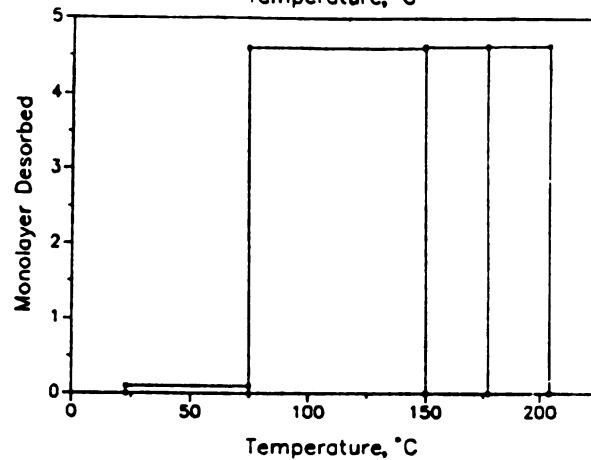


Figure II.7. Volatiles from surface-oxidized carbon fibers [8]: (a) composition versus temperature; and (b) total amount desorbed versus temperature.

Grant et al. [8] quantified the elements in the surface-oxidized carbon-fiber surface as 85 atomic percent of carbon, 11 atomic percent of oxygen, 3.5 atomic percent of nitrogen, 1.0 atomic percent of sodium, and negligible amounts of sulfur. A comparison of the surface elements on untreated and surface-oxidized carbon fiber is given in Table II.4. Based on the findings presented in this section, a schematic illustration of the potential carbon-fiber surface is constructed in Figure II.8.

Table II.4. Atomic percentages of constituents on the carbon-fiber surface [8,31].

Element	Untreated	Surface-Oxidized
C	92.0	85.0
O	5.0	10.0
N	2.0	3.5
S	<0.2	<0.5
Na	1.0	1.0

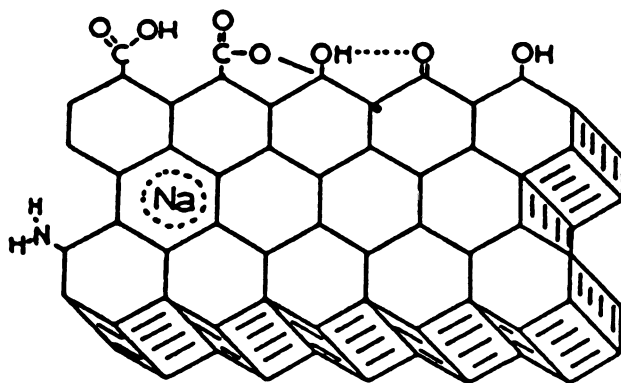
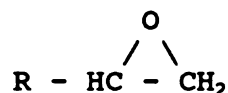


Figure II.8. Schematic illustration of the potential carbon-fiber surface groups [18].

B. Epoxy Resin

Epoxy resins are commonly used in high-performance fiber composites because of their strength, chemical resistance, toughness, and low thermal expansion on curing [32-34]. An epoxy resin is a thermoset composed of polymer chains which are formed from epoxy monomers:



In this study, a diglycidyl ether of bisphenol A, DGEBA, epoxy monomer was cured. Figure II.9 shows how the DGEBA epoxy monomer can be formed by condensing an excess of epichlorohydrin with bisphenol A, diphenylol propane A [33].

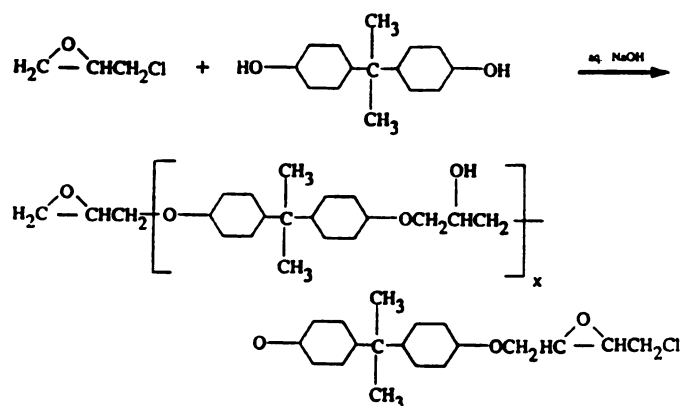


Figure II.9. Reaction of epichlorodyfrin and bisphenol A, diphenyl propane A produces the epoxy monomer, difunctional diglycidyl ether of bisphenol A [33].

Thermosetting epoxy monomers have been polymerized with hardeners such as amines or anhydrides under the application of heat and pressure as shown in Figure II.10. Under reduced pressure, the cure temperature was increased and maintained at a level such that the liquid epoxy resin polymerized and underwent a sudden and irreversible transformation to an elastic gel. After gelation, the epoxy resin was subjected to a higher cure temperature and the pressure was released. During this post-cure stage, the epoxy resin crosslinked and transformed from an elastic gel to a hard, brittle glass. Unlike thermoplastic resins which melt when re-exposed to either heat or pressure, thermosetting epoxy resins cannot reliquidify under further applications of heat and pressure [33].

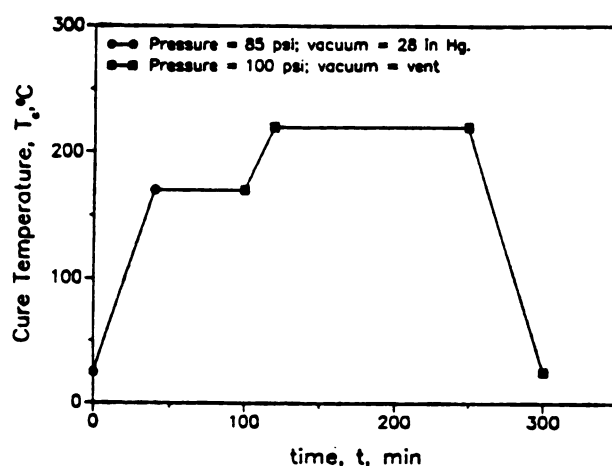


Figure II.10. Typical cure schedule for an epoxy resin.

1. Time-Temperature-Transformation, TTT, Cure Diagrams — A Model of the Isothermal Cure Behavior

As Figure II.10 shows, isothermal curing of epoxy resin was an important part of the cure process. The time and temperature necessary to transfer the liquid epoxy resin into a glass-like material must be known. A typical time-temperature-transformation, TTT, diagram is shown in Figure II.11. This diagram delineated five different regions of state encountered during an isothermal epoxy-resin cure: ungelled glass, gelled glass, liquid, gelled rubber, and char [35].

A fully-cured epoxy resin underwent two cure stages: gelation and vitrification. Gelation signified the transformation from a liquid to a gel state and is shown by the isoconversion gelation line in the TTT diagram. Vitrification signified the transformation from a gel to a glassy state and is shown by the 'S'-shaped line in the TTT diagram.

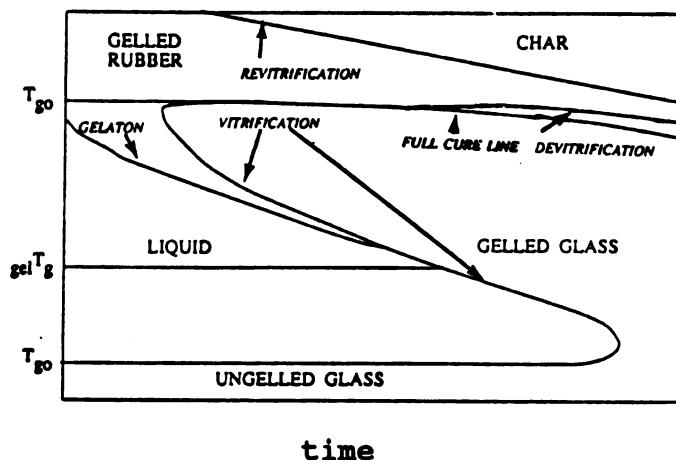


Figure II.11. Time-temperature-transformation, TTT, diagram.

The relationship between the extent of cure, α , at gelation and vitrification during isothermal cures formed the basis of the TTT diagram. This model demonstrated that gelation and vitrification depend on the cure kinetics, as well as the physical parameters of the epoxy resin, i.e., the $T_{g,ult}$, the T_g of the unreacted epoxy resin, T_{g0} , and the T_g of the gelled epoxy resin, $T_{g,gel}$.

In the glassy state, large-scale molecular motion did not occur. Rather, atoms moved around their equilibrium positions in an irregular crystal lattice. If the cure temperature, T_c , remained below T_{g0} , reactive species were immobilized in the ungelled glassy state and the epoxy resin remained unreacted and processable.

If the isothermal T_c exceeded the $T_{g,gel}$, the epoxy resin gelled. In the gelled-glass state, flow characteristics of the epoxy resin were inhibited by interchain forces originating from either secondary forces or chemical bonds.

If the T_c remained between the $T_{g,gel}$ and $T_{g,ult}$, the epoxy resin stayed in a liquid state prior to gelation. In the liquid state, polymer chains moved freely and molecules easily slid past one another when a force was applied.

If the T_c exceeded the $T_{g,ult}$, the epoxy resin gelled and became rubber-like. The local freedom of motion of the polymer chains was not restricted enabling epoxy polymers to slide past one another causing the epoxy resin to exhibit elastic properties which were associated with typical rubbers [33]. Theoretically, in this gelled-rubber state, the epoxy-resin cure can proceed to completion. Unfortunately, completion of the cure reaction rarely occurred due to thermal degradation.

Thermal degradation usually occurred at temperatures near the $T_{g,ult}$. Thermal degradation was characterized by two processes, devitrification and revitrification. Devitrification marked the glass-to-rubber transformation and corresponded to a decrease of T_g . Revitrification

marked a rubber-to-glass transformation and lead to the formation of char [36].

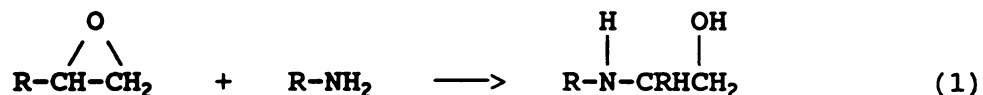
The full-cure line in Figure II.12 represented the conditions at which the maximum reaction has occurred or the maximum epoxy monomers have reacted. At these conditions, the ultimate reaction exotherm, H_{ult} , and $T_{g,ult}$ were reached. Manufacturers strive to achieve full-cure conditions because at full cure, the material properties were optimized.

This section has shown that transition states of an epoxy resin were dependent on both the T_c and t . The T_c and t helped determine the epoxy-resin cure kinetics and the final physical properties. By developing and using TTT diagrams, manufacturers were able to predetermine the final epoxy-resin properties.

2. Cure Reactions

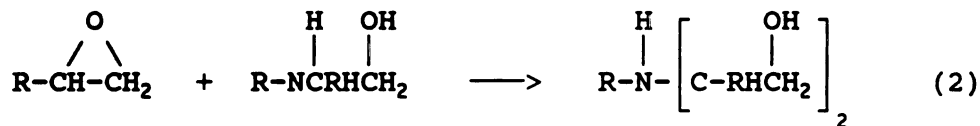
In the following, cure reactions responsible for the phase transitions in the TTT diagram were discussed. During cure, the polyfunctional epoxy monomers were polymerized with a hardener and transformed into a crosslinked macromolecular structure. The most common hardeners were difunctional or tetrafunctional amines.

The polymerization reactions can be described with two reactions. The first reaction involved an epoxy monomer and the hydrogen of a primary amine to form a branched secondary amine [37-39]:



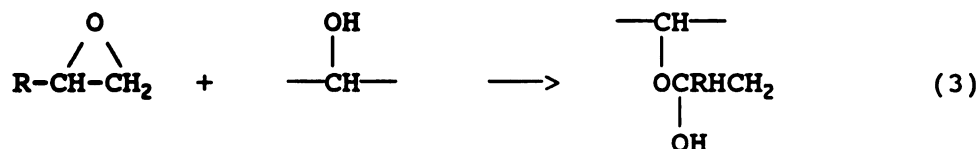
Hydrogen-donor groups, such as moisture or impurities, catalyzed this epoxy-amine reaction. The hydrogen-donor group attracted the oxygen atom of the epoxy leaving the carbon atoms with a slightly positive charge. Then a nitrogen atom on the nucleophilic hardener reacted with a carbon atom on the epoxy. The product was a secondary amine, which contained a hydroxyl group.

The other polymerization reaction was autocatalyzed by the hydroxyl of the secondary amine. The secondary amine reacted with another epoxy monomer to form [37,39]:



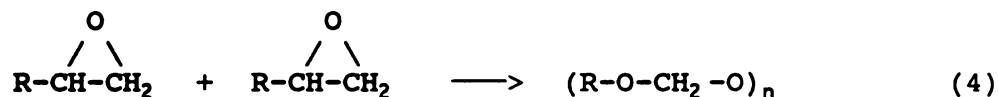
Here, the nucleophilic nitrogen attacked another carbon atom of an epoxy extending the polymer chain and formed a tertiary amine which contained an additional hydroxyl group.

At gelation, the onset of the diffusion-controlled crosslinking reaction caused a reaction-rate decrease. This reaction-rate decrease was attributed to: (1) the increase in viscosity imposed on the system due to lack of diffusional transport to a reaction site; and (2) the difficulty of forming bonds due to steric hinderance of the polymerization products. The crosslinking reaction,



involved the reaction between epoxy and hydroxyl groups on either a secondary or tertiary amine [37,39].

Researchers [34,37,40] have generally agreed that there is no large selectivity in the reaction of a primary amine with an epoxy group over a secondary amine. They also have found no evidence to support an etherification reaction between two epoxies:

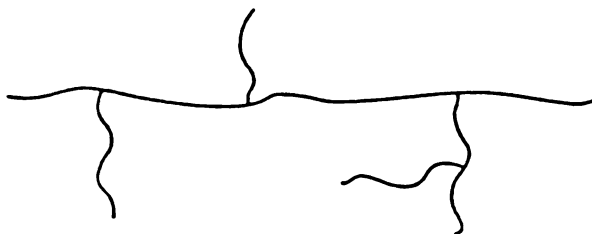


3. Cure Characteristics

The polymerization reactions, shown in Equations 4 and 5, caused the linear polyfunctional epoxy monomers to form

branched polymers [32] as shown in Figure II.12(a). After 40 to 60 percent of the epoxy monomers have reacted [33], gelation occurred. At gelation, the cure reactions shifted from chemical control to diffusion control and the reaction rate decreased. The diffusion-controlled crosslinking reactions, shown in Equation 6, caused the branched polymers to form network polymers as illustrated in Figure II.12(b).

a.



b.

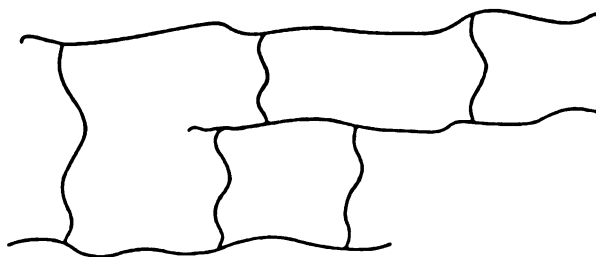


Figure II.12. Schematic representation of a: (a) branched polymer; and (b) crosslinked polymer [33].

Experimenters [2,36,41] have found that optimum properties were attained when a stoichiometric epoxy resin was cured. According to Chan et al. [41], gelation

occurred at a well-defined and calculatable stage during cure. Consider a stoichiometric epoxy resin which contained a mixture of epoxy monomers, A, with a functionality of f_e and hardener, B, with a functionality of g_e . The extent of cure at gelation, α_{gel} , was given by

$$\alpha_{gel} = [(f_e - 1)(g_e - 1)]^{-1/2}; \quad (5)$$

where f_e = epoxy monomer functionality
 g_e = hardener functionality

Beyond the gelation point, the cure proceeded to form an infinite network possessing the dimensions of the reaction vessel with increased crosslink density and increased glass transition temperature, T_g [41]. When the T_g equaled the cure temperature, T_c , vitrification occurred. Vitrification, as described by Enns et al. [36], was the transformation from a viscous gel to a glass.

a. Reaction Exotherm

The reaction exotherm was the heat liberated during an epoxy-resin cure. Two reaction exotherms have been discussed and studied in the literature, the ultimate reaction exotherm, H_{ult} , and the total reaction exotherm, H_T . The H_{ult} for an epoxy resin was the heat liberated when all epoxy monomers have reacted. The H_T was the heat liberated during an isothermal cure. Unlike the H_T , the H_{ult} was usually determined with dynamic temperature scans.

Experimental H_{ult} for stoichiometric epoxy resins are shown in Table II.5. The average experimental H_{ult} was 25.3 cal/mol. Studies have shown that the maximum obtainable H_r was only 85 to 90 percent of the H_{ult} [22,34,42].

Table II.5. Experimentally-determined ultimate reaction exotherm, H_{ult} , for an epoxy resin.

Experimenter(s)	Resin	H_{ult} cal/mol	Error
Klute et al.[43]	DGEBA-amine	26.0	±1.2
Prime [37]	DGEBA-amine	25.0	±0.94
Dutta et al.[44]	DER 332-amine	25.8	±1.0
Horie et al.[43]	DER 332-amine	24.5	±0.65
Sourour et al.[40]	DER 332-DDS	26.1	±0.70
This study	DER 332-DDS	24.6	±0.75
Average		25.3	

b. Glass Transition Temperature

Many researchers [33,40,43,45,46] have investigated the network structures of epoxy resins by studying their glass transition temperature, T_g . The T_g has been defined as the temperature at which the epoxy resin changes from an elastic gel to a hard, brittle glass. A shift in T_g depended upon: (1) the crosslinking effect, and (2) the hardener effect.

A number of studies have related the degree of crosslinking, M_c , to the shift in T_g . By averaging the

results, a rough estimate of M_c has been made [47]:

$$T_g - T_{g0} = \frac{39000}{M_c}; \quad (6)$$

where T_{g0} = unreacted T_g

DiBenedetto [48] has expanded this equation by relating the extent of cure, α , to the shift in T_g :

$$\frac{T_g - T_{g0}}{T_{g0}} = \frac{(E_x/E_m - F_x/F_m) \cdot \alpha}{(1 - (1 - F_x/F_m) \cdot \alpha)}; \quad (7)$$

where E_m = unreacted epoxy-monomer lattice energy,
 E_x = full-cure epoxy-polymer lattice energy,
 F_m = unreacted epoxy-monomer segmental mobility, and
 F_x = full-cure epoxy-polymer segmental mobility.

Bidstrup et al. [48] have DSC-cured DER 332-DDS epoxy resin and used DiBenedetto's equation to model the T_g versus α data. Their estimated values for E_x/E_m , F_x/F_m , and T_{g0} were 0.30, 0.18, and 293°K, respectively. Good agreement was found between the theoretical model and their experimental DSC data.

The hardener effect has been described as follows [47]. As Equation 3 shows, the T_g was a function of the α . From the previous section, Equation 1 showed that the α_{gel} was dependent on the functionality of the hardener. Therefore, since the number of crosslinks directly affected the T_g , the hardener functionality either increased or decreased the T_g .

Addabo et al. [49] have stated that as the cure temperature, T_c , approached the T_g , vitrification occurred. Vitrification caused the network segments to immobilize and cure reactions to cease. Barton [33] had found that vitrification slows, but does not halt, the cure reactions. Prolonged isothermal cure below the ultimate glass transition temperature, $T_{g,ult}$, resulted in a T_g greater than the T_c . The $T_{g,ult}$ was the maximum obtainable T_g and occurs when all the epoxy monomers have reacted. Experimenters [32,41] have found that epoxy resins which were isothermally cured below their $T_{g,ult}$ have a T_g approximately 10°C higher than the T_c .

The T_g was an important physical property of an epoxy resin. Manufacturers optimized cure schedules to produce epoxy resins with high glass transition temperatures. By understanding the epoxy resin cure, particularly the cure kinetics, prediction of the extent of cure or glass transition temperature was possible.

c. Cure-Kinetic Models

The two epoxy-resin cure reactions, polymerization and crosslinking, have been modeled with various cure-kinetic models. A cure-kinetic model should be selected based on how well the model describes the cure reactions. Some cure-kinetic models accurately described the epoxy cure,

while others have major deficiencies. In this section, several cure-kinetic models were evaluated.

Kinetic rate expressions describing the epoxy-resin cure have been discussed in the literature [40,33,50,51]. Some of these proposed models were semiempirical in nature, while others were based upon the detailed chemical mechanism of the epoxy-resin cure. In general, the cure kinetics of an epoxy resin have been modeled in two ways: (1) n^{th} -order kinetics; and (2) autocatalyzed reaction kinetics.

In an early investigation by Acitelli et al. [52], they fit their epoxy-resin cure data to an n^{th} -order equation,

$$\frac{d\alpha}{dt} = K (1 - \alpha)^N; \quad (8)$$

where K = overall reaction-rate constant,
 α = extent of cure, and
 N = overall reaction order.

Their cure-kinetic model assumed the following: (1) identical cure kinetics over the entire reaction; (2) the same reaction occurs prior to and subsequent to gelation, and (3) the cure reaction is diffusion-controlled.

Newer findings have shown that the identical cure kinetics are not held over the entire reaction and the

epoxy-resin cure was not diffusion controlled until after gelation occurred. Therefore, this model did not accurately model the epoxy-resin cure.

In a study conducted by Hagnauer et al. [53], polymerization was assumed to be the predominant reaction during early stages of the epoxy-resin cure. Their data was described by the following third-order expression,

$$\frac{-dC_E}{dt} = KC_E C_A^2; \quad (9)$$

$$\text{where } K = \frac{2 K' (C_E^0 + C_A^0)}{C_E^0 C_A^{0.2}},$$

$$K' = \left[\frac{d\alpha}{dt} \right]_{\alpha \rightarrow 0},$$

C_E = epoxy-monomer concentration,

C_A = hardener concentration,

C_E^0 = initial epoxy-monomer concentration, and

C_A^0 = initial hardener concentration.

This kinetic expression gave the initial reaction rate as the maximum reaction rate since the rate of conversion was proportional to the unreacted epoxy-monomer concentration.

In a typical epoxy cure, the maximum reaction rate occurred at an α between 0.30 and 0.40. The model from Hagnauer et al. also neglected to describe the different transitions the epoxy resin undergoes during cure and yielded unrealistic overall reaction orders of 0.5 and 2.1 [53]. It was concluded that no n^{th} -order kinetic models have accurately described the epoxy-resin cure.

The epoxy-resin cure occurred by two simultaneous polymerization reactions. The first cure reaction was initiated and catalyzed by the hydrogen-donor groups, such as impurities or moisture. The second cure reaction was autocatalyzed by the hydroxyl groups present in the reaction products of the first polymerization reaction [54]. An expression which described these cure kinetics for a stoichiometric epoxy-resin is [43,55,56]:

$$\frac{dq}{dt} = (k_1 + k_2 \alpha^m)(1 - \alpha^n); \quad (10)$$

where k_1 = catalyzed polymerization reaction rate constant,
 k_2 = autocatalyzed polymerization reaction rate constant,
 m = autocatalyzed polymerization reaction order, and
 n = catalyzed polymerization reaction order.

The rate constants, k_1 and k_2 , obey an Arrhenius temperature model:

$$k_i = A \exp(-E_A/RT); \quad (11)$$

where i = reaction mechanism occurring chronologically during the cure,
 A = frequency factor,
 E_A = activation energy,
 R = universal gas constant,
 T = absolute temperature.

Dutta and Ryan [43] and Mijovic et al. [44], have used Equation 10 and Equation 11 to model the epoxy-resin rate constants, k_1 , and k_2 . Their experimental data fit this cure-kinetic model well.

Sourour et al. [40] have generalized Equation 10 to include non-stoichiometric epoxy resins and assumed that the reaction orders, m and n , are equal to one. Their rate equation for an epoxy resin is:

$$\frac{d\alpha}{dt} = (k_1 + k_2)(1 - \alpha)(B - \alpha); \quad (12)$$

where B = ratio of hardener equivalents to epoxy-monomer equivalents.

This model assumed that: (1) the exclusive reactions are the polymerization reactions; (2) the concentration of hydrogen-donor groups are constant throughout the reaction; (3) the concentration of the hydrogen-donor groups is negligible compared to the epoxy monomer and hardener concentrations; and (4) gelation and vitrification occur simultaneously. Unfortunately, this model was not valid during the later stages of cure, where the reaction mechanism is diffusion-controlled.

Further investigations of epoxy-resin cures were conducted by Loos and Springer [57-60]. They used DSC and found two exothermic maxima in the reaction rate, dH/dt , versus time data. They concluded these exothermic peaks were caused by the polymerization and crosslinking reactions. They felt that their data could not be correlated by a single equation. Therefore, they used the following two equations to describe their data:

$$\frac{d\alpha}{dt} = (k_1 + k_2 \alpha) (1 - \alpha) (B - \alpha) \text{ for } \alpha < \alpha_{gel} \text{ and} \quad (13)$$

$$\frac{d\alpha}{dt} = k_3 (1 - \alpha) \text{ for } \alpha > \alpha_{gel}, \quad (14)$$

where k_3 = crosslinking reaction rate constant, and
 $\alpha_{gel} = 0.3$.

Their cure-kinetic model assumed the following: (1) the rate constant, k_3 , can be correlated to an Arrhenius type equation; (2) the model is consistent with initial and final stages of cure; and (3) the α at gelation, α_{gel} , equal to 0.3.

Careful analysis of Loos et al. experimental data showed that their epoxy resin was partially cured prior to DSC curing [42]. This explained why their value for α_{gel} was only 0.3. According to Prime [32] gelation for epoxy resins occurred at an α between 0.50 and 0.80.

This concludes the literature review of the cure-kinetics models. Equations 13 and 14 were selected to model this study's experimental data and α_{gel} was calculated from Equation 1.

C. Reinforced Epoxy Composite

The subject of this study is carbon-reinforced epoxy composites. In previous sections, the chemical structure of carbon fibers and epoxy resin was reviewed. In this section, the region between carbon fibers and epoxy resin, the fiber-matrix interphase, was addressed.

The fiber-matrix interphase extended from the edge of the bulk fiber material to the edge of the bulk matrix material [1]. The "edge" of a material was defined as the point at which the local properties begin to differ from those of the bulk material. Figure I.1 shows three different regimes which were found in a carbon-reinforced composite: (1) the bulk epoxy matrix; (2) the interphase region, which includes the fiber-matrix interface; and (3) the carbon fiber.

Cured commercial carbon-reinforced epoxy composites usually have a fiber weight fraction, w_f , between 40 and 70 percent [61,62]. Since the carbon-fiber diameter was between 7 and 8 Å [63,64]; average fiber to fiber distances were on the order of several microns. Drzal et al. [1] stated that the carbon-reinforced epoxy-composite interphase was on the order of tenths of microns; and Garton et al. [65] reported that the interphase was between

0.20 and 0.40 microns. Thus, the fiber-matrix interphase could be 10 percent of the composite material.

1. Types of Adhesion

Physical and mechanical properties of carbon-reinforced epoxy composites depended on the structure and properties of the fiber-matrix interphase. Each interphase was specific to the particular fiber-matrix system used. However, there were generalities that apply to all systems. According to Hull [66], the fiber-matrix adhesion could result from any one of the following mechanisms.

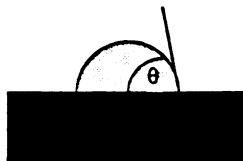
(1) Physical Absorption or Wetting

Physical absorption or the wetting of the carbon-fiber surface by the epoxy resin was critical to achieve a high degree of adhesion bonding at the fiber-matrix interphase [67]. Physical attraction was best understood by considering the wetting of a solid carbon-fiber surface by the liquid epoxy resin. Figure II.13(a) shows that wetting occurred when the contact angle between the carbon fiber and epoxy resin approached zero. Figure II.13(b) shows that nonwetting occurred when the contact angle was greater than 90° , which caused the epoxy resin to ball up and run off the carbon-fiber surface [68].

a.

Wetting

$$\theta < 90^\circ$$



b.

Nonwetting

$$\theta > 90^\circ$$

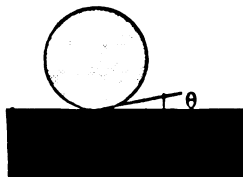


Figure II.13. Representation of: (a) wetting of a solid with a liquid; and (b) nonwetting of a solid with a liquid [68]. Note: θ = contact angle.

Wetting was explained in the terms of two theoretical equations, the Dupre equation for thermodynamic work of adhesion, W_A , and Young's equation for surface free energy. The Dupre equation represented the work necessary for an epoxy resin to wet a carbon fiber [68],

$$W_A = \tau_1 + \tau_2 - \tau_{12};$$

where τ_1 = epoxy resin surface free energy,
 τ_2 = carbon fiber surface free energy, and
 τ_{12} = epoxy-hardener surface surface free energy.

The W_A represented a physical bond resulting from highly localized intermolecular dispersion forces which, in an ideal situation, can allow for very strong adhesion between the carbon fiber and epoxy resin. The Young's equation related these surface free energy terms as follows:

$$\tau_1 = \tau_{12} + \tau_2 \cos\theta;$$

where θ = contact angle.

(15)

(16)

An epoxy resin with a surface energy of 43 mJ/m^2 readily wets carbon fibers with a surface free energy of 70 mJ/m^2 .

Schultz et al. [69] have performed wet chemistry and reverse gas-chromatography analyses on untreated, surface-oxidized, and coated carbon fibers. Coated carbon fibers were common commercial carbon fibers in which a protective coating of epoxy resin was applied to the fiber surface. Their results showed better fiber-matrix adhesion in carbon-reinforced epoxy composites containing the coated carbon-fibers. They claimed that acid-base interactions between the carbon-fiber and epoxy resin caused this increased adhesion.

Although the surface free energy was important in the initial wetting of the carbon fiber by the epoxy resin, initial free surface energies might not be important factors in the final bond between the carbon fiber and epoxy resin. Wetting was adversely affected by [70,71]: (a) a contaminated carbon-fiber surface, which reduces the effective surface area; (b) the occurrence of shrinkage stresses during cure which leads to rearrangement of the carbon-fiber surface; or (c) the overlapping of the carbon fibers, preventing the epoxy resin from completely wetting the carbon fibers. Figure II.14 illustrates how two carbon fibers averted the epoxy resin from wetting isolated contact points.

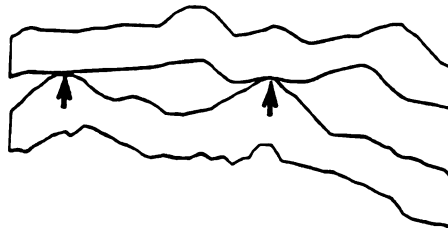


Figure II.14. Fiber-matrix adhesion between isolated contact points on a carbon fiber.

(2) Interdiffusion

The union of carbon fibers and epoxy resin could form by the diffusion of the epoxy polymers into the carbon-fiber surface. The strength of this union depended upon the amount of molecular entanglement and the type of bonding between the atomic constituents of the intertwined polymers. Interdiffusion has occurred with many resins, but because the epoxy polymers were large, the effect of molecular entanglement with the carbon-fiber surface was small [72]. Schultz et al. [69] have verified that the dispersion forces or interdiffusion of the epoxy resin and carbon-fiber surface played an insignificant role on adhesion in the fiber-matrix interphase.

(3) Electrostatic Attraction

Electrostatic attraction results from forces caused by a difference in electrostatic charge between the atoms or molecules of the carbon fiber and epoxy resin. Again, this attraction should not have a significant effect between the carbon fibers and epoxy polymers [72].

(4) Chemical Bonding

Many researchers [1,2,5,20,21] have felt that chemical bonding was an important factor in the adhesion between a carbon fiber and epoxy resin. Prior to chemical bonding, the epoxy monomer wet the carbon-fiber surface as previously described. Next, a chemical bond could form between a carbon-fiber surface group and an epoxy monomer in the fiber-matrix interphase as illustrated in Figure II.15.

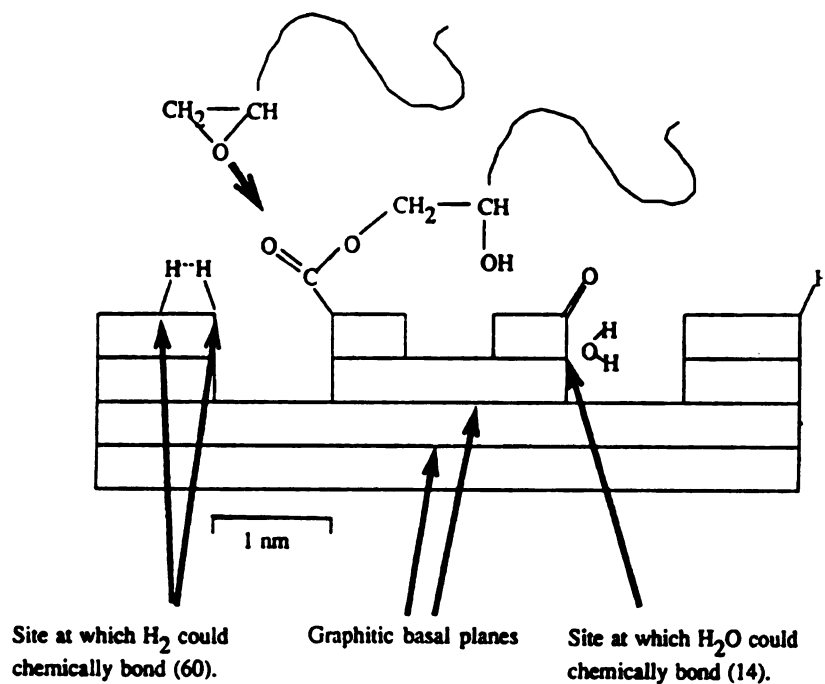


Figure II.16. Chemical reaction in the fiber-matrix interphase between the carbon-fiber surface and epoxy resin.

(5) Mechanical Adhesion

During carbon-reinforced epoxy composite cures, mechanical interlocking of the two surfaces contributed to adhesion between the carbon fibers and epoxy resin. The epoxy resin formed as a brittle glass-like material around the carbon fibers. If adhesion was solely from mechanical interlocking when the composite was stressed, the carbon fiber should pull from the epoxy resin leaving no signs of a cohesive failure.

Drzal et al. [7] have studied untreated and surface-oxidized carbon-reinforced epoxy composites. After stressing the composites, they have used an ultramicrotome to prepare samples for examination with a transmission electron microscope, TEM. Their results indicated that the failure in an untreated carbon-reinforced composite was cohesive, and failure in a surface-oxidized carbon-reinforced resin was interfacial.

Researchers [4,31] have hypothesized that onion-skin layers fracture under the residual stresses while cooling down from fiber-processing temperatures. This tendency of the onion-skin layer to break up into small particles and easily pull from the fiber-matrix interface appeared to correlate with failure at the carbon-fiber surface. This result suggested that the onion-skin layer of the untreated carbon-fiber surface was the weakest link in the fiber-matrix interphase.

Electron micrographs [23] of surface-oxidized carbon-reinforced epoxy composites have illustrated that the fracture surfaces follow the contours of the carbon fiber. That is, the fracture surfaces have propagated through the fiber-matrix interphase. The fiber-matrix interphase in surface-oxidized carbon-reinforced epoxy resins appeared to be the weakest link in the composite. They have concluded that fiber-matrix adhesion was of chemical nature, not the

result of mechanical adhesion between the fiber and matrix [3,7].

In addition to these five mechanisms, phenomena such as Van der Waals forces, hydrogen bonding, or other low energy forces might be involved with joining a fiber to the matrix. In this study, the effect of fiber-matrix adhesion on the epoxy-resin cure characteristics was considered. How the epoxy-resin cure characteristics vary gave insight as to which type of adhesions occurred.

2. Interphase Reactions

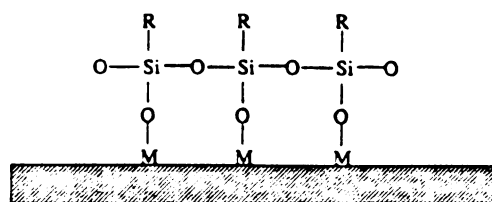
In this section, the reaction schemes of both glass-reinforced and carbon-reinforced epoxy resins were considered. The chemical reactions in the glass-reinforced epoxy interphase have been well documented [73-75]. An understanding of how a glass fiber and an uncured epoxy resin reacted may give insight into how a carbon fiber and an uncured epoxy resin reacted.

a. Glass-Epoxy

The adhesion of glass fillers to epoxy resin were due to many of the mechanisms previously described. Analogous to carbon-reinforced epoxy resins, the strength of the bonding between glass fillers and epoxy resins was enhanced

by a surface treatment, specifically a silane treatment. Silane-coated glass-filled surface contains R groups, as shown in Figure II.16(a). These R groups were any groups which can react with the epoxy monomers. Figure II.16(b) shows that during the cure, some of these R groups reacted with the epoxy monomers to form covalent bonds to the crosslinked polymer network.

a.



b.

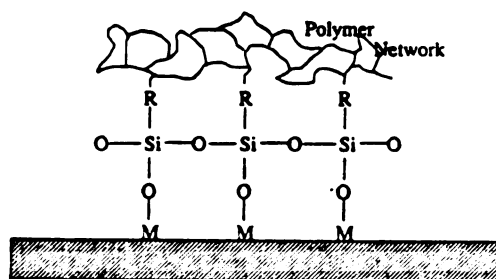


Figure II.16. Illustration of a: (a) glass-silane coupling-agent; and (b) the R groups covalently bonding with the epoxy resin [2].

Evidence of chemical bonding between a silane-coupling agent on the glass filler and epoxy resin has been obtained from both XPS and FTIR spectrometry [2,75]. Plueddeman [75] has postulated the following bonding mechanism: The

outermost layer of the glass filler consisted of physisorbed epoxy groups. The next layer consisted of physisorbed epoxy groups and a few chemical bonds between the glass fillers and epoxy. In the layer adjacent to the glass surface, interconnecting crosslinks and a three-dimensional network existed.

b. Carbon-Epoxy

Researchers have proposed that covalent bonds occur between the carbon-fiber surface groups and epoxy resin [1,2,18,65,71,74]. In Section II.A, it was shown that the most prevalent carbon-fiber surface groups were carbonyls and carboxyls. Proposed interphase reactions between a carbonyl and carboxyl with an epoxy monomer were [2]



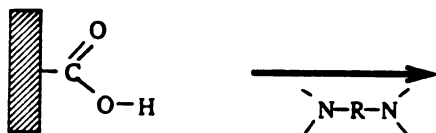
and



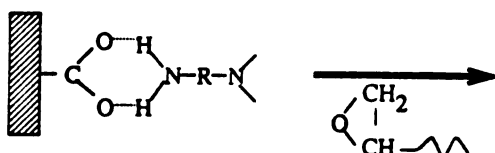
In both of these reactions, heat was required to initiate the bimolecular reaction between the acidic carbon-fiber surface groups and epoxy monomer. In Equation 17, the hydroxyl end of the carboxyl reacted with the oxygen of an epoxy monomer and bonded preferentially with the least steric-hindered carbon of the epoxy monomer. In Equation 18, an identical reaction occurred between the hydroxyl end of the carboxyl of an epoxy monomer.

Fitzer [5] has proposed the following reaction,

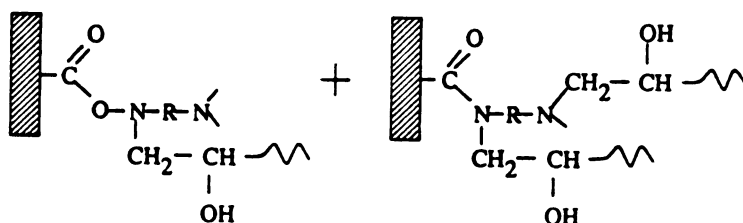
Step 1: Fiber-Hardener Coupling



Step 2: Hardener-Epoxy Coupling



(19)



between an epoxy-hardener complex and a carbon-fiber surface group. In step 1, a hydrogen bond formed between the oxygen atom of the carboxylic group and the hydrogen atom of the amine group. Step 2 represented the bonding of the epoxy monomer to a nitrogen atom of the hardener.

3. Cure Characteristics

Important reinforced epoxy-resin parameters, such as the ultimate reaction exotherm, extent of cure, glass transition temperature, and cure kinetics were determined

in the experimental study. These reinforced epoxy-resin parameters have been studied by three teams of experimenters, Dutta et al. [43], Mijovic et al. [44], and Wang et al. [74]. Dutta et al. have studied the effects of both carbon and glass fillers on the epoxy-resin cures; Mijovic et al. have studied the effect of glass fillers on epoxy-resin cures; and Wang et al. have studied the effect of carbon-filler surface functionality on the epoxy-resin cures.

Due to the lack of data on long-fiber carbon-reinforced composites, only composite systems in which fillers are used as the reinforcement were considered. Both glass and carbon filler cure data were considered.

The reader should keep in mind that the physical and morphological structure of fillers are not accurate models of the fiber surface.

a. Reaction Exotherm

Dutta et al. [43] have investigated two important parameters, the ultimate reaction exotherm, H_{ult} , and the total reaction exotherm, H_T . The H_{ult} is the maximum obtainable exotherm and occurred when all the epoxy monomers reacted; and the H_T is the reaction exotherm necessary to fully cure the epoxy resin. They have used

DSC to cure and analyze their reinforced epoxy resins. Their H_{ul} was experimentally determined from DSC analyses; whereas their H_f was experimentally determined from isothermal-DSC analyses.

Dutta et al. [43] have studied reinforced resins which contained one-, two-, four-, and six-percent filler concentrations, c. Their results showed a 12-percent increase in the H_{ul} for glass-filled epoxy-resin cures relative to the H_{ul} for neat epoxy-resin cures; and the H_{ul} for the carbon-filled epoxy-resin cures showed no significant change relative to the H_{ul} for the neat epoxy-resin cures. The H_f for glass-reinforced epoxy-resin cures was thirteen percent higher than the H_f for neat epoxy-resin cures; and the H_f for carbon-filled epoxy resin cures was unchanged from the H_f for neat epoxy-resin cures.

b. Glass Transition Temperature

Experimenters have long been aware of the mechanical changes that were induced in a polymer by the introduction of a filler. Studies where fillers were added to epoxy resins showed that the amount of filler strongly influenced the glass transition temperature, T_g [17,32,74].

Experimenters have felt that these changes in the T_g were indicative of the degree of fiber-matrix interaction and

the fiber-matrix interactions were contingent on the filler-surface properties.

Ko [17] has studied high-strength and high-modulus untreated and surface-oxidized carbon-fiber reinforced-epoxy resins. His experimental results have shown the T_g for surface-oxidized carbon-reinforced epoxy resins was as much as 25°C higher than the T_g of neat epoxy resins. His data showed that the T_g was not significantly affected by fiber-surface treatments, but the T_g was affected by the fiber type, high-strength or high-modulus, incorporated in the epoxy resin. He believed morphological changes in the epoxy resin were, presumably, induced by the graphitic basal planes at carbon-fiber surfaces. Epoxy resins were preferentially adsorbed on the graphitic basal planes, which created an epoxy-amine gradient near the fiber-matrix interphase. He credited the epoxy excess in the fiber-matrix interphase with the tighter network and increased T_g .

Ko [17] has shown the T_g increased with increasing carbon-fiber concentration, degree of fiber graphitization, and mobility of the epoxy chains at elevated temperatures. His results suggested that the chemical bonding between the fiber and epoxy resin generated by carbon-fiber surface treatments was outweighed by surface-energy effects of the carbon-fiber surface. Therefore, he believed physical

bonding was responsible for adhesion between the carbon fiber and epoxy resin.

Wang et al. [74] have considered the effect of carbon-fiber surface functionality on difunctional and tetrafunctional epoxy-resin cures. Their results showed a decreased T_g for difunctional carbon-reinforced epoxy resins and a similar T_g for tetrafunctional carbon-reinforced epoxy resins relative to neat epoxy resins. Increased functionality of the tetrafunctional epoxy resins allowed an increase in the number of cure reactions and the T_g .

These results have shown that the T_g of a carbon-reinforced epoxy-resin relative to the neat epoxy resin may increase, decrease, or remain unchanged. In summary, the epoxy or hardener functionality takes precedence over the carbon-filler effect on the T_g .

c. Cure-Kinetic Models

In this section, previous work on the effect of fillers on epoxy-resin cure kinetics was discussed. Two different approaches to modeling the carbon-reinforced epoxy-resin cure has been undertaken.

In the first approach, Dutta et al. [43] have studied glass- and carbon-reinforced epoxy-resin cures. They modeled the epoxy-resin cure with the autocatalytic cure-kinetic model given in Equation 6.

Dutta et al. have claimed that the carbon fillers have a more significant effect than the glass filler on the epoxy-resin cure. They assumed that the reaction rate constants, k_1 and k_2 , were functions of filler content, $f_1(c)$ and $f_2(c)$, and expressed mathematically as

$$k_1 = k_1' f_1(c) \text{ and} \quad (20)$$

$$k_2 = k_2' f_2(c); \quad (21)$$

where c = filler content.

They have represented $f_1(c)$ and $f_2(c)$ by fitting a third-order polynomials to their rate-constant data:

$$f_1(c) = 1 - 0.22c + 7.82 \times 10^{-2}c^2 - 6.49 \times 10^{-3}c^3 \quad (23)$$

and

$$f_2(c) = 1 - 0.14c + 5.10 \times 10^{-2}c^2 - 4.35 \times 10^{-3}c^3. \quad (24)$$

Dutta et al. have found that their cure-kinetic model fit the experimental epoxy-resin data well. Figures II.17(a) and (b) show that the carbon-reinforced epoxy-resin rate constant, k_1 , decreased to a maximum of 16 percent and k_2 decreased to a maximum of 13 percent. Figure II.17(c) and (d) show that the glass-filled epoxy-

resin rate constant, k_1 , decreased to a maximum of 13 percent and k_2 decreased to a maximum of ten percent.

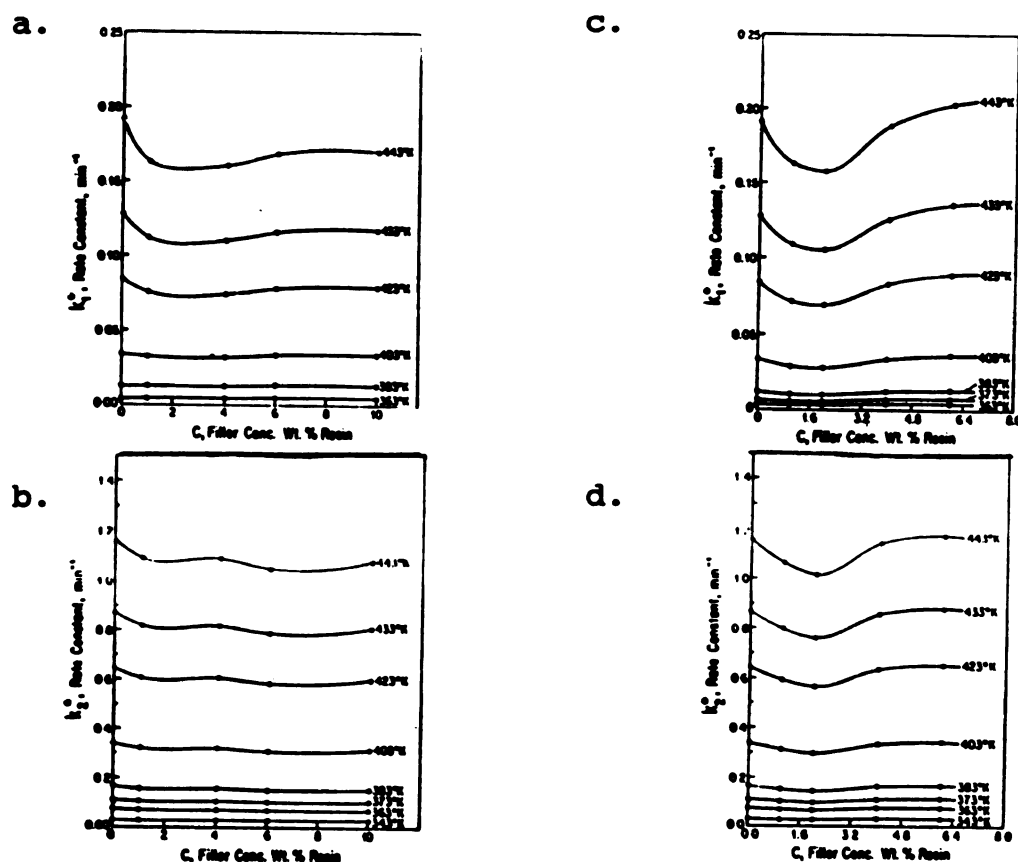


Figure II.17. Experimental results reproduced from Dutta et al. [43]: (a) k_1 for a carbon-black filled epoxy resin; (b) k_2 for a carbon-black filled epoxy resin; (c) k_1 for a glass-filled epoxy resin; and (d) k_2 for a glass-filled epoxy resin.

In the Dutta et al. [43] study, differences between neat and reinforced epoxy-resin rate constants were considered. At six-percent c, k_1 and k_2 increased and leveled off to a constant value which was not significantly different than the k_1 and k_2 values for the neat epoxy resin. Since typical commercial composites were between 40- and 70-percent filler concentration, they concluded

that filler did not significantly affect the epoxy-resin rate constants.

In the second approach, Mijovic et al. [44] have used DSC to cure a neat and 40-percent glass-reinforced epoxy resin and modeled the cure kinetics with Equation 6. Their experimental data showed a decrease in the H_T for glass-reinforced epoxy-resin cures relative to the H_T for neat epoxy-resin cures. They explained that this lower value of H_T was caused by glass fillers restricting the molecular mobility of unreacted epoxies.

Mijovic et al. [44] cure-kinetic model for neat and glass-reinforced epoxy resins is presented in Table II.6. Instead of adding a multiplication factor to the rate constants, a modified Arrhenius expression for the rate constants, k_1 and k_2 , was used. They have found similar values for k_1 and a maximum of ten-percent lower values of k_2 for glass-reinforced epoxy resin cures when compared to neat epoxy-resin cures. Their cure kinetic model showed a 98- to 99- percent decrease in frequency factors and a 34-31-percent decrease in activation energies for glass-reinforced epoxy resins relative to neat epoxy resins. An explanation for the decreased frequency factor and activation energy was offered in terms of restrictions to molecular mobility imposed by the glass filler.

Table II.6. Mijovic et al. [44] cure-kinetic model for a neat and 40% glass-reinforced epoxy resin.

Kinetic equation:

$$\frac{d\alpha}{dt} = (k_1 + k_2 \alpha^m) (1 - \alpha)^n;$$

$$\text{where } k_1 = A_1 e^{(E_A/RT)},$$

$$m = 0.5 - 0.7, \text{ and}$$

$$n = 1.3 - 1.5.$$

Kinetic parameters:

	k_1		k_2	
	A	E_A	A	E_A
neat resin	2.22 $\times 10^8$	-21.8	1.21 $\times 10^6$	-15.7
reinforced	1.34 $\times 10^6$	-15.0	2.41 $\times 10^4$	-12.3

d. Mechanical Properties

In an attempt to determine the effect of surface oxidation of a carbon fiber in promoting fiber-matrix adhesion, many researchers have studied the interfacial shear strength and tensile strength of carbon-reinforced epoxy composites [2,3,4,17,23,31,77,78]. These studies have shown that interfacial static mechanical properties nor the fracture properties were greatly affected by the fiber-matrix interphase [3].

Drzal et al. [7] have compared untreated and surface-oxidized carbon-reinforced epoxy resins. Their data showed that the interfacial shear strength for the surface-oxidized carbon-reinforced resins is over three times that of the untreated carbon-reinforced epoxy resins. Table II.4 shows that the oxygen content in the surface-oxidized carbon fibers is double that of the untreated carbon fibers. They have attributed the interfacial shear strength increase to the increased interactions between the acidic carbon-fiber surface groups on the surface-oxidized fibers and the polar-epoxy monomers.

Many experimenters [2,3,77] have studied the interfacial shear strength of a carbon-reinforced epoxy composite. Herrick [3] has shown that increasing the chemical functionality by oxidation improves the interfacial shear strengths of carbon-reinforced epoxy composites. Ko [17] has reported that the interfacial shear strengths of composites containing surface-oxidized carbon fibers are 1.6 times higher than those from untreated carbon fibers. Scola et al. [2] have shown a 90- to 120-percent improvement in the shear strengths of surface-oxidized carbon-reinforced epoxy resins relative to the neat epoxy resins. Using single fiber studies, Drzal et al. [4] have found a maximum of 100-percent increase in

the interfacial shear strength for surface-oxidized carbon-reinforced composites relative to untreated carbon-reinforced composites.

Surface-oxidized carbon-reinforced epoxy-resin experiments implied that better fiber-matrix adhesion occurred relative to the untreated carbon-reinforced epoxy composites. Results from Riggs et al. [78] showed that surface-oxidized carbon-reinforced epoxy composites exhibited increased shear strength relative to untreated carbon-reinforced epoxy composites. The data also showed that the surface-oxidized carbon-reinforced epoxy resins decreased in the tensile strength relative to untreated carbon-reinforced epoxy resins. Rand et al. [2] have found a tensile strength decreases were accompanied by increases in the Young's Modulus for surface-oxidized carbon-reinforced epoxy resins relative to untreated carbon-reinforced epoxy resins.

Wang et al. [74] have studied the effect of carbon-fiber surface functionality on epoxy-resin cure reactions. They have considered four different carbon-fiber surface treatments on an epoxy resin prepared from a difunctional epoxy monomer and difunctional hardener. Their results indicated a reduction in the H_T for reinforced epoxy-resin cures relative to the neat epoxy-resin results. They

concluded that the carbon-fiber surface functionality had little effect on the epoxy-resin cure.

Next, Wang et al. [74] have cured an epoxy resin prepared from a tetrafunctional epoxy monomer and tetrafunctional hardener. They concluded that similar H_T is found for the neat and carbon-reinforced epoxy-resin cures. They have attributed the difference in the H_T between the difunctional and tetrafunctional epoxy-resin cures on the greater importance of the crosslinking reactions during the tetrafunctional epoxy-resin cures. The increase functionality in the tetrafunctional epoxy resins allowed extra intramolecular reaction, which provided a means for the epoxy resin to bypass the inhibition caused by the filler and achieve complete cure.

D. The Role of Cure Kinetics in Composite Manufacturing

In order to manufacture quality carbon-reinforced epoxy composites, the cure was critically important. Cure conditions were determined by the cure kinetics. As previous sections have shown the cure kinetics of epoxy resins have been well studied; but, few investigations have existed on the cure kinetics of carbon-reinforced epoxy composites.

Manufacturers have improved the adhesion of the carbon fibers to epoxy resin by oxidizing the carbon-fiber surface. Section II.A.2 showed that the most common functionalities added to the carbon-fiber surface are carbonyls and carboxyls. Many researchers [1,2,5,20,21] have hypothesized that improved adhesion was the result of chemical reactions occur between the carbon fiber and epoxy resin. Presently, the carbon-fiber effect on the epoxy-resin cure kinetics is of concern to composite manufacturers.

1. Composite Cure

Composites were processed in a variety of different methods. Table II.7 lists the most common manufacturing processes.

Table II.7. Composite manufacturing processes [2].

Manufacturing Route	Outline of Fabrication and Processing Methods
Open Mold Processes:	
1. Hand Lay-up	Chopped-strand mats, woven roving, and other fabrics made from the fibers are placed on the mold and impregnated with resin by painting and rolling. Layers are built up until design thickness is achieved. Molding cures with or without heat or pressure.
2. Spray-up	Chopped rovings and resin are sprayed simultaneously into a prepared mold and rolled before the resin cures.
3. Vacuum Bag, Pressure Bag, Autoclave	Layers of fibers, usually unidirectional sheets, are preimpregnated with resin and partially cured to form a prepreg. The prepreg sheets are stacked on the mold surfaces in pre-determined orientations, covered with a flexible bag in an autoclave at the required curing temperature.
4. Filament Winding	Continuous rovings or strands of fibers are guided over rollers and guided through a bath of resin and then wound, using a program controlled machine, onto a mandrel at predetermined angles. The resin is partially or completely cured before removing the component, usually a tube, from the mandrel.
5. Centrifugal Casting	Mixtures of the fibers and resin are introduced into a rotating mold and allowed to cure in situ.

Table II.7. (continued)

Manufacturing Route	Outline of Fabrication and Processing Methods
Close Mold Processes:	
1. Hot Press Molding, Compression Molding	Heated matched dies or molds are loaded with raw material (sheet molding compound, dough molding compound, cloth or unidirectional prepreg) pressed to the shape of the cavity and cured.
2. Injection Molding, Resin Transfer Molding	Molten or plasticized polymer mixed with short fibers is injected, usually at high pressure into the cavity of a split mold and allowed to solidify or cure.
3. Pultrusion	A continuous feed of fibers, in pre-selected orientations, is impregnated with resin and pulled through a heated die to give the shape of the final section (e.g. tubes or I-beams). Partial or complete cure occurs during passage through the die.
4. Cold Press Molding	A low pressure, low temperature process in which fibers are impregnated with resin and then pressed between matched dies. Heat is generated during the cure.
5. Resin Injection	Fibers in cloth form are placed in the tool which is then closed. The resin is injected at low pressure into the cavity and flow through the fibers to fill the mold space.
6. Reinforced Reaction Injection Molding	A rapid curing resin system involving two components which are mixed immediately before injection is used. Fibers are either placed in the closed mold before resin is injected or added as short chopped fibers to one of the resin components to form a slurry before injection.

Aerospace and automotive carbon-reinforced epoxy-composite parts and structures were commonly produced by laminate-autoclave curing. In laminate-autoclave curing, the laminate or sheets of unidirectional carbon-reinforced epoxy-resin were formed into the desired shape and exposed to elevated temperatures and pressures in an autoclave for a predetermined length of time. The elevated temperature applied during cure provided the heat required for initiating and maintaining the cure reactions. The applied pressure squeezed out trapped vapor bubbles and excess epoxy resin of the composite. The magnitudes and durations of the temperatures and pressures, or the cure schedule, determined the properties of the finished composite [79].

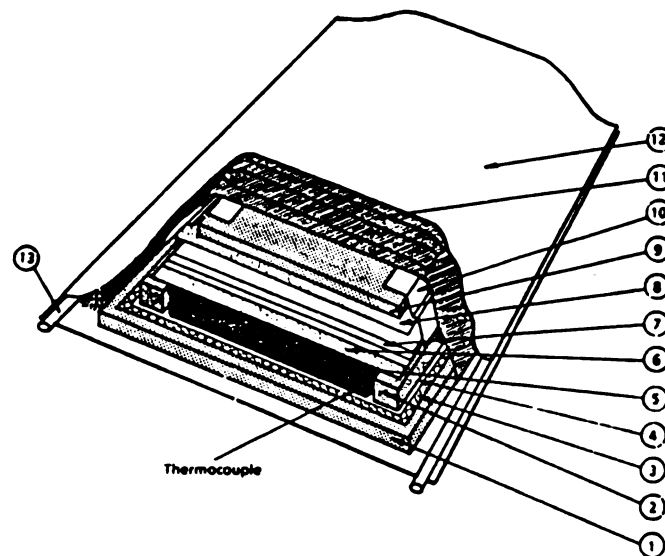
2. Laminate-Autoclave Curing

Common commercial carbon-reinforced epoxy composites have been made from laminates and cured in an autoclave. A laminate consisted of preferentially-oriented carbon-reinforced prepregs. A carbon-reinforced prepreg was a sheet of long unidirectional carbon fibers impregnated with epoxy resin.

Carbon-reinforced prepregs were fabricated with a prepregger. Prepregging was a process in which continuous fibers were pulled through a vat of liquid resin [61]. Then, these resin-impregnated fibers were wound on a

circular mandrel as a second mechanism guided the carbon fibers longitudinally across its surface with a prescribed tension and motion. The finished prepreg was removed from the mandrel and cut into sheets or prepregs. These prepregs were stacked using a predetermined-orientation to form a laminate.

Typical thermal processing began by placing the stacked laminate into a vacuum bag. A schematic of the laminate-fabrication sequence is shown in Figure II.18. The mold was necessary to form the composite and the bleeders were necessary to adsorb the excess epoxy resin.



- | | | |
|-------------------|-------------------|-----------------|
| 1. base plate | 6. release fabric | 11. air bleeder |
| 2. mold | 7. resin bleeders | 12. vacuum bag |
| 3. release film | 8. release film | 13. high- |
| 4. release fabric | 9. top plate | temperature |
| 5. laminate | 10. tape | sealant |

Figure II.18. A schematic of a laminate-fabrication sequence [61].

During autoclave curing, a vacuum was drawn on the laminate bag. The purpose of the vacuum was to consolidate the laminate and removed the excess air and moisture entrapped in the epoxy resin. Air or moisture entrapped in the composite caused voids or holes, which reduced the composite's properties.

Autoclave curing was suitable for individually cured composite structures made of thin, uniform laminates; but, autoclave curing was less appropriate for composite structures, with thick or uneven dimensions. In these cases, unavoidable temperature gradients due to the highly-exothermic reaction prevented uniformly- and completely-cured structures. Figure II.19 shows how a thick autoclave-cured specimen can be completely cured on the outside and remain uncured on the inside.

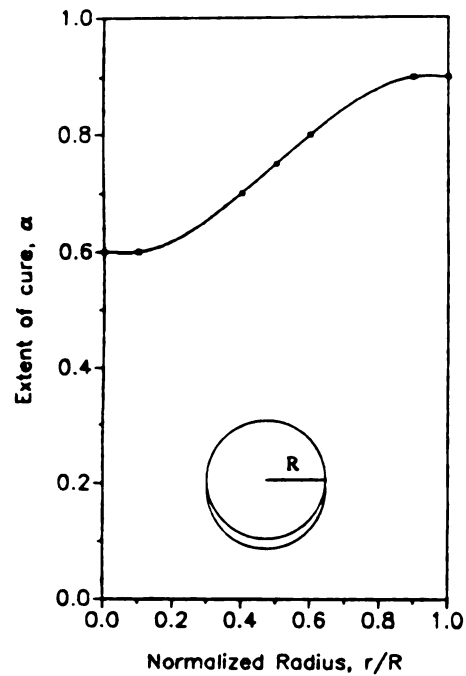


Figure II.19. Nonuniformity in conventionally-cured epoxy composite.

Upon cooling thermal stresses occurred, due to the thermal expansion differences between the outer and inner layers of the composite. This differential cooling caused more problems when curing thick composite materials relative to the thin composite materials by forming cracks or voids in the composite material.

E. Instrumentation Overview

In order to begin to understand the problems in composite manufacturing, experimenters have analyzed carbon-reinforced epoxy resins with analytical instruments, such as the differential scanning calorimeter, DSC, and Fourier transform infrared, FTIR, spectrometer. DSC and FTIR elucidated changes in the reaction exotherm and chemical structure, respectively, which accompanied the epoxy-resin cure. In this section, the theory and analysis techniques of differential scanning calorimetry and FTIR spectroscopy were discussed.

1. Differential Scanning Calorimeter, DSC

The technique of differential scanning calorimetry was introduced in the form of commercial instruments during the early 1960s. The differential scanning calorimeter, DSC, provided a convenient and useful method of monitoring the course of exothermic reactions including those occurring during epoxy-resin cures. The Nomenclature Committee of the International Confederation for Thermal Analysis, ICTA, have defined the DSC as an instrument in which the differential heat flow was measured as a function of temperature while the sample and reference were subjected to a controlled-temperature program.

A DSC was used to obtain both thermal and kinetic information on neat and carbon-reinforced epoxy resins. The techniques of differential scanning calorimetry applied to polymerization studies of epoxy resins have been investigated by many experimenters [40,54,80,81]. The DSC theory and analysis techniques were presented here.

a. Theory

A DSC works on a "null-balance" principal, whereby the heat-flow difference between the sample and a reference was translated in terms of energy per time. Parameters obtainable from DSC analyses of epoxy resins included: reaction exotherm, degree of cure, cure kinetics, and glass transition temperature [54].

The heating rate was fixed, so that there is a linear relationship between time and temperature. If m moles reacted with a constant heat of reaction per mole, then it was assumed that heat flow relative to the instrumental baseline was proportional to the reaction rate:

$$\frac{dH}{dt} = - C \cdot \frac{dm}{dt}; \quad (25)$$

where $\frac{dH}{dt}$ = differential heat flow,
 C = proportionality constant, and
 $\frac{dm}{dt}$ = differential change in moles.

Integration of Equation 25 at m equal to m_0 and H_{ult} equal to zero gave C equal to H_{ult}/m_0 , where m_0 equalled the initial number of epoxies. Integration of

$$\frac{(dH/dt)}{H_{ult}} = \frac{(-dm/dt)}{m_0} \quad (26)$$

showed that at any time, t , H/H_{ult} equalled m/m_0 .

The reaction exotherm, H , was defined as the heat flow up to time, t ,

$$H = \int_0^t \frac{dH}{dt} dt. \quad (27)$$

Most researchers have found it more convenient to work in terms of extent of cure, α , where $\alpha = H/H_{ult}$. Dividing Equation 27 by H_{ult} , became

$$\frac{d\alpha}{dt} = \frac{(dH/dt)}{H_{ult}} \quad (28)$$

Data acquisition was performed by data analyzers connected to differential scanning calorimeters.

Instantaneous data reduction allowed the experimenter to generate real-time plots. Various software packages allowed experimenter to manipulate the cure kinetic data.

b. Analysis Techniques

The main advantages of the DSC were the relative ease of operation and the requirement of small sample sizes [54]. This technique was very useful as a means of following the overall course of the cure reactions through changes in heat evolution, or changes in glass transition temperature, T_g .

Two DSC techniques used to study epoxy-resins, were dynamic and isothermal curing. Many researchers [32,80] have attempted to obtain from one dynamic-DSC experiment all the cure-kinetic information available in a series of isothermal-DSC experiments. Although dynamic-DSC experiments were easy and quick in execution, Barton [34] advised experimenters to obtain isothermal-DSC data at several different cure temperatures. Prime [37] stated that dynamic-DSC experiments gave activation energies higher than isothermal-DSC experiments. Other researchers [32,53,56] have shown that dynamic-DSC data, if modeled with the Arrhenius-temperature law, yielded kinetic parameters which were grossly in error. Based on these findings, isothermal-DSC experiments were usually conducted to obtain the epoxy-resin cure kinetics.

2. Fourier Transform Infrared, FTIR, Spectrometer

In the past, infrared spectroscopy has been proven to be time-consuming, expensive, and a very difficult task due to limited computer facilities. However, with the development of the fast Fourier transform algorithm and advancement in computer technology, this difficulty has been overcome. Today, real-time spectra could be obtained within seconds. Many experimenters feel no other analytical technique can yield so much information on the molecular constituency of organic materials as conveniently as FTIR spectroscopy [83,84]. In this section, the FTIR-spectroscopy theory and techniques applied to epoxy-resin cures were presented.

a. Theory

Detailed explanations of FTIR-spectroscopy theory were found elsewhere [83,85], only an elementary discussion was given here. A simplistic model of a FTIR spectrometer, the Michelson Interferometer, is illustrated in Figure II.20. In general, an interferometer consists of stationary and moveable perpendicular mirrors.

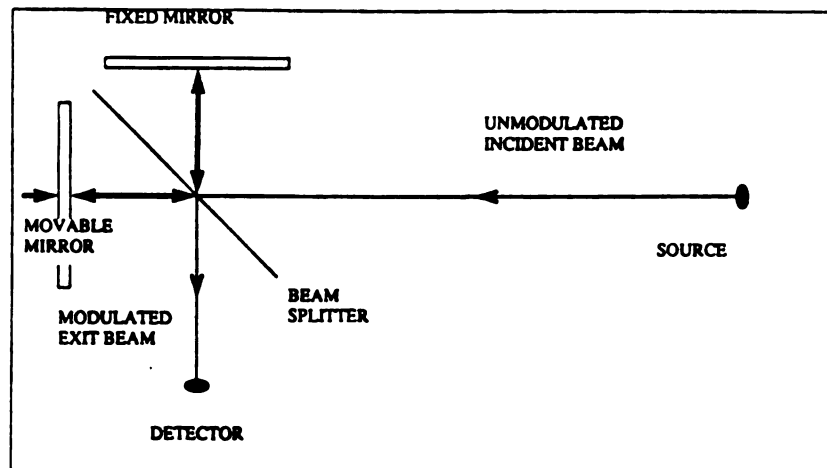


Figure II.20. Illustration of the Michelson Interferometer [28].

Once the experimenter activated the laser beam, half of its incident radiation was reflected to the fixed mirror and half of its incident radiation was reflected to the moving mirror. Assuming monochromatic light and equal pathlengths, either the two light beams returned to the beam splitter in phase and constructively interfered producing a maximum detection response, or returned out of phase and destructively interfered.

Each frequency was treated independently and the output was the sum of all the cosine oscillations caused by the optical frequencies of the source. This result was expressed mathematically as [83]:

$$I(x) = \int_{-\infty}^{+\infty} B(v) \cos(2xv) dv; \quad (29)$$

where $I(x)$ = interferogram intensity,
 x = mirror displacement,
 $B(v)$ = source intensity, and
 v = frequency.

The experimenter was usually interested in obtaining a spectra in the frequency domain. Therefore, the spectrum, $B(v)$, was transformed by the following equation, which represented one-half of the cosine Fourier transform pair [83]:

$$B(v) = \int_{-\infty}^{+\infty} I(x) \cos(2xv) dx; \quad (30)$$

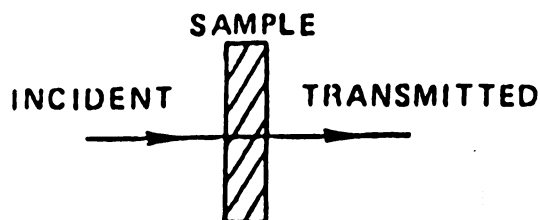
Equations 29 and 30 related the interferogram intensity $I(x)$ and the spectrum $B(v)$. A personal computer was often programmed to perform the transformation and quickly produced the resultant infrared spectrum for the experimenter.

b. Analysis Techniques

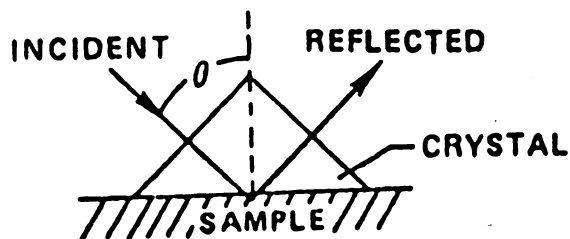
An instrumental advantage of FTIR spectroscopy was that it allows the experimenter to use a variety of sampling techniques. The techniques commonly used to characterize the epoxy resins include transmission, internal reflectance, and diffuse reflectance spectroscopy.

With FTIR spectroscopy, the most desirable sample was one producing the highest signal-to-noise ratio rather than the high signal. If transmission FTIR-spectroscopy measurements were coupled with signal averaging, very high signal-to-noise ratios were obtained. Figure II.21(a) illustrates the transmission-FTIR spectroscopy mode of analysis [83].

a.



b.



c.

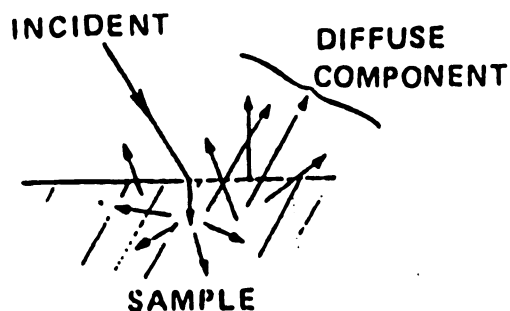


Figure II.21. FTIR-spectroscopy analysis techniques: a) transmission; b) single internal reflection, IRS; and c) diffuse-reflectance, DRIFT [83]. (Note; θ = contact angle)

One problem with transmission-FTIR spectroscopy was maintaining a straight baseline. To maintain a straight baseline, it was necessary to keep the absorbance in the linear range of the Beer-Lambert law [85],

$$I = e^{-wy}; \quad (31)$$

where I = internal transmittance,
 w = absorption coefficient of the material, and
 y = uniform sample thickness.

To achieve linearity, experimenters kept the concentration of epoxy resin in the transmission FTIR-spectroscopy specimen at sufficiently low levels so the absorbance reading was between 0 and 80 percent. This reduced the spectral artifacts generated during the data processing steps [83]. Of course, a linear optical signal required that the infrared sample had no residual orientation, such as voids or holes, and an uniform distribution of material. Thus, careful sample preparation was necessary to obtain reproducible transmission-FTIR spectra [85].

In FTIR internal reflection spectroscopy, IRS, the incident beam passes through the prism onto the sample, as illustrated in Figure II.21(b). Good optical contact between the crystal and sample was essential. The degree of contact between the crystal and sample was difficult to reproduce and restricted the comparative and quantitative aspects of the technique. Presently, the spectra obtained with FTIR-IRS is not as accurate as spectra observed with

transmission-FTIR spectroscopy [85]. The long wavelength side of the absorption bands in FTIR-IRS spectra distorted and lengthened relative to transmission-FTIR spectra.

Diffuse-reflectance, DRIFT, FTIR spectroscopy appeared to be the best suited for carbon-reinforced epoxy resins [29,83,85]. Mertzil et. al. [85] mentioned that the DRIFT-FTIR spectroscopy was superior for examining composite materials since minimal sample preparation was required. Young et. al. [83] stated that DRIFT-FTIR spectroscopy can be used successfully for the study of surfaces and of bulk samples which are finely ground. Cole et al. [29] reported that an advantage of DRIFT-FTIR over IRS was that no physical contact with the sample surface was required.

DRIFT-FTIR spectroscopy has been used in the visible and ultraviolet frequency region for a long time, but was only recently utilized in the mid-infrared region. As illustrated in Figure II.21(c), diffuse reflectance arose from radiation penetrating into the interior of an opaque sample and re-emerged after being scattered numerous times. DRIFT-FTIR spectroscopy relied on the measurement of the reflected light from a powdered sample radiated with light. Off-axis ellipsoidal mirrors collimated the reflected radiation. The measurement required sufficient scattering for isotropically reflected light. This was possible if

the powdered samples were finely ground and combined at three to five percent with a nonabsorbing powder.

In the DRIFT-FTIR spectroscopy measurements, the analog to Beer's law for transmittance-FTIR spectroscopy, was the Kubelka-Munk equation.

$$F(R_{\infty}) = \frac{(1 - R_{\infty})^2}{2 R_{\infty}} = \frac{a_m}{s}; \quad (32)$$

where R_{∞} = the sample diffuse reflectance, assumed to be infinitely thick,
 a_m = molar absorption coefficient, and
 s = scattering coefficient.

The Kubelka-Munk equation was derived for infinitely thick, weakly absorbing and highly scattering samples.

The scattering coefficient, s , was often assumed to be constant at any wave number in the spectrum, but s was affected by such variables as particle size, particle size distribution, packing density, and moisture content [86]. Fuller [28] stated that for dilute samples in low absorbing matrices,

$$a_m = 2.303 \epsilon c_m; \quad (33)$$

where ϵ = molar absorptivity, and
 c_m = molar concentration.

Substitution of Equation 33 into Equation 32 demonstrates how the Kubelka-Munk function was directly affected by the sample concentration.

A linear relationship between the Kubelka-Munk function, $F(R_\infty)$, and sample concentration occurred when s was isotropic [86]. Under this condition, the Kubelka-Munk theory related the sample concentration and scattered radiation intensity much in the same manner as the Beer-Lambert law of transmission-FTIR spectroscopy given in Equation 31. Manufacturers have utilized these two equations in software applications which provided experimenters with comparable transmission-FTIR and DRIFT-FTIR spectra.

In light of these findings, the uncured epoxy resins are usually analyzed with transmission-FTIR spectroscopy and the cured epoxy resins are analyzed with DRIFT-FTIR spectroscopy. Irregardless of either FTIR-spectroscopy technique used, the extent of cure, α , for the fully-cured DGEBA epoxy resin was calculated by [87,88]

$$\alpha = 1 - \frac{A(916)}{A(1184)} \frac{A_0(1184)}{A_0(916)}; \quad (34)$$

where $A(916)$ = absorbance at 916 cm^{-1} of fully-cured epoxy resin,
 $A_0(1184)$ = absorbance at 1184 cm^{-1} of unreacted epoxy resin,
 $A(1184)$ = absorbance at 1184 cm^{-1} of fully-cured epoxy resin, and
 $A_0(916)$ = absorbance at 916 cm^{-1} of unreacted epoxy resin.

To help eliminate sample path-length variations, the epoxy-intensity peak area was normalized by dividing by the reference peak area at 1184 cm^{-1} . The intensity peak at

1184 cm^{-1} was caused from the C-C bond stretching of the bridge carbon atom between the two p-phenylene groups [85]. Some experimenters have used the aromatic intensity peaks at 1501 or 1607 cm^{-1} for the reference [87]. In this study, the intensity peak at 1184 cm^{-1} peak was selected over the aromatic intensity peaks at 1501 and 1607 cm^{-1} due to the interference with the changing primary- and secondary-amine bands at 1508 cm^{-1} and 1625 cm^{-1} [88].

CHAPTER III

EXPERIMENTAL STUDY

An experimental study was conducted to determine the effect of carbon fibers on the cure characteristics of an epoxy resin. Any cure differences found between neat and carbon-reinforced epoxy-resin cures were attributed to interactions in the fiber-matrix interphase. Two analytical instruments, a differential scanning calorimeter, DSC, and Fourier transform infrared, FTIR, spectrometer, were used to analyze cured epoxy resins. Extent of cure and glass transition temperature data were generated for both neat and carbon-reinforced epoxy resins. Then, cure-kinetic parameters for neat and carbon-reinforced epoxy resins were modeled with the proposed autocatalytic cure-kinetic model and Arrhenius-temperature law. These cure characteristics were compared to gain insight into interactions between carbon fibers and epoxy resin.

A. Sample Preparation

All of the following materials were stored at room temperature under dark, dry conditions until needed to

prevent degradation. The materials were used as supplied without further purification or any other treatment. The epoxy DER 332, is a commercial diglycidyl ether of bisphenol A, manufactured by the Dow Chemical Company [89]. This epoxy was chosen because of its high purity and low viscosity. These epoxy properties facilitated the impregnation of the carbon fibers during sample preparation. The hardener was diaminodiphenyl sulfone, DDS, manufactured by the Aldrich Chemical Company [90]. Molecular structures of both the epoxy and hardener are shown in Figure III.1. This epoxy and hardener combination has been used by other experimenters, such as Chan [41], Sourour [40], and Dutta [43], allowing a direct comparison of this study's experimental results.

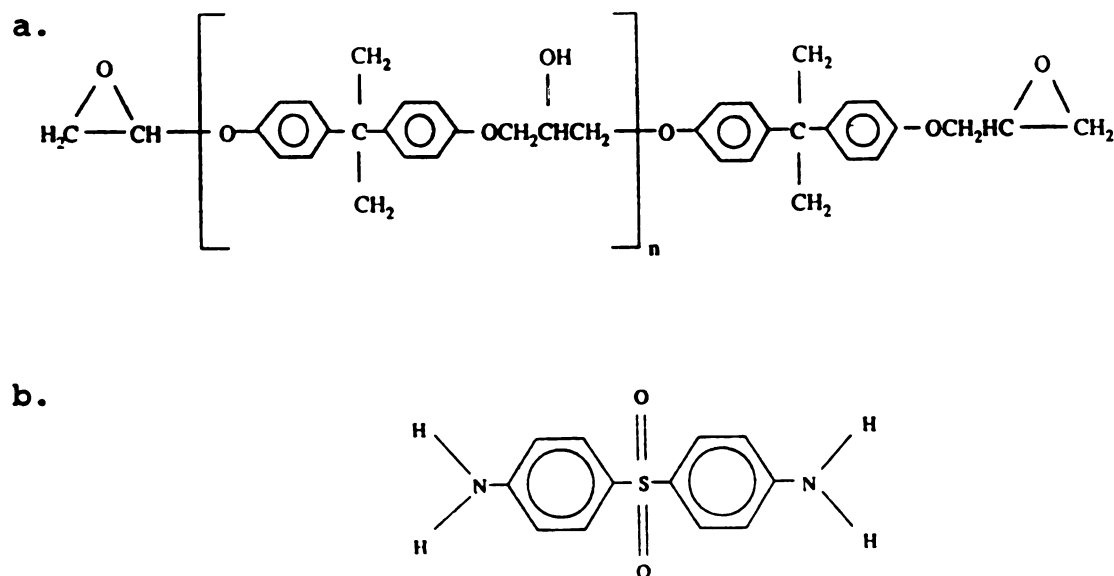


Figure III.1. The molecular structure of: (a) DER 332 [89]; and (b) DDS [90]. one equivalent of liquid epoxy and

To prepare a well-mixed, stoichiometric epoxy resin, powdered hardener were weighed. One mole of epoxy, molecular weight equal to 342.5 g/mol, equals two equivalents of epoxy groups and one mole of hardener, molecular weight equal to 168.0 g/gmol, equals four equivalents of amine groups. The epoxy was agitated and heated at 5°C/min. At 100°C, the hardener was added to the epoxy forming a milky-white suspension. At 130°C, this epoxy resin abruptly turned into a clear, homogeneous, amber-yellow liquid. When the last hardener crystal dissolved, the epoxy resin was removed from the heat source and quenched to room temperature. Then, the epoxy resin was degassed in a vacuum oven at 80°C and 30 inches of mercury for three hours. This epoxy resin was either used immediately or stored in a desiccator at 4°C for no more than 30 days.

Long, high-strength, untreated carbon fibers, AU4, and surface-oxidized carbon fibers, AS4, manufactured by Hercules Incorporated, were used as reinforcements. Considerable care was warranted to develop a suitable laboratory technique for the preparation of carbon-reinforced epoxy composites. The technique that evolved met the criteria of minimum void space, good wetting of the carbon-fiber surface, and a random distribution of fibers. Carbon-reinforced epoxy-composite specimens were prepared from a prepreg, a film of epoxy-resin impregnated

unidirectional carbon fibers. In this study, carbon-reinforced epoxy prepregs were prepared with a prepregger machine manufactured by the Research Tool Company, shown in Figure III.2.



Figure III.2. Photograph of a prepregger machine manufactured by the Research Tool Company.

Figure III.2 illustrates how a carbon-fiber tow, a bundle of 12,000 fibers, was spooled on the back of the prepregger (a). Then, the carbon-fiber tow was threaded through a heater (b) in which the fibers were preheated to 180°C to allow the desorption of volatiles. Finally, the carbon-fiber tow was pulled through the prepregger-resin vat (c) and spun onto a polycarbonate-covered 14-inch diameter mandrel (d). Polycarbonate was used to prevent the prepreg from adhering to the mandrel.

Caution was taken to avoid overheating the epoxy resin in the prepregger-resin vat to minimize the possibility of reaction. Prior to impregnation, the gelation glass transition temperature, $T_{g,gel}$, was determined with a Brookfield viscometer. The $T_{g,gel}$ is defined as the temperature where the epoxy resin undergoes a change from an ungelled glass to a viscous liquid. As the viscometer temperature increased, a dramatic drop in viscosity occurred at $T_{g,gel}$. The $T_{g,gel}$ for DER 332-DDS epoxy resin was found to be 80°C. Thus, the prepregger-resin vat was maintained at a 80°C throughout the impregnation process. This insured that a proper resin viscosity was maintained, which allowed the epoxy resin to flow and wet the carbon fibers.

The mandrel was rotated at a speed of 20 r.p.m., therefore, approximately two hours were needed to cover the mandrel with epoxy-impregnated fibers. A 14- by 84- inch polycarbonate film was cut and placed over the epoxy-impregnated fibers. This reinforced epoxy resin sandwiched in polycarbonate is called a prepreg.

ASTM D 792, method A1 [91], was used to find the density of the prepreg by the displacement of water. The prepreg density, d_p , was found by immersing a specimen in water and performing the following calculation:

$$d_p = d_w \cdot (m / B); \quad (35)$$

where d_w = water density,
 m = specimen weight in water, and
 B = buoyancy force of the water.

Next the fiber-weight fraction, w_f , of the uncured prepreg was determined by refluxing the specimen in acetone at 25°C for 90 hours. After drying at 100°C, the carbon fibers were weighed to give an average w_f of 0.60. The fiber-volume fraction, v_f , was calculated by

$$v_f = w_f \cdot (d_p / d_f); \quad (36)$$

where d_f = fiber density.

The average v_f for the uncured prepreg was 0.51. To ensure good matrix wetting of carbon fibers, the void fraction, v_o , of the prepreg was found. The v_o between 0.03 to 0.06 was obtained by

$$v_o = 1 - v_f - \left[\frac{d_p - v_f \cdot d_f}{d_m} \right], \quad (37)$$

where d_m = epoxy-resin density.

A photograph of a test specimen with w_f equal to 0.60, v_f equal to 0.51, and v_o equal to 0.05 is shown in Figure III.3.

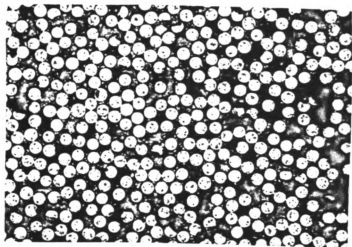


Figure III.3. A 500X photograph of a carbon-reinforced epoxy composite with a fiber-weight fraction, w_f , of 0.60.

The confidence limits on measured values of d_f , d_m , d_c , and the calculated v_f had an accumulated error of 1.5 percent [17]. However, similar consideration showed that the error transferred to v_o was 6.5 percent. Since v_o lies in the range of 0.03 to 0.06, this calculation was only helpful in eliminating grossly-flawed specimens.

Neat and reinforced epoxy resins with carbon fiber-weight fractions of 0.01, 0.10, and 0.60 were examined. To make composites with fiber-weight fractions of 0.01 and 0.10, partially-cured epoxy resin from the prepregger-resin vat was added to premeasured amounts of carbon-reinforced epoxy preregs. This mixture was agitated at 80°C until

the carbon fibers were well-distributed throughout the epoxy resin.

Next, DSC and FTIR-spectrometer test specimens were prepared. DSC test specimens were made by placing material which contained five to fifteen milligrams of resin in a 4 mm-diameter DSC-sample pan and sealed with a DSC-sample pan cover.

Uncured and cured FTIR-spectroscopy test specimens were prepared differently. Uncured-FTIR epoxy-resin samples were analyzed with transmission-FTIR spectroscopy. These transmission-FTIR test specimens were prepared by combining stoichiometric amounts of acetone-dissolved epoxy and hardener. Two to three drops of this mixture were placed on a KBr pellet and allowed to dry before analysis. A pellet was formed by pressing 300 milligrams of the KBr powder at 10,000 psi approximately five minutes or until the center of the disk was transparent.

Cured-FTIR epoxy-resin samples were analyzed with DRIFT-FTIR spectroscopy. These DRIFT-FTIR spectroscopy test specimens were prepared by placing the neat and carbon-reinforced epoxy resins in 0.5 cm X 0.5 cm X 2.5 cm silicon molds. Then, specimens were fully-cured in a convectional oven and filed into small particles which were further ground into a powder with a mortar and pestle.

Approximately fifteen milligrams of this specimen powder was homogeneously mixed with 240 milligrams of KBr powder. Then 150 milligrams of this mixture was placed on a 1-cm diameter DRIFT-FTIR spectrometer sample holder, levelled without using a spatula, and analyzed.

B. Experimental Instrumentation

In this study, the DuPont 9900 DSC and Perkin-Elmer 1800 FTIR spectrometer were used to investigate the neat and carbon-reinforced epoxy-resin cures. The DSC and FTIR spectrometer were selected because of their speed, ease of operation, availability, and low operational costs. DSC monitored the total conversion with time; whereas, FTIR spectrometer monitored the formation and disappearance of specified functionalities. Detailed discussions of both the DSC and FTIR spectrometer were given in Section II.E.

1. DSC

The DuPont 9900 DSC cell consists of a silver block chamber which contains a thermoelectric disc with raised platforms for sample and reference containers. A cross-section of the DSC cell is shown in Figure III.4. Temperature differentials between the sample and reference were monitored by thermocouples beneath the sample and reference platforms. Output from thermocouples was

controlled and amplified by DuPont's thermal analyzer, TA, as shown in Figure III.5. The TA transmits heater voltages and thermocouple signals between the programmer and the DSC cell and provides a linear-calorimetric response over a wide-temperature range, assuming the DSC is accurately calibrated [92].

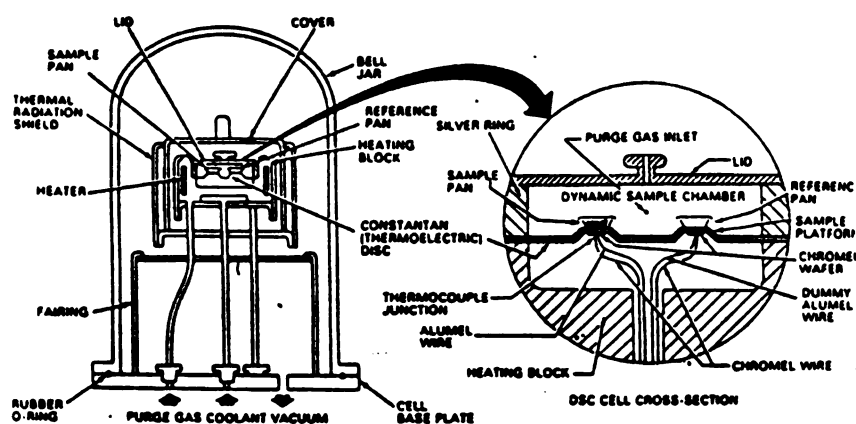


Figure III.4. Cross-section of the DuPont 9900 DSC cell [92].



Figure III.5. Photograph of the DuPont thermal analyzer, TA, and 9900 DSC.

The thermocouples were calibrated weekly using an indium standard supplied the Aldrich Chemical Company. Calibration involved exposing ten milligrams of indium to a $5^{\circ}\text{C}/\text{min}$ temperature ramp from 140°C to 170°C . The transition area and melting point were found and compared to the known heat of fusion, 28.4 J/g , and melting point, 156.6°C . The cell-coefficient constant and temperature calibration were adjusted accordingly.

Precision of the DSC was checked by subjecting two empty DSC-sample pans to a preprogrammed isothermal temperature profile. A straight baseline was achieved by adjusting the baseline-slope control on the DSC-cell base.

When balanced, the DSC monitored the differential rate of heat evolution between the specimen and reference or empty pan with a maximum nominal sensitivity of 0.6 mW/cm. This gave a experimental precision of 2.5 percent.

2. FTIR Spectrometer

Infrared spectra experiments were performed on a Perkin-Elmer 1800 FTIR spectrometer, shown in Figure III.6. Uncured epoxy resins were analyzed with transmission-FTIR spectroscopy; whereas, cured epoxy resins were analyzed with DRIFT-FTIR spectroscopy.



Figure III.6. Photograph of the Perkin-Elmer 1800 FTIR spectrometer.

Transmission-FTIR spectra were obtained by transmitting light through a sample on a KBr pellet. Signal-to-noise ratios were increased by averaging ten signals to obtain one-transmission spectrum.

Diffuse-reflectance, DRIFT, FTIR measurements were obtained with a Perkin-Elmer diffuse-reflectance, PEDR, accessory shown in Figure III.7 [93]. Incident radiation was reflected off of several mirrors before reaching the sample. Then the M4 reflector collimated the diffuse component, which was sent through another series of mirrors on its way to the detector. Poor signal-to-noise ratios were improved by averaging one-hundred signals to obtain one DRIFT-FTIR spectrum.

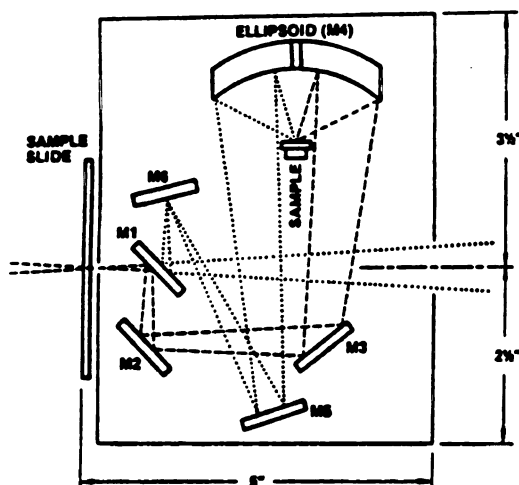


Figure III.7. Illustration of the Perkin-Elmer diffuse-reflectance, PEDR, accessory [93].

C. Experimental Procedure

Introductory experiments were performed with carbon fibers and either epoxy or hardener. Next, the epoxy and hardener were combined to form a stoichiometric epoxy resin. Finally, various amounts of long, high-strength, untreated and surface-oxidized carbon fibers were added to the epoxy resin. These neat and carbon-reinforced epoxy resins were either DSC-cured and DSC-analyzed or convectionally oven-cured and FTIR-analyzed. The experimental procedure for both analyses were given below.

1. DSC-Cured and DSC-Analyzed

Isothermal DSC analyses were employed to study changes in the reaction exotherm resulting from variations in either fiber content or fiber-surface treatment. DSC data collection was microprocessor-controlled, which allowed the operator to set various parameters for data processing.

Experimental parameters used in this study were:

Specimen:	5 to 15 mg of epoxy resin, housed in hermetically-sealed sample pans
Program:	Dynamic or Isothermal
Atmosphere:	Nitrogen at 50 cm ³ /min
Data Sampling:	0.2 sec/data point to 5.0 sec/data point

Three to five scans were obtained for each DSC data point, in an effort to reduce sampling errors and inherent

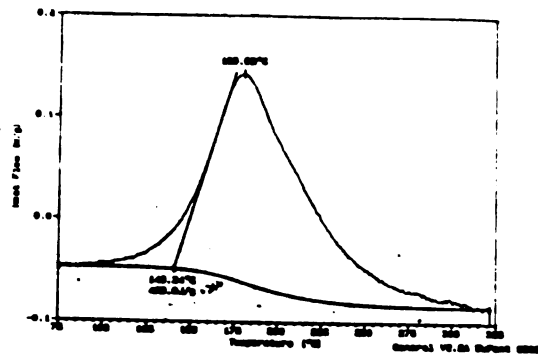
variations of the fiber content within samples. All experimental data were normalized with respect to epoxy-resin content [32,34,40]. Numerical integration of the rate of heat generation, dH/dt , as a function of time, t was performed by the DuPont TA.

DSC experiments of uncured epoxy resins were performed to obtain an estimate for the ultimate reaction exotherm, H_{ult} . The H_{ult} was defined as the maximum reaction exotherm obtainable when all epoxy monomers have reacted. DSC experiments were started by placing both sample and reference pans on the specimen holders in the DSC cell. Next, the preprogramed method was initiated. Figure III.8(a) shows that analysis was performed by drawing a sigmoidal baseline from cure initiation to cure cessation. Integration of the area under this heat generation versus time curve gave the H_{ult} .

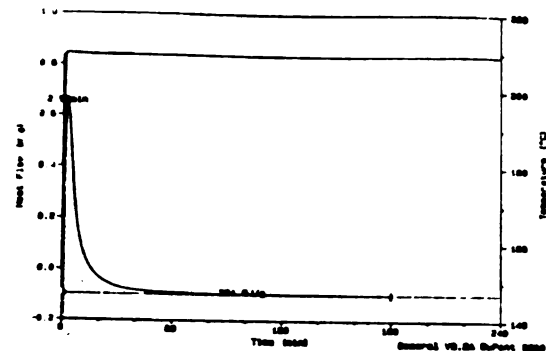
Next, uncured DSC specimens were isothermally cured to obtain a measure of the total reaction exotherm, H_T . The H_T is defined as the reaction exotherm necessary to fully cure a specimen. A reference pan was placed on the reference platform in the DSC cell as shown in Figure III.4. Then, the DSC cell was preheated to the desired cure temperature, T_c . After the DSC cell had equilibrated, the data acquisition was initiated and the specimen was placed on the sample platform. Thermal equilibrium of the

specimen as measured by the thermocouple was achieved in less than one minute. Figure III.8(b) shows a typical isothermal cure curve in which a straight baseline is drawn from cure initiation to cure cessation. The time when the reaction is considered complete or full-cure time, t_f , occurs when the baseline becomes horizontal. Integration of the area under the heat generation versus time curve determines the H_f .

a.



b.



c.

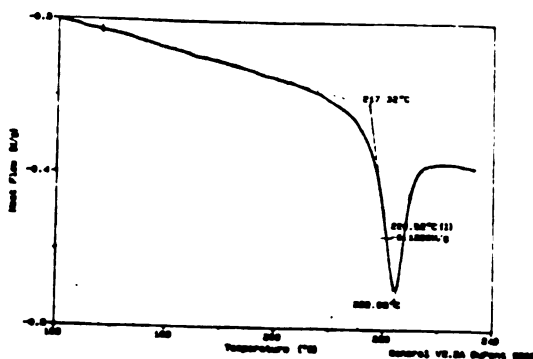


Figure III.8. Experimental DSC curves of (a) the ultimate reaction exotherm, H_{ult} , for an uncured epoxy resin; (b) the total reaction exotherm, H_f , for an uncured epoxy resin; and (c) the glass transition temperature, T_g , for a fully-cured epoxy resin.

Following each isothermal-DSC cure, the specimen was quenched to 25°C with cold tap water and the glass transition temperature, T_g , was determined. These post-cure glass transition temperatures were obtained from DSC analyses from 140°C to 240°C at a heating rate of 10°C/min.

Since the transition region embraced a temperature range of about 30°C, it was necessary to define a T_g . The T_g was taken at the intersection of the extrapolated baseline at the low temperature end and a line tangent to the inflection point. For example, the T_g in Figure III.8(c) is 220.52°C.

2. Convectionally-Cured and FTIR-Analyzed

The FTIR-spectroscopy scanning chamber was maintained at 25°C. All FTIR-spectroscopy analyses were performed in an atmosphere which was continuously purged with nitrogen. Infrared spectra were collected from 400 to 4000 cm^{-1} .

The resultant spectra for either the transmission- or DRIFT-FTIR spectroscopy specimens were the difference between a specimen and background spectrum. The background spectrum for transmission-FTIR analyses was a spectrum of the nitrogen-purged spectrometer cell. The background spectrum for the DRIFT-FTIR analyses contained non-absorbing KBr powder with a carbon-fiber concentration

identical to the carbon-fiber concentration in the specimen spectrum. The background was subtracted from the sample spectrum by automatically scaling a band common to both spectra.

Once the transmission- and DRIFT-FTIR spectra were obtained, extents of cure were calculated. Equation 34 shows that the extent of cure, α , is related to the ratio of the epoxy-intensity peak area at 916 cm^{-1} and the initial epoxy-intensity peak area at 916 cm^{-1} .

Spectra of an uncured and a fully-cured epoxy resin are given in Figure III.9. During cure, epoxy molecules reacted with primary amines to form secondary amines. These secondary amines contained hydroxyl groups. Consequently, two differences between the uncured and fully-cured spectra were found. First, a decrease in the concentration of epoxy groups corresponded to a decrease in epoxy-intensity at 916 cm^{-1} . Secondly, an increase in hydroxyl concentration caused an increase in the intensity of the broad O-H stretch between $3000 - 3500\text{ cm}^{-1}$.

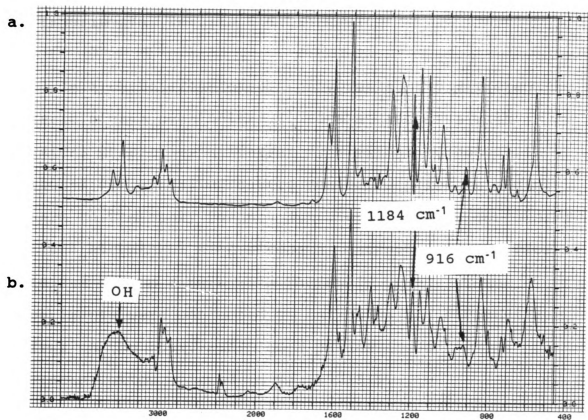


Figure III.9. FTIR-spectrometer absorbance spectra of:
(a) an uncured epoxy resin; and (b) a cured epoxy resin.

D. Experimental Results and Discussion

In a carbon-reinforced epoxy resin, two different materials have been united to form a composite with physical properties different from either component. Carbon-fiber experiments were conducted prior to adding fibers to the epoxy resin. Next, epoxy resins containing various amounts of high-strength, untreated and surface-oxidized carbon fibers were thermally cured. These experiments were conducted to determine the carbon-fiber effect on the epoxy-resin cure parameters or characteristics, listed in Table III.1.

Related terminology in the previous table include the following. The ultimate reaction exotherm, H_{ult} , and glass transition temperature, T_g , of epoxy resins were found from DSC measurements. Isothermal-DSC curing determined the total reaction exotherm, H_T , which was used to estimate the extent of cure, α , and cure kinetics. FTIR-spectra of the cured epoxy resins were also used to calculate the extents of cure. These FTIR-spectroscopy α results were compared with the DSC- α results. Finally, a comparison between neat and carbon-reinforced epoxy-resin cure characteristics was performed to determine if carbon fibers affected the epoxy-resin cure characteristics.

Table III.1. Cure Characteristics.

Symbol	Description
α	Extent of Cure
$\left[\frac{A_{916}}{A_{1184}} \right]_0$	Ratio of uncured epoxy intensity at 916 cm^{-1} to a reference intensity at 1184 cm^{-1}
$\left[\frac{A_{916}}{A_{1184}} \right]$	Ratio of epoxy intensity at 916 cm^{-1} to a reference intensity at 1184 cm^{-1}
$H_T (T_c)$	Total reaction exotherm
H_{ult}	Ultimate reaction exotherm
t_f	Full-cure time
T_g	Glass transition temperature
$T_{g, gel}$	Glass transition temperature of the gelled epoxy-resin
T_{g0}	Glass transition temperature of the uncured epoxy-resin
$T_{g, ult}$	Ultimate glass transition temperature

1. Carbon-Fiber Experiments

A literature review on the carbon-fiber surface was presented in Section II.A. Generally, carbon-fiber surfaces consist of inert graphitic basal planes with primarily carbonyl and carboxyl functionalities. Several experimenters [2,5,18,65], have proposed that chemical reactions occur between these surface groups and epoxy molecules.

Cook [2] has shown two covalent-bonded reactions between carbon fiber and epoxy resin. Such bonds were formed between an epoxy molecule and carbonyl or carboxyl on carbon-fiber surfaces to form either ether or ester bonds, respectively. Fitzer et al. [5] stated that "...the diamine hardener acts as a coupling agent between the fiber surface and the (epoxy) monomer to form strong chemical bonds between the fiber surface and the matrix." A discussion of these proposed chemical reactions between carbon-fiber surface groups and epoxy resin given in Section II.C.

Prior to experimentation, carbon fibers were stored at 25°C. Thermal analyses were performed on bare surface-oxidized carbon fibers to determine if carbon-fiber surface changes occurred during thermal heating. These fibers were analyzed with a DSC to determine if reactions can be detected between carbon-fiber surface groups. Thermal gravimetric analyzer, TGA, analyses were used to measure the amount of volatiles on carbon-fiber surfaces.

It was assumed that if chemical reactions occurred between carbon-fiber surface groups, the resultant exotherm would be too small to be detected by DSC. This assumption was verified by exposing surface-oxidized carbon fibers to DSC analyses from 25°C to 250°C at 2°C/min. No exotherm could be detected from these DSC analyses.

TGA analyses from 25°C to 500°C at 5°C/min were conducted on surface-oxidized carbon fibers. TGA recorded the weight difference as carbon fibers were heated. The 0.2-percent weight change observed was below the experimental-error detection limit of five percent. Therefore, this weight change was considered insignificant. Neither the reaction exotherm nor desorption of volatiles could be detected from thermal analyses of carbon fibers.

Next, DSC and FTIR-spectrometer experiments were conducted on mixtures of carbon fibers, carbon fibers and hardener, and carbon fibers and epoxy. Table III.2 lists these test materials and gives their composition. DSC-exothermic measurements should show an increased heat flow if epoxy molecules reacted with carbon-fiber surface groups. FTIR-spectroscopy epoxy-intensity ratio measurements should show a decrease in the epoxy intensity at 916 cm^{-1} if epoxy molecules reacted with carbon-fiber surface groups.

Table III.2. Specimens for carbon-fiber experiments.

Experiment	wt % fiber*	wt % epoxy	wt % hardener
carbon fiber epoxy	80	20	0
carbon fiber hardener	80	0	20

* - surface-oxidized carbon fibers

a. Carbon Fiber and Hardener Experiments

Experiments were carried out to determine if hardener reacts with carbon-fiber surface groups. Hardener and surface-oxidized carbon-fiber mixtures were prepared according to Table III.2. They were analyzed with DSC analyses from 25°C to 350°C at 2°C/min. The only observed baseline deviation was the hardener phase transition from a powder to a liquid at 178°C. No reaction exotherm was detected.

b. Carbon Fiber and Epoxy Experiments

Experiments were conducted to determine if epoxy molecules react with carbon-fiber surface groups. First, carbon fiber and epoxy resin mixtures were prepared according to Table III.2 and exposed to DSC analyses from

25°C to 350°C at 2°C/min. Again, no reaction exotherm was found.

This result was verified by a calculation on a 0.60 fiber-weight fraction, w_f , surface-oxidized carbon-reinforced epoxy composite, given in Appendix A. This calculation showed that if all functional carbon-fiber surface groups reacted with an epoxy molecule, the resultant exothermic increase would be less than one percent. Since the precision of the DSC is approximately 2.5 percent, detecting any reaction at the one-percent level was not possible.

The FTIR spectrometer was also used to analyze these surface-oxidized carbon fiber and epoxy mixtures. These test materials were placed in sterile beakers and isothermally heated in a convectional oven at 220°C for 170 minutes. Remaining uncured epoxy molecules dissolved in acetone; whereas, cured epoxy molecules did not. To ensure that all unreacted epoxy molecules were removed, surface-oxidized carbon fibers were refluxed with acetone for 90 hours.

Transmission-FTIR spectra of unused and acetone-washed surface-oxidized carbon fibers were obtained. Because carbon fibers tended to absorb infrared radiation across the entire range, a difference of the two spectra was

obtained to eliminate the carbon-fiber effect. Epoxy-intensity peak decreases or hydroxide-intensity peak increases would indicate that epoxy molecules reacted with carbon-fiber surface groups. Unfortunately, resultant differences were less than eight percent or less than the minimum resolution of transmission-FTIR spectroscopy analyses. Therefore, this result was not conclusive to support reaction between carbon-fiber surface groups and epoxy resin.

These carbon fibers were weighed on an analytical balance before isothermal heating and after acetone washing. No weight change could be measured beyond the instrumental error of the analytical balance.

Above experiments were inconclusive to confirm any chemical reaction between carbon-fiber surface groups and epoxy molecules. Either more precise techniques or more sensitive instrumentation were required. Recommendations for "interphase-specific" and "non-destructive" experimental techniques are given in Section V.

2. Neat and Carbon-Reinforced Epoxy-Resin Experiments

Experiments were performed to determine carbon-fiber effects on epoxy-resin cures. Neat, untreated carbon-reinforced, and surface-oxidized carbon-reinforced epoxy resins were cured to determine the cure characteristics listed in Table III.1. The ultimate reaction exotherm, H_{ult} , initial FTIR-spectroscopy epoxy-intensity ratio, $(A_{916 \text{ cm}^{-1}} / A_{1184 \text{ cm}^{-1}})_0$, and full-cure time, t_f , were found and used to determine the full-cure extent of cure, α . Next, these fully-cured extents of cure were integrated over time to obtain cure-kinetic rate constants k_1 , k_2 , and k_3 . Finally, the glass transition temperature, T_g , of fully-cured specimens were analyzed.

a. Ultimate DSC Reaction Exotherm, H_{ult}

The ultimate reaction exotherm, H_{ult} , for a stoichiometric epoxy resin was defined as the total heat liberated when all epoxy molecules reacted [40]. The H_{ult} was experimentally determined with a DSC.

DSC analyses were selected over isothermal analyses to find the H_{ult} . During DSC analyses, unreacted epoxy molecules gained energy with increasing temperature. This increased temperature enabled epoxy and hardener molecules to move faster and farther in the resin matrix. Unlike

isothermal cures, DSC analyses allowed more epoxy molecules to react before becoming trapped in the matrix network [41].

A typical DSC analysis for an epoxy resin cure is shown in Figure III.8(b). In this study, reaction exotherms were obtained using DSC-heating rates from 0.5°C/min to 20°C/min as shown in Figure III.10. Maximum reaction exotherms occurred at 2°C/min. At heating rates slower than 2°C/min, the margin of error was large relative to the error at 2°C/min.

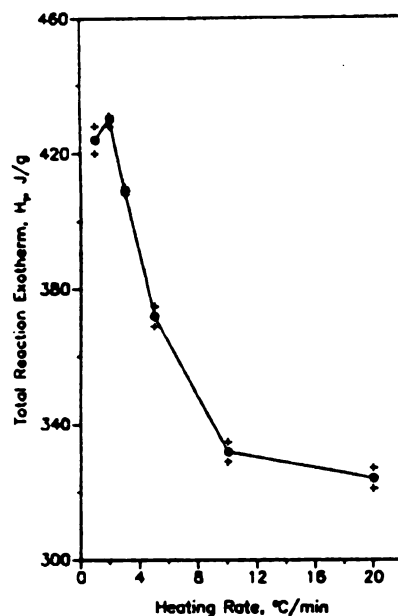


Figure III.10. Total reaction exotherm, H_T , versus DSC-heating rate for epoxy resin.

At heating rates faster than $2^{\circ}\text{C}/\text{min}$, the cure temperature, T_c , exceeded the $T_{g,ult}$ before all epoxy molecules reacted. Lower reaction exotherms were found due to revitrification and devitrification of the epoxy resin. Revitrification corresponded to a second rubber-to-glass transformation and led to char formation. Devitrification marked the glass-to-rubber transition led to thermal degradation [36,41].

Ultimate reaction exotherms for epoxy-resin were determined by integrating a DSC heat flow versus time curve from 25°C to 322°C . Experimental H_{ult} for a stoichiometric epoxy resin was found to be 24.6 ± 0.75 kcal/gmol and compared well with the literature values given in Table II.5.

Ultimate reaction exotherms for carbon-reinforced epoxy resins with 0.01, 0.10, and 0.60 fiber weight fractions, w_f , are given in Table III.3. Average ultimate reaction exotherms for untreated carbon-reinforced and carbon-reinforced epoxy resins were 25.0 ± 1.1 cal/gmol and surface-oxidized 24.9 ± 1.3 cal/gmol, respectively. This standard deviation difference among the ultimate reaction exotherms was not significant.

Table III.3. Ultimate reaction exotherm, H_{ult} , versus fiber weight fraction, w_f .

w_f	untreated	surface-oxidized
0.01	24.5	24.1
0.10	24.6	25.0
0.60	26.1	25.6
Average	25.0 ± 1.1	24.0 ± 1.3

As Table III.4 shows, the chemical functionality of the carbon fiber did not affect the H_{ult} . This result was inconsistent with Wang et al [74] findings. Wang et al. cured difunctional and tetrafunctional carbon-reinforced epoxy with difunctional hardener. They found reduced ultimate reaction exotherms by adding carbon fibers to the difunctional epoxy resin and ultimate reaction exotherms were by adding carbon fibers to the tetrafunctional epoxy resin. Wang et al. also found that the H_{ult} could be increased by 26 percent depending on the carbon-fiber surface functionality.

The H_{ult} results, shown in Table III.4, were consistent with Dutta et al. [43] finding. Dutta et al. cured glass-and carbon-filled epoxy resins. Their results showed an increased H_{ult} for glass-filled epoxy resins relative to neat epoxy resins and similar H_{ult} for carbon-filled epoxy resins relative to neat epoxy resins.

b. Initial FTIR-Spectroscopy Epoxy-Intensity Ratio,

$$(A_{916 \text{ cm}^{-1}} / A_{1184 \text{ cm}^{-1}})_0$$

Extents of cure were calculated from FTIR-spectra as a function of the fractional change in the epoxy-intensity ratio, $(A_{916 \text{ cm}^{-1}}/A_{1184 \text{ cm}^{-1}})$. The epoxy-intensity ratio is defined as the epoxy-intensity peak at 916 cm^{-1} divided by the reference-intensity peak at 1184 cm^{-1} [88].

Intensity peaks at 916 cm^{-1} and 1184 cm^{-1} were proportional to concentrations of epoxy molecules and aromatic-hydrogen bonds, respectively. The epoxy-intensity ratio decreased as the amount of unreacted epoxy molecules decreased. The reference-intensity ratio at 1184 cm^{-1} remained constant because aromatic hydrogens are not affected by the polymerization or crosslinking reactions.

The maximum amount of epoxy molecules available for reaction was estimated from transmission-FTIR spectra of an uncured epoxy-resin mixture. The epoxy-resin film was placed on a KBr pellet and infrared spectra from 400 to 4000 cm^{-1} were collected. The data were obtained at one-minute intervals and averaged over ten scans which gave a spectral resolution of 4 cm^{-1} . A spectrum of an uncured epoxy resin is shown in Figure III.6 (a). The average initial epoxy-intensity ratio equalled 0.4 and was used to calculate the FTIR-spectroscopy α , as shown in Equation 34.

c. Full-Cure Time, t_f (T_c)

Prior to fully curing the epoxy resins, the full-cure time, t_f , was determined. Neat epoxy-resin samples were isothermally DSC-cured at temperatures between 120°C to 250°C. A typical isotherm for the DER 332-DDS epoxy resin is shown in Figure III.8(b). The total reaction exotherm, H_f , is dependent on the full-cure time, t_f . The full-cure time was defined as the time between cure initiation and cure cessation. Cure initiation was chosen at the time approximately one minute after a specimen was exposed to the cure temperature, T_c . Cure cessation occurred when the incremental heat flow became constant.

Rapid increases in heat generation prior to the exotherm peak in Figure III.8(b) are characteristic of the highly-exothermic, epoxy-polymerization reactions. The decreased reaction rate after the exothermic peak was due to the onset of the diffusion-controlled crosslinking reactions. Leveling of the reaction rate to the original isothermal baseline indicated cessation of the cure reactions and the onset of vitrification [41]. The H_f was found by integrating the area under this heat flow versus time curve with a straight baseline from cure initiation to cure cessation.

The total reaction exotherm versus T_c for the fully-cured DER 332-DDS epoxy resin is given in Figure III.11(a). At lower cure temperatures, premature vitrification caused reduced total reaction exotherms. As the T_c increased, the H_T increased. The maximum H_T of 23.4 cal/gmol for the DER 332-DDS epoxy resin occurred at 220°C. Samples cured above 220°C were darkly discolored and gave smaller total reaction exotherms because of revitrification and devitrification.

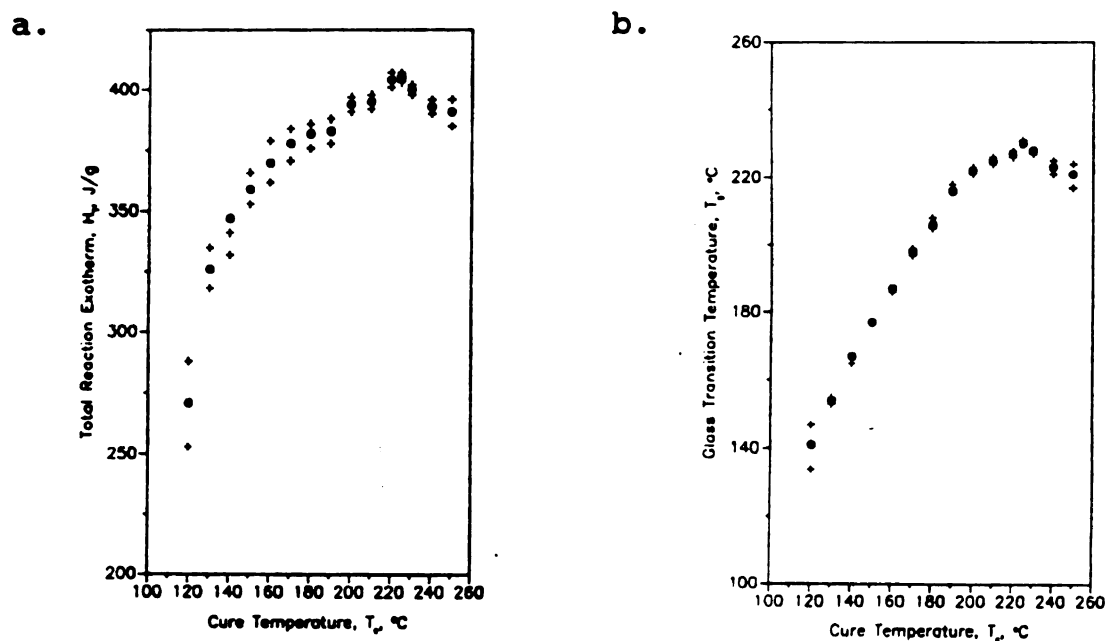


Figure III.11. DSC analyses of the: (a) total reaction exotherm, H_T , versus cure temperature, T_c ; and (b) the glass transition temperature, T_g , versus T_c .

Following the isothermal-DSC cures, the specimens were dynamically scanned to determine the glass transition temperature, T_g . DuPont, the DSC manufacturer, recommended

using a heating rate of 10°C/min for glass transition determinations because the T_g is independent of the DSC-heating rate. Glass transition temperatures for fully-cured DER 332-DDS epoxy resin are plotted in Figure III.11(b). A comparison between Figures 11(a) and 11(b) shows the T_g data followed the same trends as the H_T data. This was expected since the T_g is a function of the number of molecules between crosslinks and the H_T is a measure of the number of cure reactions. Table III.4 lists the H_T , T_g , and t_f data at various cure temperatures.

Table III.4. Total reaction exotherm, H_T , glass transition temperature, T_g , and full-cure time, t_f , versus cure temperatures, T_c , for neat epoxy-resin cures between 120°C and 250°C.

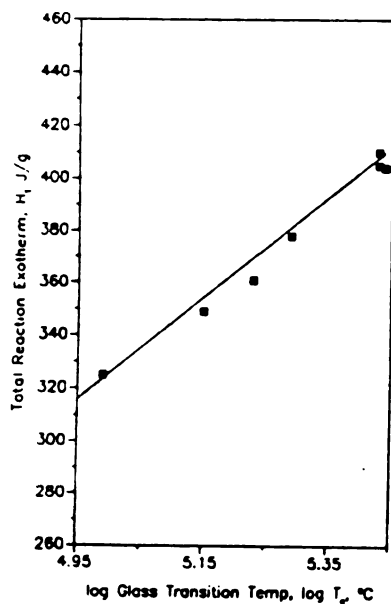
T_c	H_T	T_g	t_f
120	271	141	650
130	326	154	500
140	347	167	450
150	359	177	420
160	371	187	360
170	378	198	330
180	375	205	240
190	382	217	210
200	394	222	190
210	395	225	180
220	404	230	170
230	400	228	160
240	393	223	120
250	391	221	120

The T_g increased with increasing T_c up to the maximum or ultimate glass transition temperature, $T_{g,ult}$. For isothermal cures above 230°C, the T_g decreased with increasing T_c because of thermal degradation and charring. Chan et al. [41] used DSC analyses and determined the $T_{g,ult}$ for DER 332-DDS epoxy resin to be 229°C. This 1°C difference was well within the five-percent experimental error. Experimental precision of the DSC data is shown by standard deviation error bars in Figure III.11.

The relationship between H_T and T_c formed the basis of a theoretical model for the time-temperature-transformation, TTT, diagram. The TTT diagram, presented in Figure II.11 of Section II.B.1, is a model of an isothermally-cured thermosetting material. Appendix B outlines the procedure for estimating the full-cure line for the DER 332-DDS epoxy resin.

The full-cure line was determined as follows. The total reaction exotherms given in Figure III.11(a) are integrated at various cure times [41,94]. Next, a logarithmic relationship between H_T and T_g was assumed, as shown in Figure III.12(a). From these results, the T_g can be estimated at various cure times.

a.



b.

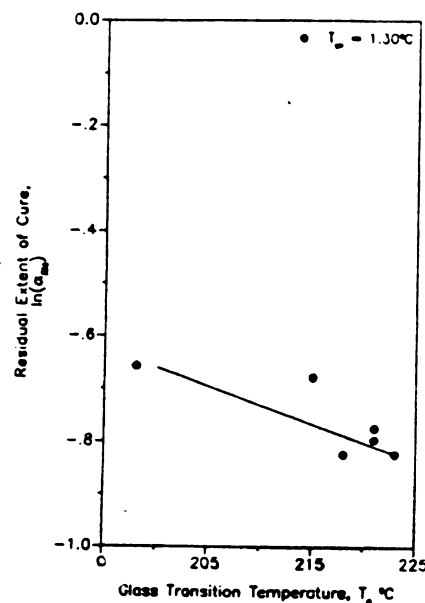


Figure III.12. Illustration of the: (a) total reaction exotherm, H_T , versus the \log_{10} (glass transition temperature, T_g); and (b) \log_1 (residual extent of cure, $\alpha_{rid} = 1 - \alpha$), versus the T_g .

Next a linear relationship was assumed to exist between T_c and T_g at each cure time,

$$T_g = A + B T_c ; \quad (37)$$

where A = intercept and
 B = slope.

After solving for A and B , Equation 37 enabled the experimenter to estimate the T_g any T_c . According to Peng et al. [94], full cure occurs when the T_g equals $T_{g,ult}$ with:

$$T_f = a + b (\log t_f), \text{ for } T_f < T_{g,ult}; \quad (38)$$

where T_f = isothermal full-cure temperature,
 a, b = fitted constants, and
 t_f = full cure time.

to correlate isothermal cure data and obtain an estimation of the t_f .

An estimation of t_f was performed by replacing t_f and T_c in Equation 38 with T_c . The constants, a and b , for DER 332-DDS resin were 232 and -5.32, respectively.

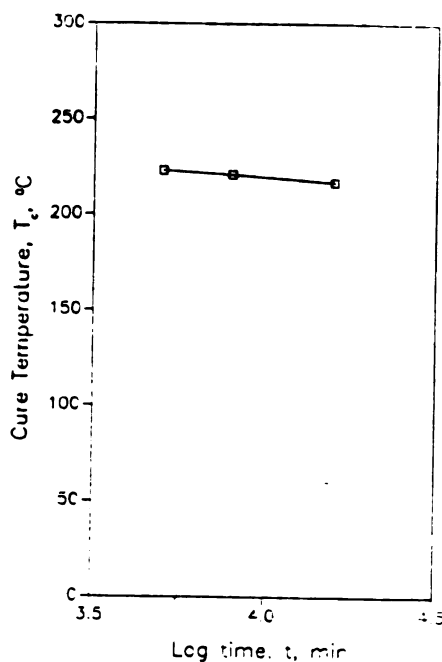


Figure III.13. Illustration of the full-cure line. Cure temperature, T_c versus log time, t .

From Equation 38, the calculated isothermal full-cure temperature, T_f , equalled the $T_{g,ult}$ of 230°C after eight minutes. An experiment was performed to test this full-cure condition. A neat epoxy resin was isothermally cured at 230°C for only eight minutes. Then the DSC exotherm was integrated which gave the extent of cure equal to 0.45. A post-cure T_g determination gave an $T_{g,ult}$ at 225°C.

Section III.2.g.(4) showed that the epoxy resin was pre-cured between ten and thirteen percent prior to DSC-curing. This explains why the extent of cure was not 0.58, the theoretical α , and maximum T_g in Figure III.11(b) was only 225°C.

Full-cure times were calculated from Equation 38, by letting T_f equal 230°C. For isothermal cures at 220, 200, and 170°C, the full-cure times are 170 minutes, 1.04×10^6 minutes or 72 days, and 4.51×10^{11} minutes or 86034 years, respectively. Fava [80] stated, "... (that the isothermal-DSC cure method) is suitable for cure times on the order of hours. If a cure proceeds for longer than about six hours, the exotherm is generally too slight to be detected accurately ...". Equation 38 verified that full cure was not practical for isothermal cure temperatures much lower than 230°C [85].

Full cure could not be achieved for T_c above 230°C because endothermic reactions, such as thermal degradation and charring, occurred before polymerization and crosslinking reactions were completed [32]. This was shown by the decreases in Figure III.12 above 230°C.

The gelation and vitrification lines for the DER 332-DDS epoxy-resin TTT diagram were also formulated in Appendix B. The gelation line represents the temperatures

where the extent of cure, α , equalled 0.58 and is given by $T_c = 281 - 93.2 \log t$. The vitrification line equals the time where the T_g equalled the T_c and is given by $T_c = 478 - 155 \log t$.

Physical parameters in the TTT diagram for the DER 332-DDS epoxy resin, T_{g0} , $T_{g, gel}$, and $T_{g, ult}$ were determined. From Figure III.11(b), the $T_{g, ult}$ was found to be 230°C. The unreacted glass transition temperature, T_{g0} , was found by extrapolating the residual extent of cure, $\alpha_{rid} = 1 - \alpha$, versus the $\log_{10}(T_g)$ curve given in Figure III.12(b) to an α_{rid} equal to one [40]. The T_{g0} for a DER 332-DDS epoxy resin was 1°C. The gelation glass transition temperature, $T_{g, gel}$, was found by placing uncured epoxy resin in a Brookfield viscometer and increasing the temperature at a rate of 5°C/min. A sudden decrease in viscosity at 80°C marked the transition from a gelled glass to a viscous liquid where $T_{g, gel}$ occurred. These data are in agreement with Chan et al. [41] results. They reported a $T_{g, gel}$ for DER 332-DDS epoxy resin of approximately 80°C. The DER 332-DDS TTT diagram is illustrated in Figure III.14.

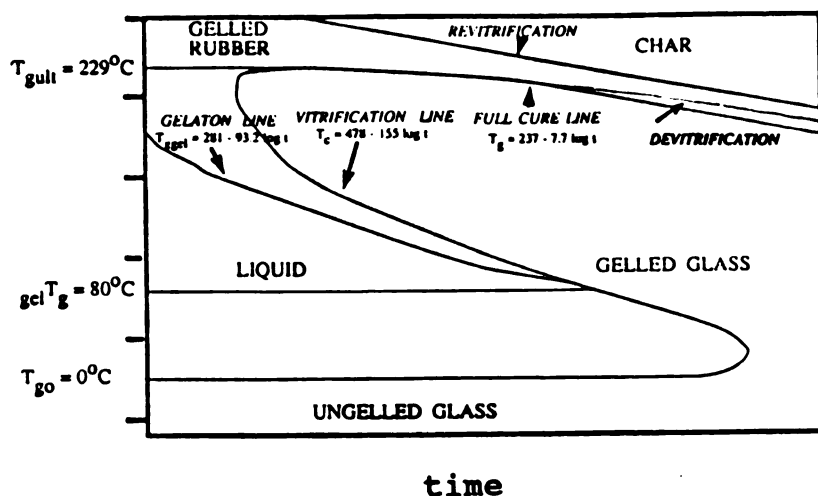


Figure III.14. Time-temperature-transition, TTT, diagram for a stoichiometric DER 332-DDS epoxy resin.

This exercise demonstrated how a TTT diagram can be formulated. The physical parameters, T_{g0} , $T_{g,gel}$, and $T_{g,ult}$, was in excellent agreement with literature values [36,41,94]. This TTT diagram was used to predict the full-cure times.

d. Full-cure Extent of Cure, α (T_c)

Isothermal experiments were performed and analyzed with both DSC and FTIR spectrometer to determine the full-cure extent of cure, α . Isothermal-DSC full-cure α equals the quotient of total reaction exotherm, H_T , divided by the ultimate reaction exotherm, H_{ult} . FTIR-spectroscopy full-cure α is a function of the epoxy-intensity ratio as shown in Equation 34.

Neat, untreated carbon-reinforced, and surface-oxidized carbon-reinforced epoxy resins were fully cured at temperatures of 170, 190, 200, 210, 220, 230, and 250°C at times equal to 300, 240, 190, 180, 170, 150, and 120 minutes, respectively. Table III.5 shows an analysis of variance, ANOVA, of isothermal-DSC total reaction exotherms for neat and surface-oxidized carbon-reinforced epoxy-resin cures. A high F-ratio, the ratio of the variation standard deviation divided by the residual standard deviation, in the ANOVA implied that isothermal-DSC H_T data were greatly dependent on the cure temperature, T_c . A low F-ratio implied that isothermal-DSC H_T data are independent of the amount of surface-oxidized carbon fiber weight fraction, w_f .

Table III.5. Analysis of variance, ANOVA, of the total reaction exotherm, H_T , for the following sources of variation: (a) cure temperature, T_c ; and (b) fiber weight fraction, w_f .

Variation	Sum of Squares	Degree of Freedom	Standard Deviation	F-Ratio
T_c	2800	6	470	8.6
w_f^*	14	3	4.5	0.09

* - fiber-weight fraction of surface-oxidized carbon fibers.

These difunctional epoxy-resin H_f results were consistent with the findings reported by Dutta et al. [43] and inconsistent with the findings of Wang et al. [74]. Dutta et al. cured glass- and carbon-filled difunctional epoxy resin. They found no statistical significant difference between total reaction exotherms for filled epoxy-resin cures and neat epoxy-resin cures. Wang et al. [74] cured a difunctional and tetrafunctional epoxy resin. Then they added carbon fillers to determine the effect of epoxy functionality on carbon-reinforced epoxy resin cures. They found that difunctional epoxy-resin cures gave reduced H_f relative to neat epoxy-resin cures and tetrafunctional epoxy-resin cures gave similar H_f relative to neat epoxy-resin cures.

Full-cure α versus T_c curves for untreated carbon-reinforced, and surface-oxidized carbon-reinforced epoxy resins are shown in Figure III.15(a) and (b), respectively. Isothermal-DSC full-cure α results reached a maximum between 210°C and 230°C. Isothermal curing below 230°C resulted in an undercured epoxy resin and isothermal curing above 230°C resulted in a thermal-degraded or charred epoxy resin. Inspection of fully-cured epoxy resins showed full-cure α versus T_c data were well within the five-percent experimental error. No significant differences between neat and carbon-reinforced epoxy resins were observed.

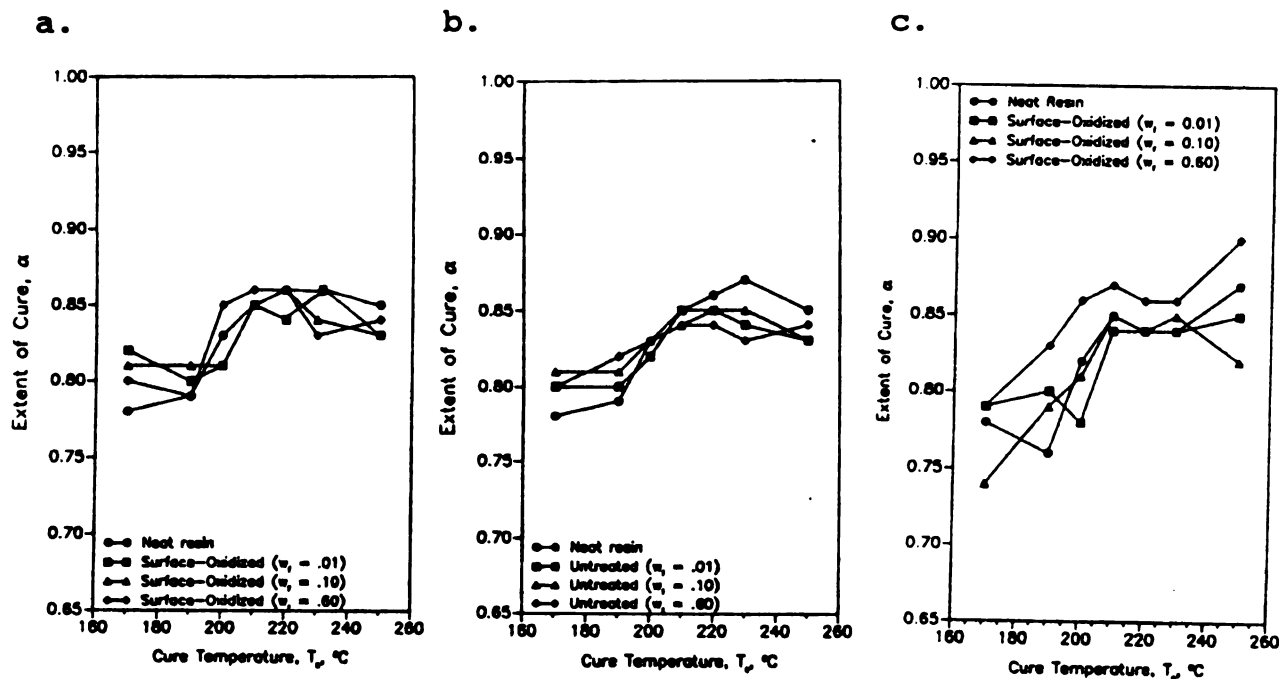


Figure III.15. Full-cure extent of cure, α , versus cure temperature, T_c , for the: (a) DSC-cured and DSC-analyzed untreated carbon-reinforced epoxy resin; (b) DSC-cured and DSC-analyzed surface-oxidized carbon-reinforced epoxy resin; and (c) convectionally-cured and FTIR-analyzed surface-oxidized carbon-reinforced epoxy resin.

Surface-oxidized carbon-reinforced resins were also analyzed with diffuse-reflectance, DRIFT, FTIR spectroscopy. Before DRIFT-FTIR spectroscopy analyses, samples were fully-cured in a conventional oven at cure temperatures and times identical to the DSC-cured specimens. A typical DRIFT-FTIR spectrum for a fully-cured DER 332-DDS epoxy resin was shown in Figure III.9(b).

A comparison of the uncured and fully-cured FTIR spectra presented in Figure III.9 showed a smaller epoxy-intensity peak at 916 cm^{-1} for the fully-cured specimen.

This decrease was due to epoxy molecules reacting with amines and forming secondary amines, which contained hydroxyl groups. An increase in hydroxyl groups was represented by the broad intensity strength from 3000 to 3500 cm^{-1} .

FTIR-spectroscopy full-cure α results for neat and surface-oxidized carbon-reinforced resins is shown in Figure III.15(c). Two-percent higher FTIR- α results relative to the DSC- α results for the 0.60 carbon-reinforced specimens was believed to be due to nonuniform sample sizes and high infrared absorbance of the carbon fibers. In DRIFT-FTIR spectroscopy, the infrared beam penetrated the epoxy-resin specimen completely and part of the beam was reflected back to a detector [29]. This reflected light was scattered by the specimen to produce the infrared spectrum. Unfortunately, the infrared beam was absorbed by carbon fibers across the total spectral range [29,86].

An investigation on the FTIR-spectroscopy errors will be addressed in Section III.D.2.g.(4). The errors due to the high infrared absorbance of the carbon fibers can be explained by high scattering coefficient, s , values in the Kubelka-Munk equation, Equation 32 [28]. High values of s caused increased absorbance across the entire FTIR

spectrum, reduced sample intensity separation, and poor spectral resolution.

The maximum FTIR-spectroscopy full-cure α occurred at 250°C. Figure III.15(a) shows the maximum isothermal-DSC full-cure α occurred at 220°C. The FTIR-spectroscopy full-cure α implied that more epoxy molecules react as the T_c increased. Since more epoxy molecules should react at a higher cure temperatures, T_c , the lower DSC full-cure α at 250°C was believed to be caused from endothermic reactions, such as thermal degradation and charring.

These extent of cure results showed that full-cure α for carbon-reinforced epoxy-resin cures were not statistically different from full-cure α for neat epoxy-resin cures. A comparison of DSC-cured and DSC-analyzed specimens versus convectional-oven cured and FTIR-spectroscopy analyzed specimens showed no significant difference between full-cure extents of cure.

E. Cure Kinetics

Physical, mechanical, and electrical properties of an epoxy resin depend to a large extent on the extent of cure, α , [7]. Qualitative analyses showed no significant difference between full-cure extents of cure for neat and carbon-reinforced epoxy resins. A cure-kinetic analysis quantified these α results.

Criterion for selecting the cure type for kinetic analysis is the ability to accurately describe the α at any given temperature. Dynamic curing was appealing because much information can be obtained from a single-temperature programmed experiment. Unfortunately, dynamic cures are not reliable for depicting the course of a reaction over a wide time-temperature range [54]. For this reason, isothermal cures were used to experimentally determine the α and, ultimately, the cure kinetics.

DSC-analyzed full-cure α data from Section III.2.D were integrated at various times, t . These α versus t data were fit to a cure-kinetic model to attain a better understanding of the carbon-reinforced epoxy-resin cures.

A comparison between neat and carbon-reinforced epoxy-resin cure kinetics would demonstrate whether carbon fibers affect the reaction rate. A comparison between untreated

and surface-oxidized carbon-reinforced epoxy-resin cure kinetics would give insight into what interphase mechanisms are occurring.

In Section II.B.3., it was determined that n^{th} -order kinetics can not predict the sigmoidal shape of an isothermal reaction exotherm. Furthermore, n^{th} -order cure-kinetic equations cannot realistically describe polymerization and crosslinking reactions which occur during an epoxy-resin cure [80].

Polymerization reactions are catalyzed by hydrogen-bond donor and hydroxyl groups [34]. If it is assumed that amine-hydrogen atoms have equal reactivity [32], then epoxy molecules are consumed in two simultaneous reactions. The first reaction was catalyzed by hydrogen-bond donor groups, and the second reaction autocatalyzed by hydroxyl groups in the reaction products. The rate equation which described these polymerization reactions was:

$$\frac{d\alpha}{dt} = (k_1 + k_2 \alpha) (1 - \alpha); \text{ for } \alpha \leq \alpha_{gel} \quad (13)$$

where α = extent of cure,

$$\begin{aligned} k_1 &= A_1 \exp(-E_{A1}/RT), \\ k_2 &= A_2 \exp(-E_{A2}/RT), \\ A_1 &= \text{frequency factor for } k_1, \\ A_2 &= \text{frequency factor for } k_2, \\ E_{A1} &= \text{activation energy for } k_1, \\ E_{A2} &= \text{frequency factors for } k_2, \text{ and} \\ \alpha_{gel} &= 0.48. \end{aligned}$$

Gelation marked the change from the rate-controlled polymerization reactions to diffusion-controlled crosslinking reactions. The theoretical extent of cure at gelation, α_{gel} , for a tetrafunctional epoxy and difunctional amine is calculated from Equation 1 to equal 0.58. Section III.E.2.g.(3) showed the epoxy resin is between ten- and thirteen-percent cured prior to DSC-curing. Therefore α_{gel} was assumed to equal only 0.48.

The rate equation which described the diffusion-controlled crosslinking reactions was [42,57]:

$$\frac{d\alpha}{dt} = k_3 e^{-D\alpha/RT} (1 - \alpha); \quad \text{for } \alpha > \alpha_{gel} \quad (14)$$

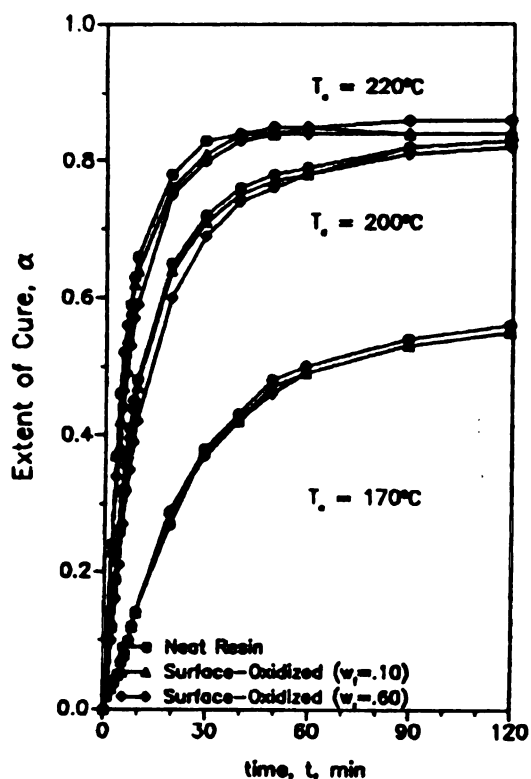
where D = fitted diffusion-limited constant,
 $k_3 = A_3 \exp(-E_{A3}/RT)$,
 A_3 = frequency factor for k_3 , and
 E_{A3} = activation energy for k_3 .

The polymerization rate equation, shown in Equation 13, has been used by numerous experimenters [34,40,43,44,55]. The crosslinking rate equation, represented by Equation 14, has been developed by Loos et al. [57] and used by Finzel [42] to model the crosslinking reaction mechanism which other experimenters neglect.

Cure-kinetic analyses were conducted as follows: Full-cure α data for neat, untreated carbon-reinforced, and surface-oxidized carbon-reinforced epoxy resins at cure temperatures equal to 170, 200, and 220°C were integrated

over time, t . These α versus t data are shown in Figure III.16 and tabulated in Table C.1. The most pronounced decrease in the reaction rate, $d\alpha/dt$, occurred near gelation.

a.



b.

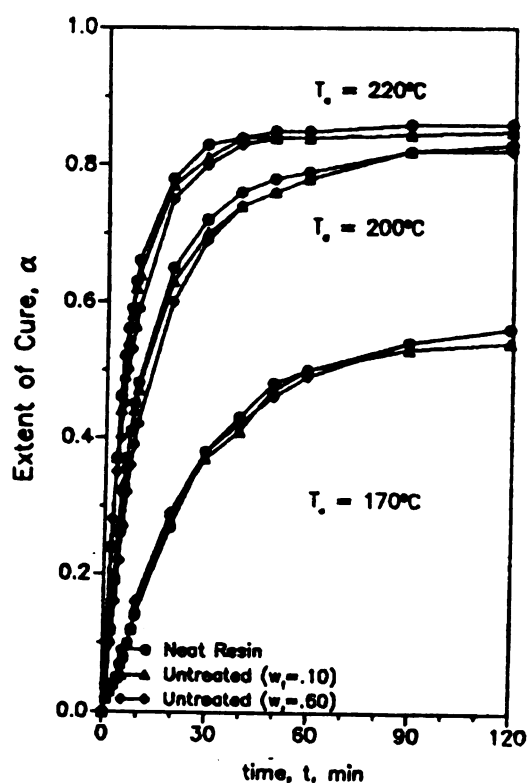


Figure III.16. Extent of cure, α , versus time, t , for a: (a) DSC-cured and DSC-analyzed untreated carbon-reinforced epoxy resin; and (b) DSC-cured and DSC-analyzed surface-oxidized carbon-reinforced epoxy resin.

A comparison between the gelation time, t_{gel} , for untreated and surface-oxidized carbon-reinforced epoxy-resin cures is given in Table III.6. The maximum t_{gel} difference between neat epoxy resin and carbon-reinforced epoxy resins was ten percent. These t_{gel}

differences are significant and consistent findings reported by Mijovic [44]. He found that the time to the exothermic peak was lengthened adding fillers to an epoxy resin.

At gelation, an increased local viscosity and steric hindrance of the reactants caused the diffusion-limited crosslinking reactions. In a carbon-reinforced epoxy resin, the epoxy molecules in the vicinity of the reinforcement were "shielded" by the carbon fibers and, hence, were less likely to encounter reactive species than epoxy molecules in the bulk epoxy matrix.

Table III.6. Gelation time, t_{gel} , versus cure temperature, T_c , and fiber weight fraction, w_f , for: (a) untreated carbon-reinforced epoxy resin; and (b) surface-oxidized carbon-reinforced epoxy resin.

a.

T_c (°C)	w_f	t_{gel}^* (min)
220	0.0	4.63
	0.01	4.97
	0.10	5.25
	0.60	5.40
200	0.0	13.2
	0.01	13.1
	0.10	13.8
	0.60	14.2
170	0.0	64.5
	0.01	65.2
	0.10	67.08
	0.60	70.15

Table III.6 (continued)

b.

T_c (°C)	w_f	t_{gel}^* (min)
220	0.0	4.63
	0.01	5.23
	0.10	5.79
	0.60	5.86
200	0.0	13.2
	0.01	12.9
	0.10	13.3
	0.60	14.9
170	0.0	64.5
	0.01	62.0
	0.10	69.7
	0.60	69.7

Note *: The gelation extent of cure, α_{gel} , is based on the assumption that the resin is already ten-percent cured prior to DSC-curing, as shown in Section III.2.g.(5); therefore, α_{gel} equaled 0.48.

Table III.6 shows that the t_{gel} is not a function of carbon-fiber surface functionality. Instead, the t_{gel} varies as a function of average distance between reinforcement. At gelation, local viscosity and steric hinderance of reactants increased. Carbon fibers further resitricted the movement of epoxy molecules and lengthened the epoxy-resin cure.

Next, Equation 13 was rearranged by dividing the reaction rate by the product, $(1 - \alpha)(B - \alpha)$. This quantity is defined as the reduced polymerization reaction rate, α_{Red1} ,

$$\alpha_{Red1} = \frac{d\alpha/dt}{(1 - \alpha)(B - \alpha)} = k_1 + k_2 \alpha, \text{ where } \alpha \leq \alpha_{gel}. \quad (39)$$

The α_{Red1} versus α for the neat epoxy resin is given in Figure III.17(a). The α_{Red1} increased with α during the initial stages of cure as predicted by equation 39. At α approximately equal to 0.3, a sharp increase in α_{Red1} values was caused by the increasing importance of diffusion-controlled crosslinking reactions.

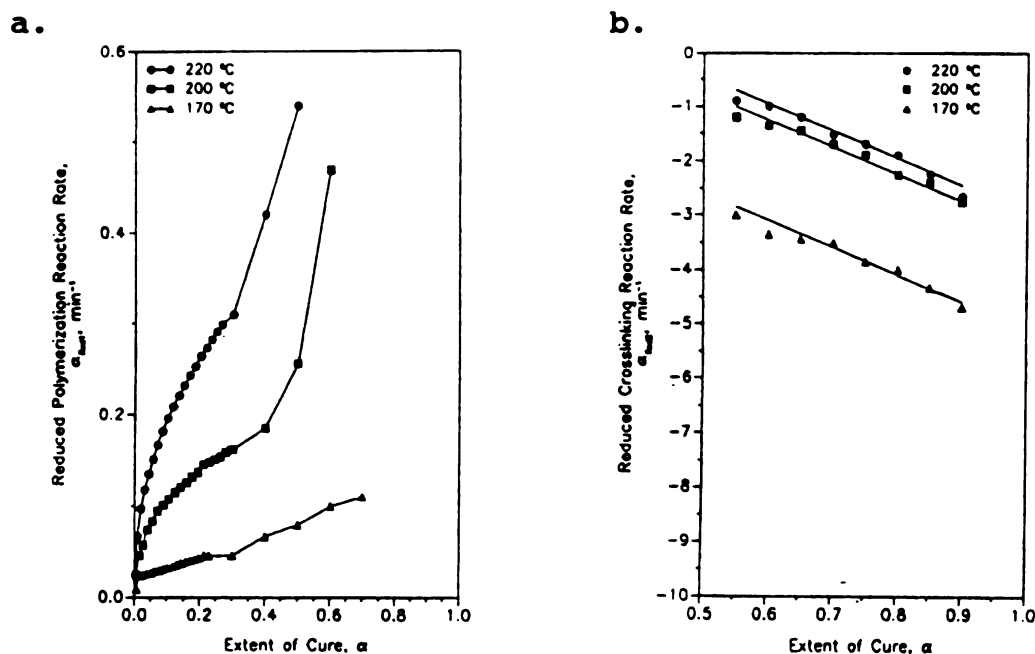


Figure III.17. Reduced: (a) polymerization reaction rate, α_{Red1} , versus extent of cure, α , for the neat epoxy resin; and (b) crosslinking reaction rate, α_{Red2} , versus α for the neat epoxy resin.

A least-squares linear regression of Equation 39 was performed between an α equal to 0.05 and 0.3. Rate constants, k_1 and k_2 , were modeled with Arrhenius kinetics and shown in Figure III.18. Lines drawn in Figure III.18

was fitted to the neat epoxy-resin rate constants.

Correlation coefficients for neat and reinforced resin rate constants, k_1 and k_2 , were between 0.969 and 0.999.

No significant difference was found between the neat and reinforced epoxy resins.

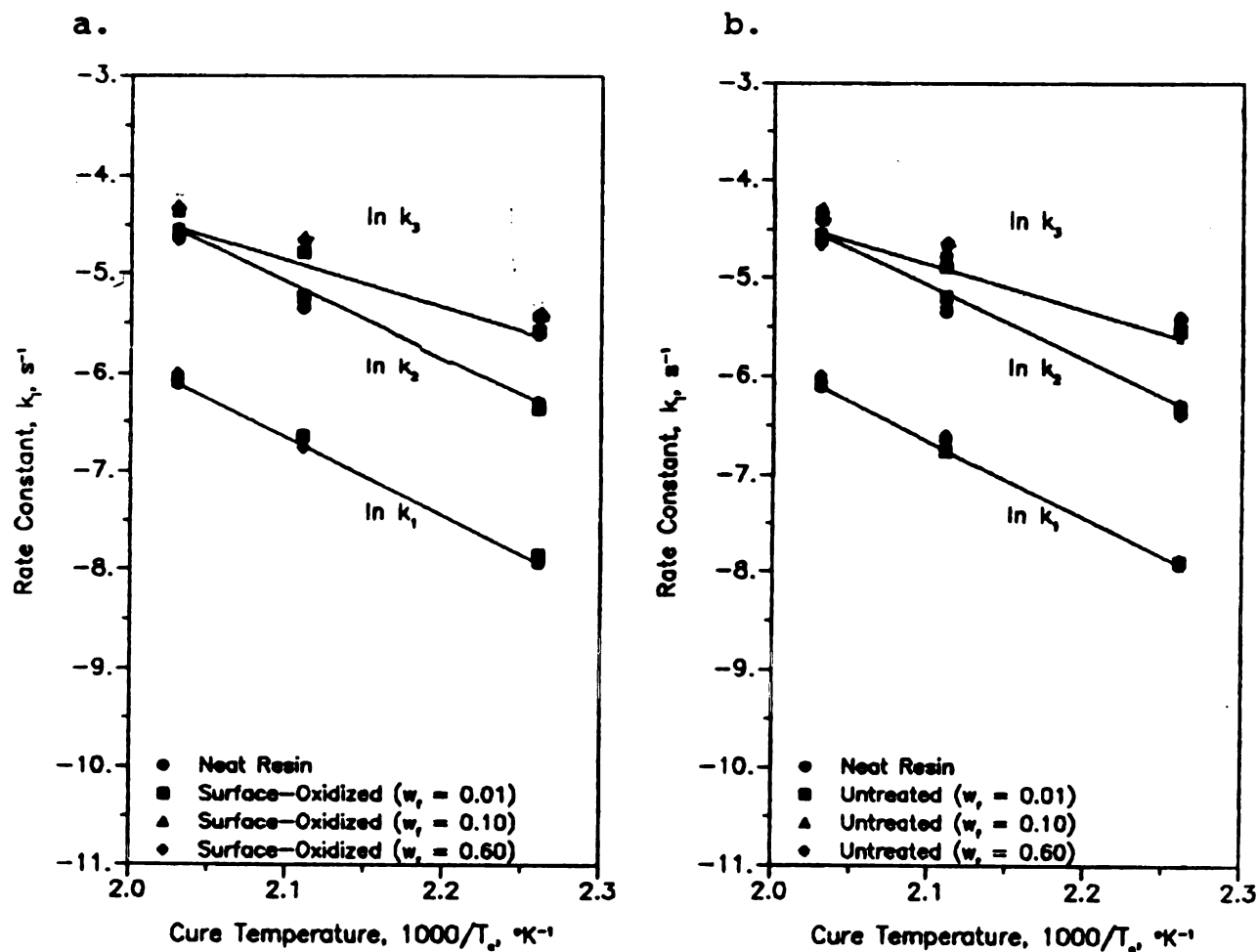


Figure III.18. Logarithm of the rate constants, k_1 , k_2 , and k_3 versus inverse absolute cure temperature, T_c , for: (a) untreated carbon-reinforced epoxy resin; and (b) surface-oxidized carbon-reinforced epoxy resins.

Values for neat and carbon-reinforced epoxy-resin reaction-rate constants, k_1 and k_2 , are given in Table III.7. Differences between neat and carbon-reinforced

epoxy-resin reaction-rate constants, k_1 and k_2 , showed no significant trends.

Table III.7. Reaction-rate constants, k_1 , k_2 , and k_3 , versus cure temperature, T_c , and fiber-weight fraction, w_f , for: (a) untreated carbon-reinforced epoxy resin; and (b) surface-oxidized carbon-reinforced epoxy resin.

a.						
T_c (°C)	k_1 (s. ⁻¹)		k_2 (s. ⁻¹)		k_3 (s. ⁻¹)	
	$w_f = 0$	$w_f = 0.01$	$w_f = 0$	$w_f = 0.01$	$w_f = 0$	$w_f = 0.01$
170	0.00036	0.00029	0.00177	0.00193	0.00038	0.00040
200	0.00119	0.00108	0.00508	0.00513	0.00107	0.00102
220	0.00237	0.00235	0.00958	0.00918	0.00199	0.00187
b.						
T_c (°C)	k_1 (s. ⁻¹)		k_2 (s. ⁻¹)		k_3 (s. ⁻¹)	
	$w_f = 0.1$	$w_f = 0.6$	$w_f = 0.1$	$w_f = 0.6$	$w_f = 0.1$	$w_f = 0.6$
170	0.00062	0.00049	0.00173	0.00176	0.00039	0.00035
200	0.00111	0.00117	0.00458	0.00495	0.00101	0.00097
220	0.00215	0.00253	0.00928	0.00872	0.00186	0.00177
b.						
T_c (°C)	k_1 (s. ⁻¹)		k_2 (s. ⁻¹)		k_3 (s. ⁻¹)	
	$w_f = 0$	$w_f = 0.01$	$w_f = 0$	$w_f = 0.01$	$w_f = 0$	$w_f = 0.01$
170	0.00036	0.00031	0.00177	0.00183	0.00038	0.00041
200	0.00117	0.00128	0.00508	0.00527	0.00107	0.00146
220	0.00237	0.00242	0.00958	0.00968	0.00199	0.00194

Table III.7 (continued)

T_c (°C)	k_1 (s. ⁻¹)		k_2 (s. ⁻¹)		k_3 (s. ⁻¹)	
	$w_f = 0.1$	$w_f = 0.6$	$w_f = 0.1$	$w_f = 0.6$	$w_f = 0.1$	$w_f = 0.6$
170	0.00036	0.00035	0.00175	0.00162	0.00043	0.00035
200	0.00119	0.00125	0.00507	0.00483	0.00104	0.00095
220	0.00225	0.00232	0.00918	0.00941	0.00183	0.00177

Cure-kinetic parameters for the crosslinking region, k_3 and D , were found by taking the logarithm of the crosslinking rate equation shown in Equation 14. Logarithm of the reaction rate multiplied by the quantity $(1 - \alpha)$ was defined as reduced crosslinking reaction rate, α_{red2} .

$$\alpha_{red2} = \ln \left[\frac{d\alpha}{dt} (1 - \alpha) \right] = \ln k_3 + D\alpha, \text{ where } \alpha \geq \alpha_{gel}. \quad (40)$$

The α_{red2} versus α curve for neat epoxy resin is shown Figure III.17(b). Higher α_{red2} values were observed at lower cure temperatures; this is due to decreasing reaction rates after gelation. The slope, D , at T_c of 170, 200, and 220°C appeared to be similar. A least-squares linear regression analysis was performed on Equation 40. The rate constant, k_3 , correlated with temperature according to the Arrhenius equation and is shown in Figure III.18. The α data fit the cure-kinetic model well, which was verified by obtaining correlation coefficients between 0.980 and 0.999.

Table III.7 shows that k_3 for carbon-reinforced epoxy resins was significantly lower than k_3 for neat epoxy resin. This is consistent with findings presented in Table III.6, which showed that carbon-fiber effects were physical. The reaction rate constant k_3 decreased with increasing w_f .

At low w_f , carbon-reinforced epoxy-resin rate constants were generally higher than neat epoxy-resin rate constants. This result was consistent with Dutta et al. [43] findings, shown in Figure II.13. They have claimed that carbon fibers helped promote or catalyze the crosslinking reactions.

The exponential kinetic parameter, D , decreased by a factor of four whenever carbon fibers are present in the epoxy resin. The change in D was due to the physical carbon-fiber effect. Initially, epoxy molecules and local viscosity were small. Polymerization reactions were not significantly affected. As the cure progresses, the network characteristic dimensions approach those of the carbon fibers and the local viscosity increased. Carbon fiber were added "barriers" to the already limited epoxy-molecule movement during the crosslinking reactions.

The frequency factor, A , and activation energy, E_A , for the neat and carbon-reinforced epoxy-resin rate

constants, k_1 , k_2 , and k_3 , are given in Table III.8. As the fiber weight fraction, w_f , increased, frequency factors and activation energies decrease. Frequency factor and activation energy decreases were probably due to chemical effects of the carbon fibers on the epoxy-resin cure.

Table III.8. Cure-kinetic parameters for the neat and: (a) untreated carbon-reinforced epoxy resin; and (b) surface-oxidized carbon-reinforced epoxy resin.

Neat	rate equation =
	$\frac{d\alpha}{dt} = (k_1 + k_2 \alpha) (1 - \alpha); \text{ for } \alpha \leq \alpha_{gel}$
	$\frac{d\alpha}{dt} = k_3 e^{-D\alpha/RT} (1 - \alpha); \text{ for } \alpha > \alpha_{gel}$
	where $k_1 = A_1 \exp(-E_1/RT)$,
	$k_2 = A_2 \exp(-E_2/RT)$,
	$k_3 = A_3 \exp(-E_3/RT)$,
	A_1 = frequency factors for k_1 ,
	A_2 = frequency factors for k_2 ,
	A_3 = frequency factors for k_3 ,
	E_1 = activation energy for k_1 ,
	E_2 = frequency factors for k_2 ,
	E_3 = activation energy for k_3 , and
	$\alpha_{gel} = 0.5$.
$A_1 = 26500$	$E_{A1} = 15.9 \text{ kcal/g}$
$A_2 = 31500$	$E_{A2} = 14.7 \text{ kcal/g}$
$A_3 = 26500$	$E_{A3} = 15.9 \text{ kcal/g}$
	$D = -2.0$

Table III.8 (continued)

a.

w_f	A			E_A (kcal/g)		
#	1	2	3	1	2	3
0.01	16600	24400	5700	16.1	14.6	11.8
0.10	16100	8820	567	15.5	14.7	10.2
0.60	15500	3650	418	15.2	13.5	10.3
$D_1 = -8.5$			$D_2 = -8.2$		$D_3 = -7.9$	

b.

w_f	A			E_A (kcal/g)		
#	1	2	3	1	2	3
0.01	17100	29400	5380	16.2	14.3	11.1
0.10	15500	13600	499	15.3	13.7	9.6
0.60	14500	7620	290	14.9	13.2	9.3
$D_1 = -8.6$			$D_2 = -8.6$		$D_3 = -8.2$	

Frequency factor decreases were caused by a more-ordered or less-entropy system. Ten-percent decreases in entropies were caused by acidic carbon-fiber surface groups attracting epoxy molecules. This attraction restricted the movement of the epoxy molecules and created a more-ordered system. Table III.9 shows entropy differences were

polymerization reactions and significant during crosslinking reaction.

Table III.9. Calculation of the entropy for: (a) untreated carbon-reinforced epoxy resin; and (b) surface-oxidized carbon-reinforced epoxy resin.

Arrhenius temperature law: $k = A e^{E_A/RT}$;

From the transition theory [95],

$$k = \frac{k' T}{h} e^{\delta S/R} e^{-\delta H/RT}$$

Therefore,

$$A = \frac{k' T}{h} e^{\delta S/RT};$$

where k' = Boltzmann constant,
 T = absolute temperature,
 h = Planck constant, and
 R = universal gas constant.

a.

W_f	A			$\delta S (\text{kcal/gmol}^\circ\text{K})$		
#	1	2	3	1	2	3
0.0	26500	31500	26500	-57	-57	-57
0.01	16600	24400	5700	-58	-58	-60
0.10	16100	8820	567	-58	-58	-65
0.60	15500	3650	418	-58	-58	-65

Table III.9 (continued)

b.

w_f	A					
#	1	2	3	1	2	3
0.0	26500	31500	26500	-57	-57	-57
0.01	17100	29400	5380	-58	-57	-60
0.10	15500	13600	499	-58	-58	-65
0.60	14500	7620	290	-58	-58	-66

Activation energy decreases were believed to be caused from hydrogen-donor groups present on carbon-fiber surfaces catalyzing cure reactions. Such fiber-matrix bonding has been suggested by other experimenters [5,55,65]. Moroni et al. [55] have used FTIR spectroscopy to determine hydrogen-bonding occurred between carbon-fiber surface groups and epoxy molecules. Both Horie and Fitzer [5] have studied carbon-reinforced epoxy resins and also proposed hydrogen bonds exist between carbon-fiber surface groups and epoxy molecules. Garton et al. [65] have used FTIR spectroscopy and reported polymerization reactions were influenced by carbon-fiber surface groups.

Table III.10 shows that good agreement between this study's activation energies and literature values.

Average-reported activation energiers for catalyzed polymerization reactions, E_{A1} , for stoichiometric epoxy resins were 17.0 ± 3.8 . Average reported activation energies for autocatalyzed polymerization reactions, E_{A2} , for stoichiometric epoxy resins were 13.9 ± 1.8 .

Table III.10. Comparison of activation energy, E_A , for epoxy resins modeled with the autocatalytic cure-kinetic equation given in Equation 13.

Experimenter(s)	Resin System	E_A (kcal/gmol)
Kamal et al. [55]	DGEBA-DDS	14.8, 14.5
Horie et al. [55]	"	13.9, 13.4
Sourour et al. [40]	"	20.0, 11.0
Monori et al. [55]	"	13.5, 12.0
Mijovic [44]	"	22.0, 16.0
Smith et al. [55]	DGEBA-amine ^a	14-16
Kil et al. [55]	"	14.2, 14.4
Prime [32]	"	11-14
Average E_{A1}		17.0 ± 3.8
Average E_{A2}		13.9 ± 1.8

a - amine other than DDS

Table III.10 shows activation energies found by Sourour et al. [40] and Mijovic [44] were high when compared to other activation-energy values. Inspection of their data suggested that Sourour et al. and Mijovic et al. used α data greater than $\alpha_{g,1}$ to model k_1 and k_2 . These α data were influenced by crosslinking reactions. Since crosslinking reaction rates are slower than polymerization

reaction rates, Sourour et al. and Mijovic et al. obtained rate constants with higher frequency factors and activation energies.

Frequency factors and activation energies found in this study for carbon-reinforced epoxy resins were compared with cure-kinetic parameters reported by Mijovic [44] for a 40-percent glass-reinforced epoxy resin. Table II.5 showed Mijovic found a 98- to 99-percent frequency-factor decrease and a 23- to 35-percent activation-energy decrease for glass-reinforced epoxy-resin cures relative to neat epoxy-resin cures. Their kinetic parameters followed trends identical to trends found in this study. His reinforced rate constants have decreased frequency factors and activation energies relative to neat epoxy-resin cure-kinetic parameters. Mijovic attributed these decreases in A and E_a to glass fillers restricting the mobility of unreacted epoxy molecules.

Dutta et al. [43] findings were compared with this study's results. They DSC-cured a neat, glass-filled and carbon-filled epoxy resins. Their reinforced epoxy-resin formulation contained one-, two-, four- and six-percent filler concentration. They modelled reaction rates with a single autocatalytic equation and rate constants as third- and fourth-order functions of filler content as shown in Section II.C.3.c. The glass-reinforced epoxy resins showed

a maximum reduction in E_a for k_1 from 15.4 to 14.4 kcal/mol [32]. The E_a reduction they reported was consistent with results of this study.

Figure II.12 showed Dutta et al. [43] carbon- and glass-reinforced epoxy-resin rate constants, k_1 and k_2 , decreased to a minimum value at two-percent filler concentration relative to neat epoxy-resin rate constants. Above this filler concentration rate constants increased and leveled off to a constant value, which was not significantly different than neat epoxy-resin rate constants. These results were inconsistent with findings of this study.

Two major conclusions drawn from this cure-kinetic study were summarized as follows. First, carbon fibers have a physical effect on epoxy-resin cure kinetics. As more carbon-fibers were added to epoxy resins, gelation times increased and reaction rate constants k_2 decreased. These results implied carbon fibers "hindered" epoxy molecules and slowed crosslinking reactions. Secondly, the carbon-fiber surface treatment have a small effect on epoxy-resin cure kinetics. Frequency factors and activation energies for carbon-reinforced epoxy resins decreased relative to neat epoxy-resin values. These results implied that carbon-fiber surface groups attracted epoxy molecules catalyzed cure reactions.

f. Glass Transition Temperature, $T_g(\alpha)$

After isothermally curing neat and carbon-reinforced epoxy resins, glass transition temperatures were found. A comparison between neat and carbon-reinforced resins was conducted to determine whether the epoxy-resin bulk matrix changed.

In the liquid state, molecular structure is disordered and atoms do not behave with the regularity exhibited in the glassy state. In the glassy state, however, molecules are ordered and atoms move around equilibrium positions. In glassy state, large-scale molecular motion does not occur, but atoms or small groups of atoms move against local restraints of secondary bond forces. The glass transition temperature, T_g , corresponds to the transition from liquid-like movement which is characteristic of the liquid state to limited movement which is characteristic of the glassy state.

Neat and carbon-reinforced epoxy-resin samples were isothermally cured at temperatures ranging from 170°C to 250°C. Initially, liquid epoxy resins polymerized and the T_g increased with increasing extent of cure, α [80]. When the T_g equaled the cure temperature, T_c , vitrification occurred. During vitrification the epoxy resin became glass-like and diffusion-controlled crosslinking reactions

began. Further curing beyond vitrification caused increased glass transition temperatures above the T_c . When no further reaction exotherm was detectable with DSC, isothermal cures were terminated. Following cure, samples were scanned at 10°C/min to observe the T_g .

The ultimate glass transition temperature, $T_{g,ult}$ is defined as the maximum T_g when all epoxy molecules have reacted. At cure temperatures below the $T_{g,ult}$, epoxy-resin samples were undercured and formed loose-network structures. DSC analyses performed on these undercured specimens showed an "overshoot" in the heat flow versus temperature diagram. This "overshoot" was explained by a free-volume changes as the temperature increases. Liquid-like motion of atoms in the rubbery state requires more free volume than short-range excursions of atoms in the glassy state.

Since the fully-extended chain is the conformation of minimum energy, it occurred more frequently during isothermal cures below $T_{g,ult}$. The free volume was defined as [33]

$$\begin{aligned} f &= f_g + (T - T_{g,ult}) \delta\alpha_e & \text{for } T \geq T_{g,ult} & \text{ or} \\ f &= f_g & \text{for } T < T_{g,ult} & , \end{aligned} \quad (41)$$

where $\delta\alpha_e$ = change in volume expansion coefficient and f_g = free volume at temperatures below $T_{g,ult}$.

The volume expansion coefficient, α_v , is a measure of the amplitude of molecular vibrations with temperature. As cure temperatures increased, cured epoxy resins have more crosslinked chains. When samples were heated beyond the $T_{g_{ult}}$, epoxy molecules became more energetic and increased in volume. This rapid increase in energy manifested itself as an "overshoot" on DSC heat flow versus temperature diagram as shown in Figure III.19(a). As temperatures increased, cured epoxy resins remained in a crosslinked-chain conformation and little or no "overshoot" was seen as shown Figure III.19(g).

A difference of 20°C was found between T_g and T_c for samples isothermally cured below $T_{g_{ult}}$. This trend has been reported for similar epoxy resins [32,40]. During low temperature cures, epoxy resins vitrified prior to completion of polymerization reactions. At low cure temperatures, reduced molecular energy slowed diffusion of reactive species in the glassy matrix and decreased the amount of cure reactions.

Glass transition temperature versus T_c data for neat, untreated carbon-reinforced, and surface-oxidized carbon-reinforced epoxy resins are shown in Figure III.20. A comparison of Figure III.11 and III.20 show that precuring epoxy resins, during fiber impregnation, prior to cure decreased the final T_g from 230°C to 225°C.

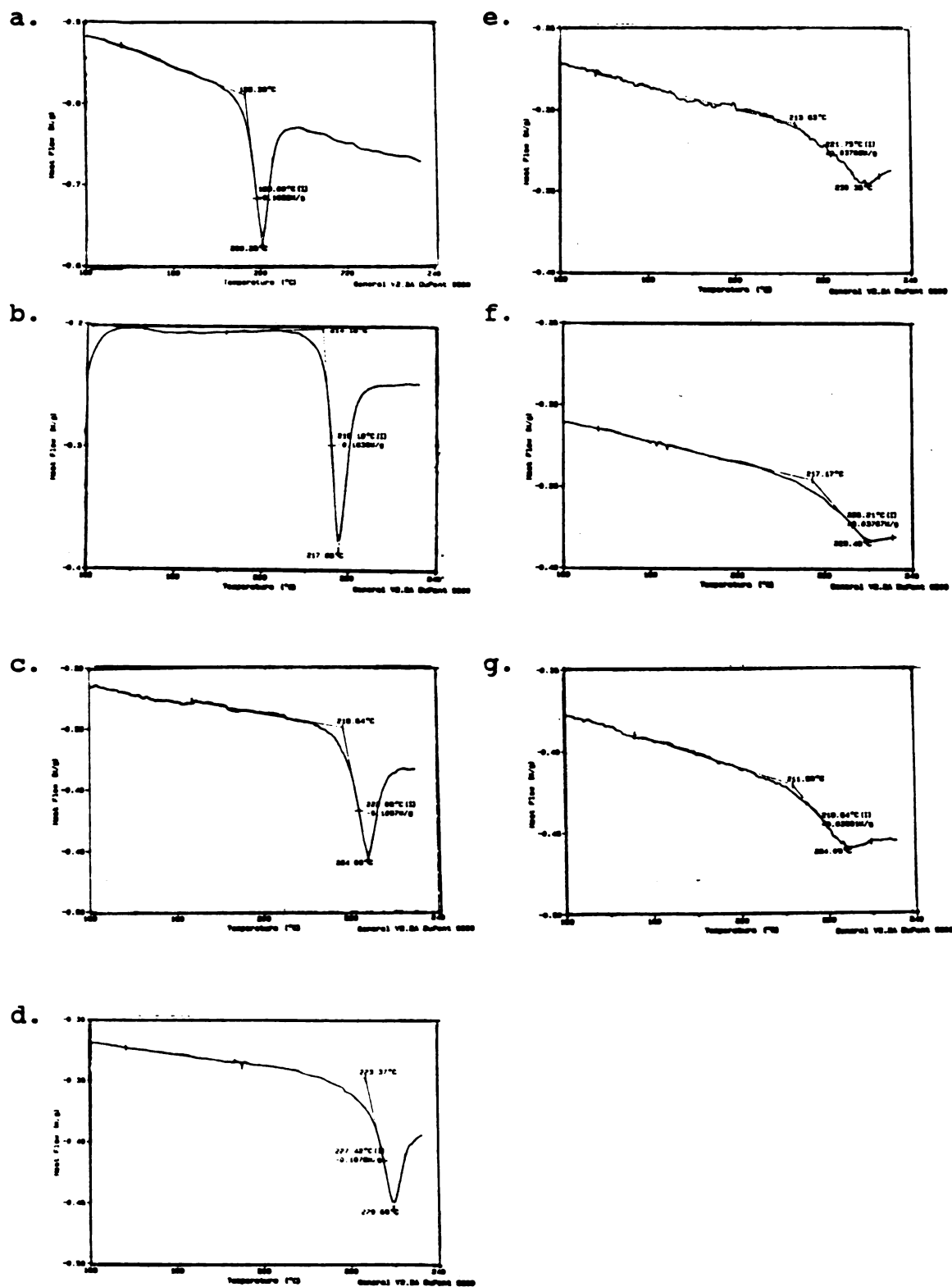


Figure III.18. DSC analyses of fully-cured epoxy resin at: (a) 170°C; (b) 190°C; (c) 200°C; (d) 210°C; (e) 220°C; (f) 230°C; and (g) 250°C.

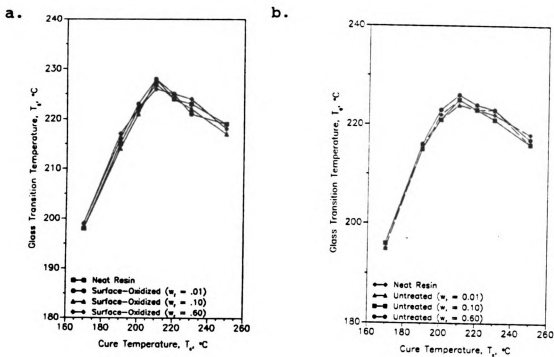


Figure III.20. Glass transition temperature, T_g , versus cure temperature, T_c , for: (a) untreated carbon-reinforced epoxy resin; and (b) surface-oxidized carbon-reinforced epoxy resin.

Figure III.11(b) shows that the highest T_g of 225°C occurred at a T_c equal to 210°C. Epoxy resins cured above 210°C show a decreased T_g . Note that T_g equal to $T_{g_{ult}}$ of 230°C was not attained. This can be explained by rearrangement of crosslinked epoxy-resin networks and degradation of samples prior to completion of cure reactions.

Glass transition temperatures given in this study were inconsistent with findings reported by Ko [17]. He found a 25°C increase in the T_g for untreated carbon-reinforced

epoxy resins and 45°C increase in T_g for surface-oxidized carbon-reinforced epoxy resins relative to the T_g for neat epoxy resins. He believed epoxy molecules adsorbed on graphitic basal planes of carbon-fiber surface and created an epoxy-amine gradient in the fiber-matrix interphase.

These difunctional epoxy-resin T_g results were also indifferent with Wang et al. [74]. They found carbon-fiber effects on tetrafunctional epoxy-resin cures did not change the epoxy-resin glass transition temperatures; but, carbon-fiber effects on difunctional epoxy-resin cures reduced glass transition temperatures by 25°C. They have concluded epoxy-resin functionality plays a large role in the matrix network formation.

This study showed no significant differences existed between glass transition temperatures of neat and carbon-reinforced epoxy resins. Therefore, regardless of the carbon-fiber type or content added to epoxy resins, identical crosslinked matrices resulted.

g. Reproducibility and Accuracy

Sample preparation was the major cause of variability in the reproducibility and accuracy of this study. The following sample-preparation techniques were investigated: 1. hardener addition, 2. fiber impregnation, 3. prevention of environmental contamination, and 4. transmission- and DRIFT-FTIR spectroscopy.

(1) Hardener Addition

The powdered hardener was dissolved in the epoxy resin prior to curing. The purpose of these experiments was to determine: (1) How the cure characteristics of a non-stoichiometric epoxy-resin compares to the cure characteristics of a stoichiometric epoxy resin; and (2) if the epoxy resin partially cures prior to DSC-curing or convectional-oven curing.

(a) Stoichiometric Variations

A stoichiometric epoxy resin consisted of 35.8 grams of DDS 100 grams of DER 332 epoxy monomer. The precision of the analytical balance used to measure the reactants was ± 0.5 mg. Assuming error occurred during mixing or measuring, slight non-stoichiometric mixtures with epoxy-amine equivalent ratios of 1:1.01 and 1:0.99 were prepared.

Then, these unstoichiometric samples were isothermally DSC-cured and DSC-analyzed to obtain the extent of cure and glass transition temperature, T_g .

The extent of cure, α , and T_g for each nonstoichiometric specimens were compared with the α and T_g for a stoichiometric epoxy resin. No significant difference in α or T_g was observed between the stoichiometric and either non-stoichiometric epoxy resin.

(b) Extent of Cure, α

The purpose of this experiment was to determine if the epoxy resin partially cures prior to DSC-curing or convectional-oven curing. In order to combine the liquid epoxy monomer and powdered hardener, the hardener was dissolved in the epoxy monomer by heating the epoxy resin from 100°C to 130°C over a period to approximately five minutes. A DSC analysis which simulated heating during the mixing process was performed. The average DSC-analyzed extent of cure, α , after hardener addition equalled 0.05.

The extent of cure, α , after hardener addition was also analyzed with FTIR spectrometer. Totally unreacted epoxy resins were prepared by measuring stoichiometric amounts of epoxy monomer and hardener, then dissolved each in acetone. Next, these stoichiometric acetone-dissolved

epoxy monomer and hardener mixtures were combined. Several drops of this uncured mixture were placed and allowed to dry on a KBr plate.

FTIR-transmission spectra of this uncured mixture and neat epoxy resin were performed. Equation 27 was used to calculate FTIR-spectroscopy epoxy-intensity ratios. The average FTIR-spectroscopy α after hardener addition equalled 0.11.

These results showed that the epoxy resin was precured between five and eleven percent after hardener addition. Why the FTIR data differs from the DSC data will be considered in Section III.D.g.(4).

(2) Fiber Impregnation

Commerical fiber composites were often made from laminates. A laminate is defined as several layers of prepregs or sheets of fibers impregnated with epoxy resin. In this study, a prepreg was created by pulling a carbon fiber bundle through a prepregger-resin vat of liquid epoxy resin and winding the impregnated fiber bundle on a mandrel.

The extent of cure, α , for the prepreg was determined from the residual exotherms of several 80°C oven-aged

epoxy-resin samples. The term "residual exotherm" refers to the magnitude of the remaining exotherm as measured by DSC after the epoxy resin is partially cured. DSC analyses of the residual exotherms for a stoichiometric epoxy resin cured at 80°C gave the α versus time, t , data shown in Figure III.21. Since the average residence time in the prepregger-resin vat was estimated at two hours, the curve was integrated after two hours to give an α equal to ten percent.

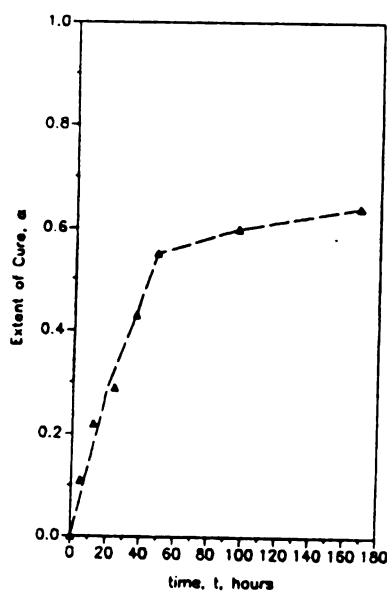


Figure III.21. Extent of cure, α , versus time, t , for a neat epoxy resin cured at 80°C.

The extent of cure after fiber impregnation was also analyzed with the FTIR-spectrometer. A thin film of the epoxy resin from the prepregger-resin vat was cast on a KBr plate and analyzed with the FTIR spectrometer. The

difference between this epoxy resin and the stoichiometric acetone-dissolved uncured epoxy mixture described in Section III.2.g.(3) as measured from the transmission-FTIR analysis was 13 percent.

The α data after hardener addition and fiber impregnation as measured by DSC and FTIR spectroscopy is summarized in Table III.11. The difference between the DSC and FTIR-spectroscopy data was considered insignificant since Section III.E.e.g(4) shows that the experimental error of the transmission-FTIR spectroscopy data was eight percent.

Table III.11. Extent of cure, α , after hardener addition and fiber impregnation.

	DSC	FTIR-Spectrometer
After Hardener Addition	0.05	0.11
After Fiber Impregnation	0.10	0.13

(3) Prevention of Environmental Contamination

Protecting samples from environmental contamination was imperative. A five-percent decrease in total reaction exotherm, H_r , was seen when the epoxy resin was not

contained in a desiccator. Reduced H_f due to adsorbed volatiles from the environment have been reported by other investigators [25,32].

Initially, neat and carbon-reinforced samples were stored in dry ice at -40°C to facilitate handling and prevent premature curing. Stored samples were assumed to absorb water or volatiles from the dry ice. Drzal et al. [25] reported that the major epoxy-resin absorbate is water and minor absorbates are carbon dioxide and carbon monoxide. They implied that the absorbates diffuse into the free volume present in the epoxy resin and associate with hydroxyl groups present in the network. Absorbed volatiles were believed to interfere with the hydroxyls causing a reduction in the number of cure reactions and forming a looser matrix network.

Isothermal-DSC analyses showed a two-percent decrease in the total reaction exotherm, H_f , for a carbon-reinforced sample with a 0.10 fiber weight fraction, w_f , when compared with non-contaminated samples [96]; whereas, the H_f for a carbon-reinforced sample with a 0.60 w_f was reduced by ten percent relative to a non-contaminated samples. Corresponding glass transition temperatures for contaminated samples with a 0.10 w_f showed a 5°C decrease relative to non-contaminated samples; whereas, the T_g for

carbon-reinforced samples with a 0.60 w_f was reduced by 10°C relative to non-contaminated sample.

This decrease in T_g was consistent with the results of Brant [32]. He found a 10°C decrease in T_g for epoxy resins which were exposed to water. Drzal et al. [25] and Peyser et al. [81] also reported a decrease in T_g for water-absorbed epoxy resins.

Reduced total reaction exotherms and glass transition temperatures for the contaminated reinforced resin cures suggested that absorbed volatiles interfere with the polymerization and crosslinking reactions. The greater reduction in the total reaction exotherms and glass transition temperatures for 0.60 w_f carbon-reinforced samples suggest that volatiles adsorb more readily on the carbon-fiber surface than in the epoxy resin. After dry ice was found to contain volatiles which reduce the H_f and T_g , the dry ice was not used for sample preparation. Instead, a desiccator was used to store the epoxy resin sample prior to DSC-cured convectional curing.

(4) Transmission- and DRIFT-FTIR Spectroscopy

In this study, stoichiometric epoxy resins were DSC-cured and compared with literature values. Excellent agreement was found; therefore, the DSC experimentation and

methodology appeared to accurately characterize the thermal and kinetic cure parameters. As Figure III.15 shows, the FTIR-spectroscopy α results differed from the DSC- α results. Uncured epoxy-resin data from transmission-FTIR spectroscopy analyses and cured epoxy resin data from diffuse-reflectance, DRIFT, FTIR spectroscopy analyses were not as accurate.

Hamadeh et al. [86] found that obtaining accurate FTIR-spectroscopy measurements were difficult due to numerous variables that affect the reproducibility of sample preparation. As Table C.2 shows, poor reproducibility existed among the FTIR-spectroscopy data. This lack of accuracy in FTIR-spectroscopy data was assumed to be due to the sample make-up and poor sample preparation [97].

Mertzel [85] and Cole [29] stated that the variability of film thicknesses on the KBr plates is the major cause of variation among transmission-FTIR spectra. Young et al. [83] also reported that transmission-FTIR spectroscopy was subjected to substantial error caused from non-uniform film thickness. Differences between the reference-intensity ratio, $1146\text{ cm}^{-1}/1184\text{ cm}^{-1}$, between two identical transmission-FTIR sample spectra were acceptable at four

percent. Table III.12 shows that the error for the epoxy-intensity ratio, $916\text{ cm}^{-1}/1184\text{ cm}^{-1}$, was unacceptable at thirteen percent.

Table III.12. FTIR-spectroscopy sample-preparation errors.

Relative Standard Deviation Between FTIR-Spectroscopy Intensity-Peak Measurements [‡]		
Sources of Error	Epoxy Peak [*] (%)	Reference Peak ⁺ (%)
Transmission: Uniform Film Thickness	13	4
DRIFT:		
Particle Size	24	4
Particle-Size Distribution	17	2
Packing Density	15	1
Day-to-Day Reproducibility	28	3
Sample Concentration	45	2
Using a Broader Baseline	17	1
No Liquid N ₂ Purge of FTIR-Spectroscopy Chamber	11	1
& - experimental data for these results can be found in Table C.2. * - epoxy-intensity ratio = $(916\text{cm}^{-1}/1184\text{cm}^{-1})$ + - reference-intensity ratio = $(1146\text{cm}^{-1}/1184\text{cm}^{-1})$		

According to Mertzel [85], DRIFT-FTIR spectroscopy has been successfully used for the study of surfaces and bulk materials. Mertzel et al. also emphasized that careful control of the sample preparation must be practiced to

achieve reproducible measurements in the infrared examination.

DRIFT-FTIR spectra gave acceptable differences among reference-intensity ratios between one to four percent. Unfortunately, as Table III.11 shows, the small but important cured epoxy-intensity ratios gave large experimental errors.

Two consecutive spectra of the same sample gave epoxy-intensity ratios which differed by fifteen percent. This difference in epoxy-intensity ratios are believed to be caused from the dissimilar packing of the sample powder in the sample holder.

FTIR spectra of a specimen with large-particle sizes gave inaccurate spectral intensities. Larger peaks, such as the reference-intensity peak at 1184 cm^{-1} , gave reduced intensities relative to smaller peaks. These findings were consistent with Fuller et al. [28]. Their results also showed that FTIR-spectra bandwidths and relative intensities change considerably with particle size.

Next, studies were conducted to determine sources of variation. Obtaining FTIR-spectra of fine and coarse specimen particles showed a maximum epoxy-intensity ratio difference of 24 percent. FTIR-spectroscopy analyses of a

sample containing a wide particle distribution (ie. fine and coarse specimen particles) tended to give spectral intensities which varied by seventeen percent.

Environmental contamination was considered. Samples were analyzed before and after a 24-hour exposure to 25°C and 50 percent relative humidity environment. A 28-percent decrease in the FTIR-spectroscopy epoxy-intensity ratio was found.

In conclusion, the maximum difference in the epoxy-intensity ratio among the different particle sizes, particle-size distributions, packing density, and moisture absorption were 24, 17, 15 and 28 percent, respectively. Variables such as particle size, particle-size distribution, packing density, and moisture content affected the scattering coefficient, s , in the Kubelka-Munk equation shown in Equation II.32. Presumably, dry small, evenly-distributed particles loaded into a sample cup as a loose powder were more closely packed yielded a smaller s . A smaller s would decrease the absorbance signal, and therefore, produces a better spectra.

Other experimenters [27,83,86,97] have experienced similar problems. Sellitti et al. [27] used FTIR spectroscopy to study carbon-reinforced epoxy composites and claimed that analyses were difficult due to severe

scattering and high carbon-fiber absorptivity. Painter et al. [97] also found that obtaining reproducible FTIR-spectroscopy data was greatly effected by sample preparation procedures. Hammadeh et al. [86] could not obtain reproducible DRIFT-FTIR spectroscopy data and recommended using a Wig-L-Bug to obtain suitable DRIFT-FTIR spectroscopy samples with uniform particle size and particle-size distribution.

Cole et al. [29] claimed that the DRIFT-FTIR spectra of carbon-reinforced epoxy composites are not accurately characterized because of complications arising from the reflective effects of the carbon fibers. They found poor data reproducibility and reported a relative standard deviation between the epoxy-intensity peaks as high as 15 percent.

In summary, neither transmission- nor DRIFT-FTIR spectroscopy were perfected. These FTIR analyses were too variable to obtain quantitative thermal or kinetic data due to errors caused by sample preparation and carbon-fiber absorbance. Therefore, the FTIR-spectroscopy data was only used to qualitatively verify DSC extent of cure data.

CHAPTER IV

CONCLUSIONS

Effects of carbon fibers on the epoxy-resin cure were determined and results were compared with published data. Long, high-strength, untreated and surface-oxidized carbon fibers were added to an epoxy resin in concentrations equal to 0.01, 0.10, and 0.60. DSC and FTIR-spectroscopy analyses were conducted to obtain extents of cure, glass transition temperatures, and cure kinetics. It was determined that the addition of carbon fibers to an epoxy resins: (1) did not cause more or less epoxy molecules to react; (2) did not significantly affect thermal cure characteristics; and 3) did significantly affect kinetic-cure parameters.

Major conclusions of the literature review were summarized as follows:

1. Carbonyls and carboxyls are the most prevalent carbon-fiber surface functionalities [6-8,18,21,24,27]. Surface-oxidized carbon fibers contained twice as many functional groups as untreated carbon fibers. Many experimenters have

reported that physical and chemical interactions between carbon fibers and epoxy resin exist [2,5,25,55,65].

2. This region, where physical and chemical interactions existed, is called the fiber-matrix interphase. The fiber-matrix interphase has been described as the three-dimensional region between the bulk epoxy matrix and a carbon fiber, which included the two-dimensional interface [4].

3. Cure kinetics for an epoxy-resin cure were modeled with the following two equations [52,57-60]:

$$\frac{d\alpha}{dt} = (k_1 + k_2 \alpha) (1 - \alpha); \text{ for } \alpha \leq \alpha_{gel} \quad (13)$$

$$\frac{d\alpha}{dt} = k_3 e^{-D\alpha/RT} (1 - \alpha); \text{ for } \alpha > \alpha_{gel} \quad (14)$$

where $k_i = A_i \exp (-E_i/RT)$,

A_i = frequency factors for k_i ,

E_i = activation energy for k_i ,

$\alpha_{gel} = 0.48$.

Initially, the reaction rate was modelled with

Equation 13, which represented the rate-controlled autocatalytic-polymerization reactions. At a particular extent of cure, gelation occurred and increased local viscosity and steric hinderance of the reactants was found [32-34,40,44]. Following gelation, the diffusion-limited crosslinking reactions dominated and reaction rates were modelled with Equation 14.

4. Neat versus reinforced epoxy-resin cures have been discussed in the literature. Results from such studies were summarized as follows: (1) Dutta et al. [43] had found that glass-reinforced epoxy-resin cures gave 12-percent higher extents of cure relative to neat epoxy-resin cures; but carbon-reinforced epoxy-resin cures gave extents of cure which were not significantly different than neat epoxy-resin cures; (2) Wang et al. [74] cured neat and carbon-reinforced difunctional and tetrafunctional epoxy resins and found that reinforced difunctional epoxy resins a maximum of 25°C reduction in glass transition temperature, T_g , relative to neat epoxy resins, and reinforced tetrafunctional epoxy-resin glass transition temperatures were not significantly different than neat epoxy resins; (3) Ko [17] had used various carbon fibers for reinforcements to find that glass transition temperatures for high-strength carbon-reinforced epoxy composites 25°C higher than glass transition temperatures for neat epoxy resins and concluded that the T_g was affected by fiber type; and (4) Mijovic [44] have studied a glass-reinforced epoxy resin and found a 98- to 99-percent frequency-factor decrease and a 23- to 31-percent activation-energy decrease relative to neat epoxy resins.

Major conclusions of the experimental study were summarized as follows:

1. Experimental DSC full-cure extent of cure data showed no significant difference between the neat and carbon-reinforced epoxy resins. FTIR-spectroscopy full-cure extent of cure data were also inconclusive in detecting any difference between neat and carbon-reinforced epoxy resins. These findings were consistent with carbon-reinforced epoxy-resin results of Dutta et al. [43]. Small changes in reaction exotherm and chemical structure due to fiber-matrix interactions can not be measured by DSC and FTIR, a more "interphase-specific" instrument was needed.

2. No significant difference was found between glass transition temperatures for neat, untreated carbon-reinforced, and surface-oxidized carbon-reinforced epoxy resins. Similar glass transition temperatures suggested that similar network formation occurred in the bulk-epoxy matrix. The glass transition temperature, T_g , results presented in study were different than results given by Wang et al. [74] and Ko [17]. Wang et al. [74] cured neat and reinforced difunctional epoxy resins and found a 25°C T_g reduction for the reinforced formulations. Ko [17] found a 45°C T_g increase for high-modulus carbon-reinforced epoxy resins and a 25°C T_g increase for high-strength carbon-reinforced epoxy resins relative to neat epoxy resins. Ko concluded the fiber type, not the fiber surface, affected glass transition temperatures.

3. Fully-reacted extents of cure for neat and carbon-reinforced epoxy resins were integrated over time.

Gelation times increased to a maximum of ten percent when the fiber-weight fraction increased to 0.60. At gelation, the movement of unreacted epoxy molecules was restricted by concurrent local increases in viscosity and steric hindrance of reactants. This physical carbon-fiber effect created another "barrier" the epoxy molecules must encounter and lengthened the epoxy-resin cure.

4. The diffusion-controlled crosslinking reaction rate constant k_3 decreased with increasing fiber-weight fraction. The maximum decrease relative to the neat epoxy resins occurred at ten percent when the fiber-weight fraction equalled to 0.60. This result also showed carbon fibers affected the epoxy molecules' mobility in an epoxy-resin cure.

5. An Arrhenius-temperature model of these reaction rate constants showed frequency factors decreased by 99 percent and activation energies decrease by 35 percent with increased fiber-weight fractions. Decreased frequency factors and activation energies were attributed to a chemical effect of carbon-fiber surface groups on epoxy-resin cure reactions. Decreased frequency factors were likely caused from polar carbon-fiber surface groups attracting polar groups in the epoxy resin. Decreased

activation energies were caused from carbon-fiber surface groups catalyzing epoxy-resin cure reactions. Such fiber-matrix bonding has been investigated by other experimenters [5,55,65]. Reduced frequency factors and activation energies were consistent with Mijovic [44]. He has shown that carbon-reinforced resins have 99-percent frequency factor decreases and 21-35 percent activation-energy decreases relative to frequency factors and activation energy decreases for neat epoxy resins. Surface-oxidized carbon-reinforced epoxy resins showed that frequency factors and activation-energies were decreased by approximately ten percent relative to untreated carbon-reinforced epoxy resins. These decreases were expected since surface-oxidized carbon fibers contained twice as many polar surface groups as untreated carbon fibers.

6. This study did not confirm whether chemical reactions occurred in the fiber-matrix interphase. This study did show that using DSC and FTIR spectroscopy to analyze cured epoxy composites can not give quantitative fiber-matrix interphase cure characteristics. "Interphase-specific" instrumentation must be used, such as an X-ray Photoelectron Spectroscopy, XPS.

7. Recently, XPS study performed by Hooke [89] showed a small, but significant change subsequent to reaction with

a thermally-heated epoxy. There was an approximate three-to five-percent increase in the carbonyl concentration at the carbon-fiber surface. This increase indicated a chemical interaction between carbon fiber and epoxy molecule. The XPS result further supported this study's finding that a chemical carbon-fiber effect existed.

The amount of carbon fibers and the carbon-fiber surface treatment had a small, but significant effect on the epoxy-resin cure kinetics. Kinetic differences between neat and carbon-reinforced epoxy-resin cures were explained by carbon fibers possibly restricting the molecular mobility of reactants and forming chemical interactions with epoxy molecules. These carbon-fiber effects were considered significant because a composite material's performance is highly dependent on interactions in the fiber-matrix interphase.

CHAPTER V

RECOMMENDATIONS

A major problem encountered in this experimental study was the inability of the DSC and FTIR spectrometer to give quantative "interphase-specific" data. This problem will be addressed and accompanied with suggestions. Then recommendations for alternative curing methods will be presented based on insight obtained from this study.

A. Problems and Suggestions

A major difficulty found in this study was that experimental techniques used were not "interphase-specific". Differential scanning calorimetry analyses were not sensitive enough to detect the small variations in the reaction exotherm; FTIR-spectroscopy methods were not precise enough to accurately detect the variations in the chemical structure of the fiber-matrix interphase.

Two high-vacuum techniques, not accessible at the start of this research project, now available in the Composite Materials and Structures Center Laboratory at Michigan State University, are the electron spectroscopy

for chemical analysis, ESCA, and Auger spectroscopy. Both instruments are "interphase-specific".

ESCA- and Auger-spectroscopy techniques irradiate the specimen with an incident beam set at a grazing angle to the sample surface. ESCA bombards the sample surface with monoenergetic x-rays and ejects inner, 1s, 2s, and 2p, electrons from various atomic levels. Auger spectroscopy bombards the surface with high-energy electrons and an inner electrons are ejected. The vacancy is filled by an outer electron and energy is released which causes an Auger electron to be ejected. The energy of the ejected electrons is determined by means of an electron spectrometer which quantifies the chemical structure of the sample surface. Unfortunately, neither the ESCA nor Auger spectroscopy are "non-destructive". They require the interphase to be fractured to expose the sample surfaces.

According to Sellitti et al. [27], an analytical technique which can satisfactorily characterize the carbon-epoxy interphase must be "interphase-specific" and "non-destructive". Both Sellitti et al. [27] and Garton et al. [65] claimed that FTIR internal reflection spectroscopy, IRS, was both "interphase-specific" and "non-destructive".

Other FTIR-spectroscopy techniques that show promise are using microscope and heating attachments with

transmission-FTIR spectroscopy. These attachments would allow the epoxy-resin to be cured while focusing on a region as small as 10 Å in diameter [87]. These two FTIR-spectroscopy techniques would enable the experimenter to obtain a spectra of the fiber-matrix interphase at various cure times and use these data to model the cure kinetics.

Today, a complete understanding of the carbon-epoxy interphase falls short of being fully adequate to control and optimize the composite interphase. The critical gaps in knowledge are primarily related to the detailed structure of the interphase and its implication with respect to chemical and mechanical behavior. The delicacy and dimensional scale of the fiber-matrix interphase make them very difficult to address experimentally.

One of the more promising experimental approaches to these problems is through the use of scanning tunneling microscopy, STM. In the past, STM has been applied to atomic imaging of carbon fibers [5]. Commercial STM instruments are available which are capable of producing images ranging from atomic resolution up to areas of square micrometers. Sophisticated tools, such as the STM, could make it possible to obtain the information about the carbon surface-defect structure and epoxy-resin chemistry required to formulate valid quantitative theories of the fiber-matrix interphase.

This study and recommendations should help future experimenters gain insight on how to better study composite interphases. In the next section, several suggestions will be given which may also assist in further composite research and experimentation.

B. Further Research

The major problem facing epoxy manufacturers is achieving a fast, efficient, and uniform epoxy-resin cure. Today, conventional curing is limited to only thin epoxy resins, because large thermal gradients which are generated during epoxy-resin cures. Typically, epoxy resins are cured under heat and pressure in autoclaves. As Figure II.19 shows the heating mechanism for a convectionally-cured specimen is through its boundaries. Upon cooling, these epoxy resins develop residual stresses in the matrix due to differences in the thermal expansion and, then, fracture.

Microwave and laser curing provides sufficient energy to initiate the polymerization reactions in the epoxy matrix [95,99]. With electromagnetic or laser curing, manufacturers may achieve a more efficient, uniform, complete, and economical cure than convectional-oven curing regardless of the composite's geometry. Microwave curing enables specimens to be cured from its interior to its

boundaries. Laser curing enables the beam to be focused at any point on a specimen.

Experimenters [57-60,99,101-103], have cured epoxy resins using microwave energy. Microwave energy is the energy associated with electromagnetic radiation within the microwave frequency range. Energy density stored in the electric field is always equal to the energy density stored in the magnetic field for electromagnetic radiation [101]. From electrostatics, the dielectric media includes both polar and non-polar molecular structures. Polar molecules align themselves with the oscillating electric field. Non-polar molecules take on an induced dipole, then orient themselves in the electric field. These molecules also adsorb rotational and vibrational energy from electromagnetic radiation of the appropriate frequency. When a dielectric material is placed in this field, epoxy molecules attempt to move and align themselves with it. However, since the field is oscillating, epoxy molecules are continually redirected. The increased movement of epoxy molecules creates an increase in the thermal energy of the system [102,103].

Since carbon fibers are much more lossy than the epoxy resin, the carbon fibers will increase in temperature faster than the epoxy resin. Whether the increase in carbon-fiber temperature will advantageously or adversely

affect the ultimate structure and properties of the composite material is not known. It may be possible that the conductive carbon fibers will distribute the heat more efficiently and uniformly; or the carbon fibers may excite polar carbon-fiber surface groups, such as carboxyls and carbonyls, and cause more epoxy monomers to react.

One disadvantage of microwave curing is that the experimenter has little control over the direction of the radiation. Laser curing of resins can offer more flexibility by directing the beam to only certain areas of a composite material. Unfortunately, the laser curing of composites has been less studied than the microwave curing of resins.

New research indicates that laser can be directed such that one part of a material may be cured while an adjacent part is left unaffected. Studies have been conducted where a carbon-dioxide infrared laser is used to cure an epoxy resin [104]. After a simulated production cure, the shear strength of the epoxy-resin samples are tested. The shear strength of the laser-cured samples are found to be equal to those obtained with the conventionally-cured samples. Newbould et al. [104] has reported that the failure modes are cohesive rather than adhesive. They also believed that laser curing has much potential once stable power

deliveries are obtained and laser beam equipment capable of scanning complex surfaces is available.

As a direct benefit, this study can be used as an aid in the designing and processing of composites. Comparative studies of conventionally-cured versus microwave- or laser-cured composites should be performed to gain insight on whether other types of curing are superior to conventional curing.

Due to the lack of understanding of the fiber-matrix interphase, currently marketed commercial composites are optimized with respect to information available. In order to aid in future "a priori" selection of composite components, other fiber composites such as glass or Kevlar should be cured, modeled, and compared with this study. Gaining an understanding of the structure and composition of different fiber-matrix interphases should enable a future "a priori" selection of composites based on the needs of composite-material users.

Appendix A

MAXIMUM EXOTHERM BETWEEN CARBON FIBERS AND EPOXY MATRIX

The difference in the atomic percentage of oxygen on the surface-oxidized and untreated fiber surface was 0.09 and 0.05, respectively. The actual surface of the fiber which was available for reaction with an epoxy molecule remained very small. Using bond lengths and geometry, the maximum number of sites containing functional, oxidized, the number groups on the surface of the surface-oxidized-carbon fiber, is 4.99×10^{15} sites/cm² or 4.88×10^{-8} g/mol/cm². This value is multiplied by the reaction exotherm and the surface area of the reinforced formulations, to determine the maximum change in the reaction exotherm. The calculated maximum increase in the reaction exotherm for the surface-oxidized carbon-reinforced composite is 5.40 cal/g; and the maximum increase in the reaction exotherm due to physisorption is 0.022 cal/g.

Adhesion at the Fiber-matrix Interface:

The carbon fiber consists of layers of basal planes [8] with an interplanar distance of 3.35 Å and a planar distance of 7.7 Å. The distance between a C-C bond is 1.42 Å. All angles in a perfect hexagon are 120°, and an equilateral triangle can be drawn between the center of the hexagon and two neighboring perimeter points of the hexagon.

Suppose the graphitic basal plane of a carbon fiber surface can be illustrated as follows:

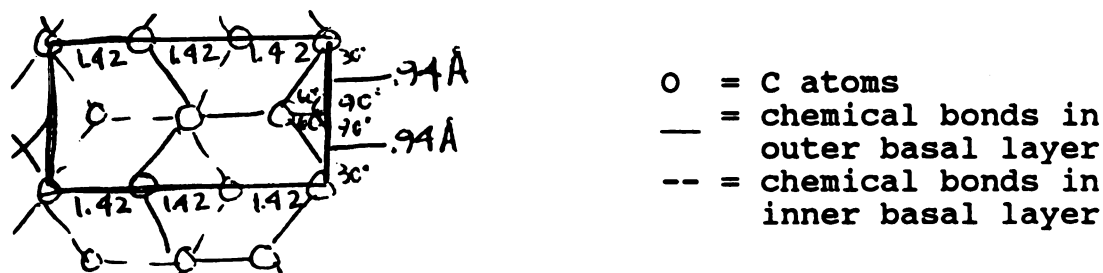


Figure A.1. Chemical reaction of a carbon fiber and an epoxy resin.

$$3(1.42 \text{ \AA}) \cdot 2 \cdot (0.94 \text{ \AA}) = 8.01 \text{ \AA}$$

$$4(1/4) + 2(1/2) + 2 = 4 \text{ atoms}$$

$$\frac{(4 \text{ atoms})(1 \times 10^8 \text{ \AA})^2}{(8.01 \text{ \AA})(1 \text{ cm}^2)} = \frac{4.99 \times 10^{15} \text{ atoms of C}}{\text{cm}^2}$$

- Assume: 1. The surface area, S, per gram of epoxy equals 4500 cm². This surface area was observed with by using a krypton adsorption technique or BET analysis [7]
2. Equilmolar reaction between an epoxy and a carbon-fiber surface group. The reaction exotherm for this reaction equals 24.6 kcal/g_{epoxy}.

Therefore, the maximum change in the ultimate reaction exotherm, δH_{ult} , due to chemical reaction between the epoxies and the carbon-fiber surface groups is

$$\delta H_{ult} = \left[\frac{24.6 \text{ kcal}}{\text{gmol}} \right] \left[\frac{1000 \text{ cal}}{\text{kcal}} \right] \left[\frac{4500 \text{ cm}^2}{g_{\text{epoxy}}} \right] \cdot \left[\frac{4.99 \times 10^{15} \text{ sites possible}}{\text{cm}^2} \right] \left[\frac{\text{gmol}}{1.023 \times 10^{23} \text{ atoms}} \right]$$

or $\delta H_{ult} = 5.40 \text{ cal/g}$ or 22.6 J/g . This value is only 1.26% of the ultimate reaction exotherm, H_{ult} . Since the precision of the DSC is $\pm 2.5\%$, sample error, detecting such a small change in reaction exotherm is unobtainable with the DSC.

Let's consider the δH_{ult} due to physisorption, from Adamson the physisorption reaction exotherm equals 0.1 kcal/g_{epoxy}. Therefore the

$$\delta H_{ult} = \left[\frac{0.1 \text{ kcal}}{\text{gmol}} \right] \left[\frac{1000 \text{ cal}}{\text{kcal}} \right] \left[\frac{4500 \text{ cm}^2}{g_{\text{epoxy}}} \right] \cdot \left[\frac{4.99 \times 10^{15} \text{ sites possible}}{\text{cm}^2} \right] \left[\frac{\text{gmol}}{1.023 \times 10^{23} \text{ atoms}} \right]$$

or $\delta H_{ult} = 0.022 \text{ kcal/g}$ or 0.092 J/g . Obviously, this value can not be determined from DSC analyses either.

Appendix B

TTT DIAGRAM TRANSITIONS

DETERMINING THE FULL CURE LINE

The full cure line on a TTT diagram represents the time where the all cure reactions cease. This method is similar to a procedure outlined by Peng et al.

1. Assume a linear relationship exists between T_g and H_{ult} , for isothermal cures below the ultimate glass transition temperature.

T_c ($^{\circ}\text{C}$)	T_g ($^{\circ}\text{C}$)	H_{ult} (J/gmol)
170	198	330
190	215	358
200	222	374
210	225	386
220	227	394

The following equation fit the data: $T_g = 33.2 + 0.503 H_{ult}$. The correlation coefficient equalled 0.9902.

2. Next the glass transition temperature at different times during the isothermal cures at 170, 200, and 220 $^{\circ}\text{C}$ are calculated using the previous equation.

t (min)	H (170,t)	T_g (170,t)	H (200,t)	T_g (200,t)	H (220,t)	T_g (220,t)
30	241	157	348	188	361	215
40	276	172	354	211	376	220
50	289	179	358	213	378	223
70	295	182	364	216	380	224
100	314	191	371	220	381	225

3. A linear relationship exists between T_g and T_c . The previous data was fit to the equation, $t_g = A + B T_c$.

t(min)	data	A	B	r^*
30	T_c 170 200 220 T_g 154 208 215	-52.9	1.21	0.9988
40	T_c 170 200 220 T_g 172 211 220	6.92	0.987	0.9734

t(min)	data	A	B	r*
50	$\frac{T_c}{T_g} \frac{170}{179} \frac{200}{213} \frac{220}{223}$	28.0	0.900	0.9820
70	$\frac{T_c}{T_g} \frac{170}{182} \frac{200}{216} \frac{220}{224}$	37.6	0.863	0.9741
100	$\frac{T_c}{T_g} \frac{170}{191} \frac{200}{220} \frac{220}{225}$	73.8	0.702	0.9632

* = correlation coefficient

4. Determine the isothermal cure temperature needed to achieve full cure at the times of 30, 40, 50, 70, and 100 minutes.

t(min)	30	40	50	70	100
$T_f (^{\circ}\text{C})$	224	223	222	222	221

The data fit the following equation:

$$T_f = 232 - 5.32 \log t.$$

The correlation coefficient is 0.9557.

DETERMINING THE GELATION LINE

The gelation line represents the line in a TTT diagram in which the extent of cure, α , equals the extent of cure at gelation, α_{gel} .

1. Assume a linear relationship between gelation temperature, T_{gel} , and the \log_{10} of the gelation time, $\log t_{gel}$, or

$$T_{gel} = a + b \log t_{gel};$$

where a, b = fitted constants.

The theoretical α_{gel} for a stoichiometric difunctional epoxy is 0.58, and the resin is found to be five to ten percent precured; therefore, the α_{gel} is assumed to be 0.50.

$T_c (^{\circ}\text{C})$	$t_{gel} (\text{min})^{**}$	$\log_{10} t_{gel}$
170	16.60	1.2
200	7.10	0.85
220	4.70	0.67

** = Data from Table III.7.

2. This data is fit to:

$$T_f = 232 - 5.32 \log t.$$

DETERMINING THE VITRIFICATION LINE

The vitrification line in a TTT diagram represents the line when the T_g equals the T_c .

1. The experimental T_c versus H_f data has been extrapolated to determine the vitrification time, t_{vit} , or the time when T_g equals T_c .

<u>T_c ($^{\circ}\text{C}$)</u>	<u>t_{vit} (min)</u>
170	100
200	57
220	50

2. A linear regression is performed on the previous table. The resultant equation is:

$$T_c = 478 - 155 \log t.$$

Appendix C

DSC AND FTIR-SPECTROSCOPY EXPERIMENTAL DATA

Table C.1. The DSC extent of cure, α , versus time, t , and fiber weight fraction, w_f , for the neat, surface-oxidized carbon-reinforced and untreated carbon-reinforced isothermally-cured at: (a) 170°C; (b) 200°C; (c) 220°C.

(a)

t	w_f			
	neat	0.01	0.10	0.60
2	0.02	0.02	0.01	0.02
3	0.03	0.03	0.03	0.03
4	0.04	0.04	0.04	0.04
5	0.05	0.05	0.06	0.06
6	0.08	0.07	0.08	0.08
7	0.10	0.09	0.10	0.17
8	0.12	0.12	0.11	0.12
9	0.14	0.14	0.13	0.13
19	0.27	0.26	0.26	0.25
29	0.38	0.38	0.37	0.36
39	0.43	0.42	0.41	0.43
49	0.48	0.48	0.48	0.47
59	0.50	0.49	0.49	0.48
89	0.54	0.53	0.53	0.52
119	0.54	0.54	0.53	0.52
149	0.55	0.54	0.54	0.53
179	0.56	0.55	0.55	0.54
329	0.56	0.56	0.55	0.55

Table C.1 (continued)

(b)

t	w_f			
	neat	0.01	0.10	0.60
2	0.04	0.04	0.04	0.04
3	0.12	0.12	0.13	0.12
4	0.19	0.20	0.20	0.19
5	0.26	0.25	0.25	0.24
6	0.32	0.32	0.33	0.32
7	0.37	0.36	0.36	0.35
8	0.41	0.40	0.40	0.39
9	0.45	0.45	0.44	0.43
19	0.48	0.48	0.47	0.47
29	0.65	0.64	0.64	0.63
39	0.72	0.71	0.71	0.71
49	0.76	0.76	0.75	0.74
59	0.78	0.78	0.77	0.76
69	0.79	0.78	0.78	0.78
79	0.80	0.80	0.79	0.80
89	0.81	0.81	0.80	0.80
99	0.82	0.82	0.81	0.81
119	0.82	0.82	0.81	0.81

(c)

t	w_f			
	neat	0.01	0.10	0.60
2	0.24	0.25	0.25	0.23
3	0.37	0.38	0.37	0.37
4	0.46	0.44	0.45	0.44
5	0.52	0.52	0.51	0.51
6	0.56	0.56	0.56	0.55
7	0.59	0.59	0.58	0.58
8	0.63	0.63	0.62	0.61
9	0.66	0.65	0.63	0.62
19	0.78	0.77	0.76	0.76
29	0.83	0.82	0.82	0.82
39	0.84	0.83	0.82	0.82
49	0.85	0.84	0.83	0.82
59	0.85	0.84	0.83	0.83
89	0.86	0.85	0.85	0.84
119	0.86	0.85	0.85	0.85
149	0.86	0.86	0.86	0.85
179	0.86	0.86	0.86	0.85
329	0.86	0.86	0.86	0.86

Table C.2. FTIR epoxy intensity peaks data.

Epoxy intensity peak peak*	Source/ Relative Error (%)
Transmission: 0.05476 0.05154 0.05348 0.05125	Particle size 13
DRIFT-FTIR: 0.09878 0.08465 0.05274 0.05016	Particle size distribution 24
 0.09332 0.07811 0.06615 0.08125	Packing Density 17
Day 1 Day2	Day-to-Day Reproducibility 28
0.05696 0.04274	
0.06189 0.04016	
0.06655 0.04494	
0.05016 0.04222	
 0.05050 0.1028 0.09682 0.05125	Sample Concentration 45

Table C.2. (continued)

0.1694 0.1761 0.2048 0.1502	Broader Baseline 17
0.06154 0.05860 0.06690 0.06257	No N ₂ Purge 11

LIST OF REFERENCES

1. Drzal, L.T., "The Interphases in Epoxy Composites," Advances in Polymer Science, Dusek, K., ed., Vol. 75, pp 1-32, (1985).
2. Cooke, T.F., "High Performance Fiber Composites with Special Emphasis on the Interface," Journal of Polymer Engineering, Vol. 7, pp 197-254, (1987).
3. Herrick, J.W., Proceedings of the 23rd Annual Technical Conference, The Society of the Plastics Industry, Session 16A, (1968).
4. Drzal, L.T., Rich, M.J., and Lloyd, P.A., "Adhesion of Graphite Fibers to Epoxy Matrix I - Role of Fiber Surface Treatment," Journal of Adhesion, Vol. 16, pp 1-30, (1982).
5. Fitzer, E., Geige, K.H., Huffner, W., and Weiss, R., "Chemical Interactions Between the Carbon Fiber Surface and Epoxy Resins," Carbon, Vol. 18, pp 189-191, (1980).
6. Thomas, C.R. and Walker, B.J., Proceedings from the Fifth London International Conference on Carbon and Graphite, p 520, (1978).
7. Drzal, L.T., Rich, M.J., and Lloyd, P.F., "Adhesion of Graphite Fibers to Epoxy Matrices: II. Effect of Fiber Finish," Journal of Adhesion, Vol. 16, pp 133-152, (1983).
8. Grant, J.T., Kim, R.Y., and Soni, S.R., "Improved Materials for Composite Adhesives," AFWAL-81-4154, (1984).
9. Reynolds, W.N., "Structure and Physical Properties of Carbon Fibers," Chemistry and Physics of Carbon, Vol. 11, p 1, (1973).
10. McKey, D.W. and Mimeault, "Surface Properties of Carbon Fibers," Chemistry and Physics of Carbon, Vol. 8, p 151, (1973).

11. Donnet, J.B. and Bansal R.C., Carbon Fibers, Marcel Dekker, p 27, (1987).
12. Donnet, J.B. and Voet, A., Carbon Black, Marcel Dekker, p 50, (1976).
13. Jenkins, G.M. and Kawamura, K., Polymeric Carbons-Carbon Fiber, Glass, and Char, Cambridge University Press, (1976).
14. Bacon, R., "High Temperature Resistant Fibers from Organic Polymers," Interscience, p 213, (1969).
15. Hercules, Inc, Wilmington, Delaware.
16. Reynolds, W.N., "Physical Properties of Graphite," Elsevier Publishing Company, (1968).
17. Ko, Y.S., "Carbon Fiber-Reinforced Composites: Effect of Fiber Surface on Polymer Properties," Polymer Engineering and Science, Vol. 22, No. 3, pp 805-814, (1982).
18. Denison, P., Jones, F.R., and Watts, J.F., "The Use of XPS and Labeling Techniques to Study the Surface Chemistry of Carbon Fibers," Journal of Applied Physics, Vol. 20, p 368, (1987).
19. Boehm, H.P., Diehl, E., and Heck, W., "Identification of Functional Graphite Surface Oxids of Carbon," p 369.
20. Boehm, H.P., "Chemical Identification of Surface Groups, Advances in Catalysis," Vol. 16, Academic Press, (1966).
21. Kozlowski, C. and Sherwood, P.M.A., "X-Ray Photoelectron Spectroscopic Studies of Carbon Fibre Surfaces VII - Electrochemical Treatment in Ammonium Salt Electrolytes," Carbon, Vol. 24, No. 3, pp 357.
22. Ubbelohte, A.R. and Lewis, F.A., "Graphite and IB Crystal Compounds," Oxford University Press, p 1, (1960).
23. Diefendorf, R.J. and Tokarky, E.W., "The Relationship of Structure to Properties in Graphite Fibers," APML-TR-72-133, (1977).
24. Hennig, G.R., "Electron Microscopy of Reactivity Changes Near Lattice Defects in Graphite," Chemistry and Physics of Carbon, Vol. 2, Marcell Dekker, p 6, (1966).

25. Drzal, L.T., Rich, M.J., Koeing, M.F., and Lloyd, P.A., "Adhesion of Graphite Fibers to Epoxy Matrices III - The Effect of Hypothermal Exposures," Journal of Adhesion, Vol. 18, p 49-72, (1985).
26. Tsai, S.W. and Hahn, H.T., Introduction to Composite Materials, Technomic Publishing Company, (1980).
27. Sellitte, C., Koeing, J.L., and Ishida, "Surface Characterization of Graphitized Carbon Fibers by Attenuated Total Reflective Fourier Transform Infrared Spectroscopy," Interfaces in Polymer, Ceramic, and Metal Matrix Composites, Elsevier Science Publishing, p 110.
28. Fuller, M.P. and Griffiths, P.R., "Diffuse Reflectance Measurements by Infrared Fourier Transform Spectrometry," Analytical Chemistry, Vol. 50, No. 13, pp 1906-1910, (1978).
29. Cole, K.C., Pilon, A., Hechler, J.J., Choriliotis, A., and Overbury, K.C., "Comparison of Infrared Spectroscopic Methods for the Quantitative Analysis of Epoxy Resins Used in Carbon-Epoxy Composite Materials," Applied Spectroscopy, Vol. 42, No. 5, pp 761-769, (1988).
30. Goodman, S.H., ed., Handbook of Thermoset Plastics, Naves Publication, p 258, (1986).
31. Rich, M.J. and Drzal, L.T., "Interfacial Properties of Some High-Strain Carbon Fibers in an Epoxy Matrix," Proceedings of the 41st Annual Technical Conference, Society of the Plastics Industry, Session 2, (1986).
32. Prime, R.B., Thermo Characterization of Polymeric Materials, Turi, E, ed., Chapter 5, Academic Press, p 435, (1982).
33. Billmeyer, F.N., Textbook of Polymer Science, Wiley, p 445, (1984).
34. Barton, T.M., "Application of Differential Scanning Calorimetry to the Study of Epoxy Resin Curing Reactions," Thermochemic Acta, Vol. 72, p 111-154, (1985).
35. Gillham, J.K., "Relationship Between Cure and Properties of Thermosetting Resins," Encyclopedia of Polymer Science and Engineering, Vol. 4, 2nd Edition, pp 519-524, (1986).

36. Enns, J.R. and Gillham, J.K., "Time-Temperature-Transformation Cure Diagram: Modeling the Cure Behavior of Thermosets," Journal of Applied Polymer Science, Vol 28, pp 2567-2591, (1983).
37. Prime, R.B., "Differential Scanning Calorimetry of the Epoxy Cure Reaction," Polymer Engineering and Science, Vol. 13, pp 435-569, (1973).
38. Riccardi, C.C. and Williams, J.J., "A Kinetic Scheme for an Amine-Epoxy Reaction with Simultaneous Etherification," Journal of Applied Polymer Science, Vol 32, pp 3445-3456, (1986).
39. King, J.J. and Bell, T.P., "Reactions in a Typical Epoxy - Aliphatic Diamine System," ASC Symposium Series, No. 114, Chapter 10, pp 225-257, (1979).
40. Sourour, S. and Kamal, M.R., "Differential Scanning Calorimetry of Epoxy Cure: Isothermal Cure Kinetics," Thermochimic Acta, Vol. 14, pp 49-59, (1976).
41. Chan, L.C., Nae, M.N., and Gillham, J.K., "Time-Temperature-Transformation Diagrams of High T_g Epoxy Systems and Competition Between Cure and Thermal Degradation," Journal of Applied Physical Science, Vol. 29, pp 3307-3327, (1984).
42. Finzel, M., Personal Communication, (1988).
43. Dutta, A. and Ryan, M.E., "Effect of Follers on Kinetics of Epoxy Cure," Journal of Applied Polymer Science, Vol. 24, pp 635-664, (1979).
44. Mijovic, J., "Cure Kinetics of Neat Versus Reinforced Epoxies," Journal of Applied Polymer Science, Vol. 31, pp 1177-1187, (1986).
45. Lee, G. and Hartmann, B., "Effects of Test Frequency and Cure or Glass Transformation Temperature Predictions on Some Epoxy Polymers," Journal of Applied Polymer Science, Vol. 22, pp 1471-1474, (1984).
46. Dusek, K, "Network Formation in Curing of Epoxy Resins," Advances in Polymer Science, Vol. 78, pp 2-59, (1986).
47. Nielsen, L.E., "Cross-Linking-Effect on Physical Properties of Polymers," Journal of Macromolecule Science, Vol. 3(1), pp 69-103, (1969).

48. Bidstrip, S.A., Sheppard, N.F. Jr., and Senturn, S.D., "Dielectric Analysis of the Cure of Thermosetting Epoxy Amine Systems," Technical Report 8, Office of Naval Research, Contract No. N00014-84-K-/0274, (1986).
49. Addabo, H.E. and Williams, R.J., "The Evolution of Thermosetting Polymers in a Conversion-Time Phase Diagram," Journal of Applied Science, Vol. 27, p 1327, (1986).
50. Charlesworth, J.M., "The Relative Reactivity of Primary and Secondary Amine Hydrogens deu The Bulk Polymerization of Aromatic Amines with Glyeidyl Ethers," Journal of Polymer Science and Polymer Chemistry, Vol. 25, pp 231-734, (1987).
51. Moacanin, J., Cizmechiouglu, M., Horg, S.D., and Gupta, A., "Mechanism and Kinetics of the Curing Process in a Resin System," Chemorheology of Thermosetting Polymers, pp 83-94, (1983).
52. Acitelli, M.A., Prime, R.B., and Sacher, E., "Kinetics of Epoxy Cure: (1) The System Bisphenol-A Diglycidyl Ether/m-Phenylene Diamine," Polymer, pp 335-342, (1971).
53. Hagnauer, G.L., Pearce, P.J., LaLiberte, B.R., and Roylance, M.E., "Cure Kinetics and Mechanical Properties of a Resin Matrix," Chemorheology of Thermosetting Polymers, pp 25-47, (1983).
54. Barton, T.M., "Kinetics of Cure of Epoxy Resin Systems: Bisphenol-A, Diglycidylether, Dic4, Aminophenyl Sulphane," Polymer, Vol. 21, pp 603-606, (1986).
55. Moroni, A., Mijovic, J., Pearce, E.M., and Foun, C.C., "Cure Kinetics of Epoxy Resins and Aromatic Dramines," Journal of Applied Polymer Science, Vol. 32, p 3761, (1986).
56. Sichina, W.J., "Autocatalyzed Epoxy Cure Prediction Using Isothermal DSC Kinetics," DuPont Company Applications Brief, No. TA-93.
57. Lee, W.I., Loos, A.C., and Springer, G.S., "Heat of Reaction, Degree of Cure, and Viscosity of Hercules 3501-6 Resin," Journal of Composite Materials, Vol. 16, pp 510-520, (1982).

58. Lee, W.I. and Springer, G.S., "Interaction of Electromagnetic Radiation with Organic Matrix Composites," Journal of Composite Materials, Vol. 18, pp 357-385, (1984).
59. Loos, A.C. and Springer, G.S., "Curing of Epoxy Matrix Composites," Journal of Composite Materials, Vol. 17, pp 135-169, (1983).
60. Lee, W.I. and Springer, G.S., "Microwave Curing of Composites," Journal of Composite Materials, Vol. 18, pp 387-409, (1984).
61. Shribley, A.M., Handbook of Composites, Van Nostrand Reinhold Company, (1982).
62. Hercules Incorporated, Graphite Fibers Business Center, Utah.
63. Thornel, "Technical Information," Product Information on T-300 Thornel Carbon Fibers, Union Carbide Corporation, Danbury, Connecticut.
64. Hercules, "Product Data on Magnamite Graphite Fibers, Type AS4," Hercules Incorporated, Wilmington, Delaware.
65. Garton, A. and Doley, J.M., "Characterization of the Aramid: Epoxy and Carbon:Epoxy Interphases," Polymer Composites, Vol. 6, pp 195-199, (1985).
66. Hull, D., Introduction to Composite Materials, Cambridge University Press, pp 9-48, (1981).
67. Needles, H.L., Alger, K.W., and Okamoto, R., "Adhesion at the Interface in Cured Graphite Fiber Epoxy-Amine Resin Composites," Journal of Reinforced Plastics and Composites, Vol. 6, pp 357-366, (1987).
68. Adamson, A.W., Physical Chemistry of Surfaces, John Wiley & Sons, pp 57-119, pp 150-160, (1982).
69. Schultz, J., Lavielle, L., and Martin, C., "The Role of the Interface in Carbon Fiber-Epoxy Composites," Journal of Adhesion, Vol. 23, pp 45-60, (1987).
70. Hartshorn, S.R., Structural Adhesives, Plenum Press, pp 366-367, (1986).
71. Adamson, M.J., "Thermal Expansion and Swelling of Cured Epoxy Resins Using in Graphite/Epoxy Composite Materials," Journal of Materials Science, Vol. 15, pp 1736-1754, (1980).

72. Rich, M.J., Personal Communications, (1988).
73. Plueddeman, E.P., "Mechanisms of Adhesion through Silane Coupling Agents," Composite Materials, Broutman, L.T. and Krock, R.H., eds., Academic Press, Vol. 6, (1974).
74. Wang, S. and Garton, A., "The Effect of Carbon Surface Functionality on MY720/DDS Cure Reactions," Polymeric Materials Science and Engineering, Vol. 60, pp 805-809, (1989).
75. Plueddemann, E.P., "Bonding through Coupling Agents," American Chemical Society, Polymer Reprints, Vol. 24, pp 196-203, (1983).
76. Eckstein, Y. and Berge, E., "Proceedings for the Symposium on Recent Developments in Adhesive Chemistry," Lee, C.H. ed., Dlenur Publishing Company, p 139, (1984).
77. Zukas, W.X., MacKnight, W.J., and Schneider, N.S., "Dynamic Mechanical and Dielectric Properties of an Epoxy Resin During Cure," Chemorheology of Thermosetting Polymers, pp 223-250, (1983).
78. Riggs, D.M., Shuford, T.J., and Levels, R.P., "Graphite Fibers and Composites," Handbook of Composites, Lubin, G., ed., Van Nostrand-Reinhold Company, Section 11, (1982).
79. Wenz, S.M., and Mijovic, J., "The Effect of Cure Schedule on Physical/Mechanical Properties of Graphite/Epoxy Composites," SAMPE Journal, pp 31-45, (1986).
80. Fava, R.A., "Differential Scanning Calorimetry of Epoxy Resins," Polymer, Vol. 13, pp 137-151, (1968).
81. Peyser, P. and Bacon, W.D., "Kinetics of Epoxy Resin Polymerization Using Differential Scanning Calorimetry," Journal of Applied Polymer Science, Vol. 21, p 2359, (1977).
82. Prime, R.B. and Sacher, E., "Kinetics of Epoxy Cure: 2. The System Bisphenol-A, Diglycidyl Ether Polyamide," Polymer, Vol. 13, pp 455-458, (1972).
83. Young, P.R. and Chang, A.C., "FTIR Characterization of Advanced Materials," SAMPE Quarterly, Vol. 17, No. 4, pp 32-39, (1986).

84. Koeing, J.L., "Spectroscopic Characterization of Polymers," Analytic Chemistry, Vol. 59, No. 19, pp 1141-1155, (1987).
85. Mertz, E. and Koeing, J.L., "Application of FT-IR and NMR to Epoxy Resins," Advances in Polymer Science, Dusek, K., ed., Vol. 75, pp 74-112, (1985).
86. Hamadeh, I.M., Yeboah, S.A., Trumbull, K.A., and Griffiths, P.R., "Preparation of Calibration Standards for Quantitative Diffuse Reflectance Infrared Spectrometry," Vol. 38, No. 4, pp 426-491, (1984).
87. Buckley, L. and Roylance, D., "Kinetics of a Sterically Hindered Amine-Cured Epoxy Resin System," Polymer Engineering and Science, Vol. 22, No. 3, pp 166-171, (1982).
88. DeLong, J.D., Personal Communication, (1988).
89. Dow Chemical Company, Midland, Michigan.
90. Aldrich Chemical Company, Milwaukee, Wisconsin.
91. ASTM D 792, Annual Book of ASTM Standards, Philadelphia, PA, (1986).
92. E.I. Dupont Corporation, Wilmington, Delaware.
93. Perkin-Elmer Corporation, Perkin-Elmer Diffuse Reflectance Accessory Instructions, Norwalk, Colorado, (1986).
94. Peng, X. and Gillham, J.K., "Time-Temperature-Transformation (TTT) Cure Diagrams: Relationship Between T_g and the Temperature and Time of Cure for Epoxy Systems," Journal of Applied Polymer Science, Vol. 30, pp 4685-4696, (1985).
95. Levenspiel, O., Chemical Reaction Engineering, second edition, John Wiley & Sons, p.25, (1972).
96. Schwalm, C.A., Hawley, M.C., and DeLong, J.D., "Study of Interphase Reactions During the Cure of Composites," Navy Defense Support Program, Champagne, Illinois, Nov. 8-10, (1987).
97. Painter, P.C., Snyder, R.W., Starsinic, M. Coleman, M.M., Kuchn, D.W., and Davis, A., "Concerning the Application of FT-IR to the Study of Coal: A Critical Assessment of Band Assignments and the Application of Spectral Analysis Programs," Applied Spectroscopy, Vol. 35, No. 5, pp 475-485, (1981).

98. Hooke, K., Personal Communication, (1989).
99. Hawley, M.C., Jow, J., Schwalm, C.A., Singer, S.M., and DeLong, J.D., "Microwave Processing and Measurement of Properties for Various Fiber/Epoxy Ratios," Fourth Annual Meeting, Polymer Processing Society, Orlando, Florida, May 8-11, (1988).
100. Feenstra, R., ed., Proceeding for the Second International Conference of Scanning Tunneling Microscopy, Oxnard, California, July 20-24, Amer. Vac. Soc., New York, (1987).
101. Gourdenne, A., Massarani, J.H., Monchaux, P., Aussudre, S., and Thourel, L., "Cross-Linking of Thermosetting Resins by Microwave Heating: Quantitative Approach," American Chemical Society, Division of Polymer Chemistry, Polymer Reprints, Vol. 20, pp 471-474, (1979).
102. Strand, N.S., "Microwave Curing of Thermoset Resins," Society of Manufacturing Engineers, Technical Paper EM79-368, (1979).
103. Gourdenne, A. and LeVan, Q., "Intimate Study of the Microwave Curing," American Chemical Society, Division of Polymer Chemistry, Polymer Reprints, Vol. 22, pp 125-127, (1981).
104. Newbould, J. and Legumina, A., "New Technology: GM's Lasablate Aids SMC Surface Prep," Auto Plastic News, Vol. 19, No. 4, pg 9, (1989).